VINCENZO D'ALESSANDRO

INVESTIGATION AND ASSESSMENT OF THE WAVE AND FINITE ELEMENT METHOD FOR STRUCTURAL WAVEGUIDES

"Investigation and assessment of the Wave and Finite Element Method for structural waveguides"

3D TECH SRLS Via San Vito, 65, 80014, Giugliano in Campania, Naples, Italy.

Typeset with LaTeXand PGF/TikZ.

This document was typeset using the LaTeXstyle `classicthesis`, developed by André Miede.

Text printed in Italy at Universal Book SRL, Via S. Botticelli, 22, 87036 Rende, Cosenza.

ISBN 978-88-98382-06-4

UNIVERSITÀ DEGLI STUDI DI NAPOLI
FEDERICO II

Department of Industrial Engineering
Doctoral School of Industrial Engineering
Ph. D. Course in Aerospace, Naval and Quality Engineering

Investigation and Assessment of the Wave and Finite Element Method for structural waveguides

Candidate
Vincenzo D'Alessandro

Supervisors
Prof. Sergio De Rosa
Prof. Francesco Franco

Coordinator
Prof. Luigi de Luca

Submitted on March 2014 for the XXVI cycle

Vincenzo D'Alessandro: *Investigation and assessment of the Wave and Finite Element Method for structural waveguides* , March 2014

I, Vincenzo D'Alessandro, declare that this thesis titled "Investigation and assessment of the Wave and Finite Element Method for structural waveguides" and the work presented in it are my own work. I confirm that:

- this work was done wholly or mainly while in candidature for a doctoral degree at this University;
- where any part of this thesis has previously been submitted for a degree or any other qualification at this University or any other institution, this has been clearly stated;
- where I have consulted the published work of others, this is always clearly attributed;
- where I have quoted from the work of others, the source is always given and with the exception of such quotations, this thesis is entirely my own work;
- I have acknowledged all main sources of help;
- where the thesis is based on work done by myself jointly with others, I have made clear exactly what was done by others and what I have contributed myself.

This Ph.D. thesis will be defended in a public dissertation on May 16, 2014 under the judgement of a specialised commission composed by:

- Prof. Annalisa Fregolent, Department of Mechanical and Aerospace Engineering, Universitá di Roma "La Sapienza";
- Dr. Elena Ciappi, Marine Technology Research Institute INSEAN, National Research Council of Italy (CNR), Roma
- Prof. Herve Riou, Department of Mechanical Engineering, Structure and System division, Ecole Normale Supérieure de Cachan;
- Prof. Walter D'Ambrogio, Department of Industrial Engineering, Information and Economy, Universitá degli Studi dell'Aquila.

March 2014
Department of Industrial Engineering
Universitá degli Studi di Napoli "Federico II"
Napoli

Vincenzo D'Alessandro

Dedicated to my lovely Parents,
Antonio and Giuseppina

quante volte vi ho pensato nei momenti piú importanti
quando solo sopra un palco e affrontavo i miei giganti
quando in macchina di notte con l'Europa da scoprire,
a far finta di star bene per non farvi preoccupare
quante volte ho detto basta,
ma chi me lo fa fare,
peró poi pensando a voi non riuscivo mai a mollare
questa vita di speranze, ma piena di emozioni
(A. Britti, "Mamma & Papá")

ACKNOWLEDGEMENT

This thesis represents the conclusion of three years of hard and exciting work, during which I grew up as researcher, but mostly as person. Therefore, I would like to acknowledge all those people, who have played a key role during this my growth.

I wish to thank the Doctorate School in Industrial Engineering, which has gave me all the instruments I needed for my work and has partially funded my staying at McGill University in Montreal (Canada).

I wish to thank the financial support received by the European project SUPER-PANELS Strengthening and Upholding the Performances of the new Engineered Research PANELS - PEOPLE MARIE CURIE ACTIONS, International Research Staff Exchange Scheme FP7-PEOPLE-2009-IRSES), which has funded my staying at McGill University in Montreal (Canada) and the conferences I attended.

I wish to thank the Department of Industrial Engineering for giving me the possibility to improve my technical skills, providing me all the instruments I needed.

It is very hard for me to explain in few words the thankfulness I feel for my supervisors, Proffs. Sergio De Rosa and Francesco Franco. Thanks to both of them for having changed my academic career, my prospects, in that meeting occurred six years ago (it seems like yesterday!). I thank them for the trust, dedication, availability which they have given me, trying to convey knowledge and analytical skills. The possibility of having a daily conversation, talking of work and life stuffs with respect but at the same time in a friendly mood, it is a chance that not all PhD students have. Thanks a lot!

I shared the entire doctoral program with Giuseppe Petrone, and I wish to thank him because having a so prepared colleague/friend allowed me to work at my best, sometimes even having fun. I also thank Nicola Santoro, the last PhD student in the group. It has been a pleasure and a privilege to work with them.

I wish to thank the remaining part of our research group, PASTA-Lab, in particular Prof. Francesco Marulo, always generous with his life and technical lessons; Post-Docs Eng. Tiziano Polito and Eng. Michele Guida, models for me; and Ms. Carla Colino.

I thank Prof. Marco Amabili, my supervisor at McGill University in Montreal (Canada), for given me the possibility to increase my laboratory skills.

Thanks to PhD studentes/Post-Docs at the Aerospace Section of the Department of Industrial Engineering: Angelo De Fenza, Marco Barile, Natalino Boffa, Marco Di Palma, Leandro Maio, Elia Daniele and Romeo Di Leo: we have created a very nice atmosphere, made of proficient works and funny moments.

Every day within the last three years, I came back home from the university. I am a lucky guy, because very warm people was waiting for me with their lovely support and patience. For this reason, I would like to thank them for walking beside me across this path full of hard work and satisfaction.

First of all, I thank my lovely Parents, Mom Pina and Dad Antonio, to whom I dedicate this work. If I have been able to achieve all the goals I set for myself, it is for their love, their teaching and their sacrifices. Thanks for letting me grew up curious, humble and ambitious: these characteristics helped me a lot. Thanks for understanding me when I was nervous because my codes did not work. Thanks for teaching me to never give up and to fight in order to achieve what I want. I hope you can be proud of me. Thanks to my sister Imma, a model both as person and student: it has been always hard being her younger brother! Also thanks to her boyfriend Daniele, who now is as a brother for me. I thank my grandfather Vincenzo: his stories, narrated when I was a kid, made me passionate about the world of aircraft.

If a friend is a treasure, then I am the richest man in the world. In these years, there were some hard moments. Sometimes, I might fall, but there were My Friends to support me. Sharing laughs, by mostly tears. I wish to thank all of them, in our way, because we are *the most beautiful show after the Big Bang* (Jovanotti, italian song). Thanks to the Tripod which does not give to become adults, *which 40 years will not stop us* (Ligabue, italian song): Luca & Peppe A., not blood-brothers, but life-brothers. Thanks to that dream found beyond the sky, after a nightmare (Peppe B. and Peppe C.): the important people are always there. Thanks to those new wave of joy, brought my little sis and confident Anna. Thanks to the personification of goodness, a reference point for all of us (Gianmaria). Thanks to the simplicity and sweetness (Monica, the only person I can speak English with. Thanks for her teaching!). Thanks to Massimo and Antonio, the first friends who left us for other places, showing that the friendship does not change, maybe just the everyday life. Thanks to the imagination and precision (Giuseppe Paolo) and thanks to who teaches me to look at life always with a smile (Antonio R.). Thanks to The Travelers (Santo, Luigi, Gigi, in addition to Peppe C., Monica and Luca) for being my soundtrack band, my *Wonderwall*. And thanks also to who have always believed in me from the beginning, even if we took different ways (Maria).

Simply, THANKS.

RINGRAZIAMENTI

Questa tesi é l'epilogo di tre anni di duro e appassionante lavoro, durante i quali sono cresciuto come ricercatore, ma soprattutto come persona. Desidero ringraziare tutte le persone che hanno avuto un ruolo fondamentale durante questa mia crescita.

Ringrazio la Scuola di Dottorato in Ingegneria Industriale che ha messo a mia disposizione gli strumenti necessari per svolgere al meglio il mio lavoro e finanziato in parte il mio soggiorno presso la McGill University di Montreal (Canada).

Ringrazio il supporto economico ricevuto dal progetto europeo SUPERPANELS (Strengthening and Upholding the Performances of the new Engineered Research PANELS - PEOPLE MARIE CURIE ACTIONS, International Research Staff Exchange Scheme FP7-PEOPLE-2009-IRSES). Tale progetto ha finanziato in gran parte il mio periodo come tirocinante presso la McGill University di Montreal (Canada) e parte delle conferenze a cui ho presenziato.

Ringrazio il Dipartimento di Ingegneria Industriale, per avermi fornito tutti gli strumenti di cui avevo bisogno per la mia formazione tecnica.

É difficile per me trovare le parole giuste per ringraziare i miei supervisori, i Proffs. Sergio De Rosa e Francesco Franco. Ringrazio entrambi per aver cambiato il mio percorso universitario, le mie prospettive, in quell'incontro di sei anni fa (sembra ieri!). Li ringrazio per la fiducia, per la dedizione, per l'infinita disponibilitá che mi hanno dedicato, provando a trasmettermi conoscenze e capacitá di analisi. La possibilitá di avere un confronto giornaliero, con rispetto ma al tempo stesso in un clima amichevole, é una fortuna che non tutti i dottorandi hanno. Grazie, davvero.

Ho condiviso l'intero percorso di dottorato con Giuseppe Petrone, che desidero ringraziare perché avere un collega/amico cosí preparato mi ha permesso di lavorare al meglio, talvolta anche divertendoci. Ringrazio anche Nicola Santoro, l'ultimo dottorando del gruppo. É stato un piacere e un privilegio lavorare con loro.

Ringrazio la restante parte del nostro gruppo di ricerca, PASTA-Lab, nelle persone del Prof. Francesco Marulo, sempre prodigo di insegnamenti tecnici e di vita; dei ricercatori Ing. Tiziano Polito e Ing. Michele Guida, esempi per me; della Sign.ra Carla Colino.

Ringrazio il Prof. Marco Amabili, mio supervisore durante alla McGill University, per avermi dato l'opportunitá di migliorare le mie conoscenze riguardanti l'analisi sperimentale di strutture.

Come non ringraziare i dottorandi/ricercatori della Sezione Aerospaziale del Dipartimento di Ingegneria Industriale: Angelo De Fenza, Marco Barile, Natalino Boffa, Marco Di Palma, Leandro Maio, Elia Daniele e Romeo Di Leo per aver creato tutti insieme un clima sereno e di amicizia, fatto di proficuo lavoro e momenti piacevoli.

Ogni giorno di questi tre anni, tornavo a casa dall'universitá. Sono una persona fortunata, perché ad attendermi c'erano persone che mi hanno supportato e sopportato con amore. Per questo motivo desidero ringraziare coloro che hanno percorso accanto a me questa strada ricca di fatica e soddisfazioni.

Innanzitutto, ringrazio i miei Genitori, Mamma Pina e Papá Antonio, a cui dedico questo lavoro. Se sono stato in grado di raggiungere tutti gli obiettivi che mi prefissavo, é solo grazie al loro amore, sacrifici, insegnamenti. Li ringrazio per avermi fatto crescere curioso, umile ed ambizioso: queste caratteristiche mi hanno aiutato tanto. Li ringrazio per avermi capito quando ero pensieroso perché qualche codice non funzionava. Li ringrazio per avermi insegnato a non mollare mai, lottando per raggiungere ció che voglio. Spero che siano orgogliosi di me. Grazie a mia sorella Imma, da sempre esempio di persona e studentessa per me: é sempre stato difficile essere suo fratello minore! Grazie anche al suo fidanzato, Daniele, ormai un fratello per me. E grazie a mio nonno Vincenzo: le sue storie, narratemi quando ero bambino, mi hanno fatto appassionare al mondo degli aerei.

Se chi trova un amico, trova un tesoro, allora io sono l'uomo piú ricco del mondo. In questi anni, ci sono stati momenti duri. Qualche volta sarei potuto cadere, ma c'erano gli Amici Miei a sostenermi. A condividere risate, ma soprattutto a raccogliere qualche lacrima. Voglio ringraziarli, a modo nostro, perché siamo *il piú grande spettacolo dopo il Big Bang* (Jovanotti). Grazie a quel Treppiedi che non si arrende al diventare adulti, *che non ci fermano i 40 anni* (Ligabue): Luca & Peppe A., fratelli non di sangue ma di vita. Grazie a quel sogno trovato *al di lá del cielo*, dopo un brutto incubo (Peppe C. e Peppe B.): le persone importanti ci sono sempre. Grazie a quella ventata di allegria, mia piccola sorella acquisita e confidente (Anna). Grazie alla bontá fatta persona, punto di riferimento per tutti noi (Gianmaria). Grazie alla semplicitá e alla dolcezza (Monica), l'unica con la quale potessi parlare in inglese (grazie per gli insegnamenti!). Grazie a chi ha aperto le danze, andando via per primi e dimostrando che affettivamente non cambia nulla, se non la quotidianitá (Massimo e Antonio). Grazie alla fantasia e precisione (Giuseppe Paolo) e a chi mi insegna a guardare alla vita con il sorriso, sempre (Antonio R.). Grazie ai The Travelers (Santo, Luigi, Gigi, oltre a Peppe C., Monica e Luca) per essere stati la mia colonna sonora, il mio *Wonderwall*. E grazie anche a chi ha sempre creduto in me, fin dall'inizio, anche se abbiamo prese strade differenti (Maria).

Semplicemente, GRAZIE.

INTRODUCTION

MOTIVATIONS

Nowadays, passengers of all means of transport, such as aircraft, cars and trains, expect high comfort levels, in terms of both vibrations and noise. This has led to the development of always more efficient simulation tools, in order to speed up the virtual design and prototype phases.

Despite the enormous computational power available, thanks to modern computer and efficient algorithms, the development of new models is complicated because of the wide frequency range of the excitation. In fact, the vibro-acoustic behaviour of a structure is strongly influenced by the frequency range of analysis.

Let us consider a linear system (e.g. a plate), excited in a wide frequency range. If the Frequency Response Function (FRF) is estimated, three main regions can be identified, as described below.

- Low Frequencies (LF): the response exhibits isolated modal resonances and it has local characteristics. In particular, the response is strongly dependent on the positions of the excitation and of the response points, as well as the type of constraints. This region is usually investigated through deterministic methods, such as the *Finite Element Method (FEM)* and/or the *Boundary Element Method (BEM)*.

- High Frequencies (HF): the response is diffuse and does not present resonance. Furthermore, it does not depend on local parameters. Hence, the structure can be investigated through probabilistic technique, such as the *Statistical Energy Analysis (SEA)* and/or the *Energy Distribution Approach (EDA)*.

- Mid Frequencies (MF): the response in this region presents an intermediated behaviour, being a transition zone, for which well-established prediction techniques are not yet available. Conventional deterministic methods, based on finite elements, require an unacceptable computational effort due to the huge size of models; on the other hand, the assumptions of probabilistic methods are not yet valid.

In recent years, a huge effort has been done in the development of numerical methods suitable for the mid-frequency range, some of which exploit the analysis of wave propagation through structures. The knowledge of the dispersion relations and, in general, of the types of waves propagating through structures is of interests for many applications involving the fluid-structure interactions, such as transmission of structure-borne sound, shock response and so on.

Among the methods based on the wave propagation, the Wave and Finite Element Method (WFEM) is gaining interest for the analysis of periodic structures,

very common in engineering field. Periodic structures are supposed to be constituted by a set of identical elementary cell, repeated along one or two directions. The Wave and Finite Element Method allows to investigate only one cell of the structure, modelled through Finite Element. Once the mass, stiffness and damping matrices of the cell (eventually estimated through a commercial software) are estimated, they are post-processed in order to formulate an eigenvalue problem, whose solutions constitute the propagation constants of the waves travelling through the structure.

GOALS

The Wave and Finite Element Method appears to be very attractive because it allows the use of huge Finite Element libraries of commercial softwares to model the elementary cell of the periodic structure. Therefore, the goal of this dissertation is exploiting the potentiality of the Wave and Finite Element method for the analysis of structural waveguides, both one- and two-dimensional, using a commercial code for the discretisation of the elementary cell. An own-code for the analysis of such waveguides has been developed in MATLAB® environment, able to import the matrices carried out through ANSYS®. The tool is now available at the Department of Industrial Engineering – Aerospace Section of University of Napoli "Federico II".

DISSERTATION OUTLINE

The dissertation is organised as follows.

Chapter 1 is dedicated to the literature review regarding the development of the Wave and Finite Element Method for the analysis of wave propagation in waveguides and the forced response in finite structures.

In Chapter 2, the theoretical basis on the wave propagation are summarised, in order to provide to the reader all the concepts needed for the comprehension of the thesis. First, the main parameters characterising the wave propagation are defined, highlighting the meaning of the dispersion curves. Then, wave propagation in infinite media is explained, remarking the different nature of the waves occurring. The influence of boundaries in finite structures is then introduced, in order to describe the forced response of finite structures. At the end, an introduction of the wave propagation in layered media is presented, mostly referred to sandwich structures.

Chapter 3 concerns the application of the Wave and Finite Element Method (WFEM) for the analysis of uniform one-dimensional structures. The chapter is basically arranged in three main sections. In the first one, the method is formulated for the analysis of waveguides: since the generic waveguide is considered a periodic structure, the Bloch theorem allows the investigation of only one, elementary cell. The dispersion relations are carried out by solving an eigenvalue problem based on stiffness and mass finite element matrices. Once dispersion

relations are known, the analysis of the forced response through the wave propagation approach is explained. In the second section, the code implementing the WFEM for one-dimensional structures is briefly explained. In the last sections, numeric results are presented for different type of structures (isotropic, composite, sandwich), both in terms of dispersion curves and forced response, in order to exploit the potentiality of the developed method.

In Chapter 4, a first approach to the analysis of wave propagation in two-dimensional waveguides through WFEM is presented. The chapter is arranged as the previous one. First of all, the eigenvalue problem is formulated for a four-node rectangular finite element. Then, the code is briefly explained, before to report the first obtained results, oriented to the validation of experimental tests conducted on a natural fibres composite panel.

At the end, in Chapter 5 concluding remarks and possible future works are highlighted.

CONTENTS

LIST OF FIGURES

LIST OF TABLES

1 LITERATURE REVIEW

The analysis of the propagation of waves in structures is a fundamental task in many engineering applications. The knowledge of dispersion relations, providing information on the type of propagating waves as well as their velocity, is of interest for the prediction of forced response, acoustic radiation, non-destructive testing, transmission of structure-borne sound and so on, which nowadays are the subject of many studies in order to improve the vibro-acoustic comfort of passenger carries.

Wave propagation in *simple* structures can be investigated through analytical models, exact or approximated. However, the analysis of wave motion usually involves assumptions and approximation concerning the stress, strain and displacement states of the structure, and always more refined models are required as the frequency increases since the wavelength may become comparable with the cross-section dimensions. For example, if the propagation of bending waves in a beam is investigated, Euler-Bernoulli, Rayleigh, Timoshenko or 3-dimensional elasticity based theories might be used, depending on the frequency range of interest [1, 2].

For complex structures, such as layered (composite and sandwich) beam [3–5] and plate [6–12], or cylinders [13–15], the analytical formulation (if it is possible) becomes quite difficult: beyond the required assumptions and approximations in the models, the resulting dispersion relations are usually transcendental and/or of high order, therefore their resolution is not straightforward (or requires symbolic manipulation [15, 16]). For this reasons, for the analysis of complex construction, semi-analytical or numerical methods have been developed for the computation of dispersion curves.

However, if the structure under investigation presents characteristics which periodically repeat in one or more directions, different approach can be developed by exploiting the periodicity [17]. In general, a generic structure obtained as an assemble of identical elements, called cells, can be considered as periodic. Several engineering structures can be assumed as periodic, starting from simply beams and plates, moving to stiffened plate or car tyres, up to aircraft fuselage, railways tracks, and so on.

Among several methods available in literature for the analysis of the wave propagation, in the last ten years the Wave and Finite Element Method is becoming particularly attractive for the analysis of periodic structures for its direct connection to conventional FE approach.

The Wave and Finite Element Method (WFEM) is a deterministic technique which consider an homogeneous waveguide structure as a periodic system assembled by identical elementary cells. Similarly to the Spectral Finite Element

Method (SFEM) [18–20], the analysis of the waveguide is based on the analysis of one single section, but it does not require the definition of specified spectral elements because the cross section is discretised through standard Finite Element Method [21, 22]. This allows the investigation of the wave motion in waveguide having complex cross-sectional shape, with a reduced computational cost.

The WFEM integrates several positive aspects of previous works regarding the analysis of wave propagation. In fact, the method start with the modelling of a short section of the waveguide under investigation through conventional Finite Element. Supposing time-harmonic motion, the equation of motion is then expressed in discrete coordinates, relating nodal degrees of freedom $\mathbf{q}$ and forces $\mathbf{f}$ of the undamped section:

$$(\mathbf{K} - \omega^2 \mathbf{M})\mathbf{q} = \mathbf{f} \tag{1.1}$$

where $\mathbf{K}$ and $\mathbf{M}$ are the stiffness and mass finite element matrices. This relation resembles the dynamic stiffness matrix introduced by Koloušek [23], despite the matrix, in general, is not frequency-dependent. Generalising the concept of the Transfer Matrix Method (introduced by Thompson [24] to relate displacements and stresses at the top and the bottom free surfaces of a plate) by applying the periodicity condition through the Bloch theory [17], it is possible to express the nodal displacements and forces on a side of the section as a function of those on the other side, taken as reference. This relation is expressed through a transfer matrix, which is obtained directly from the dynamic stiffness matrix. The definition of the transfer matrix leads to the formulation of an eigenvalue problem, whose solutions represent the wave propagation constants (eigenvalues) and the wavemodes (eigenvectors) of the propagating waves.

As reported by Mead in his overview [25], the pioneering work by Orris and Petyt [26] is the first to apply the use of the conventional Finite Element Method for the analysis of wave propagation in one-dimensional infinite, periodic beams and rib-skin structures. Abdel Rahman [27], applying the receptance method [28], extends this FE approach for evaluating the dispersion curves of two dimensional waveguide, based on four nodes quadrangular elements, as well as three dimensional periodic beam systems. Given the needed of describe the cross-section deformation of railway tracks at high frequencies, Thompson [29] develops an FE model of a finite length of rail using beam elements for the head and plates. Then, by imposing symmetric and/or antisymmetric boundary conditions at both ends, obtained the frequency-wavenumber relations, assuming wave propagation along the track axis. A similar approach is applied by Gry [30].

Beside this first works, the research on the Wave and Finite Element Method received new emphasis in the 2000's, thanks to works conducted by Mencik and Ichchou's group [31–57] in France and those conducted under Mace's supervision [58–79] in UK.

CONTRIBUTIONS FROM LYON (FRANCE)

To the author's best knowledge, the present Wave and Finite Element method is formulated for the first time by Houillon et al. [31]. In this work, the dispersion curves of thin walled structures, such as cylinders and rectangular plate box, are

carried out, remarking the advantages connected to the possibility to use conventional existing Finite Element models for modelling of an elementary section. The comparison with analytical results are quite good. A well-posed implementation procedure is defined, highlighting the parameters playing a key role. This work is further completed by by Ichchou et al. [34], who perform a parametric analysis on a thin walled structure modelled using thin shell elements (one of the investigated FE models is shown in Figure 1.1). The influence of the length of the elementary cell (called *propagation distance*) and of the mesh of the model on the accuracy of the results is investigated, in terms of dispersion curves, group velocity and kinetic energy density.

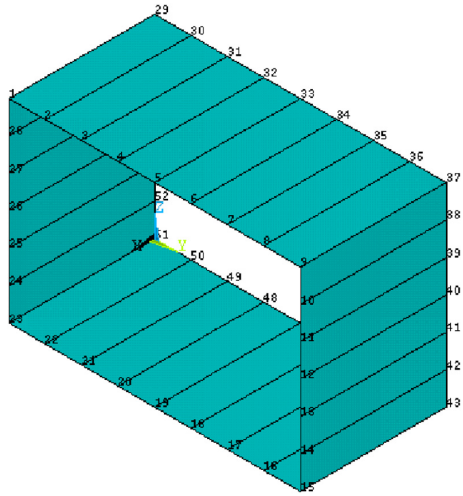

Figure 1.1: Finite Element model of a thin walled tubular box [34]

Mencik and Ichchou also investigate through the WFEM the vibroacoustic behaviour of a slender structure containing a fluid [36]. The FE model of the elementary cell is made of three-dimensional linear elements, having steel material properties for the the solid part and water properties for the fluid one. The forced response is estimated for a duct assumed clamped on both edges, whereas the fluid is excited by imposed displacements and coupled with a mass-spring system. The boundary conditions are applied in the physical domain, by expressing the displacements in terms of wavemodes obtained by the wave propagation analysis.

Ichchou et al. [38] use the WFE approach to carry out the dispersion curves of ribbed plates. In particular, analytical, numerical and experimental characterizations of flexural waves propagating along the rib are presented, comparing the results with analytical and experimental [37] ones. In the WFE model, both the plate and the rib are modelled with thin shell elements, and only the out-of-plane motion is considered (vertical displacement and rotation about the rib).

The analysis of transmission and diffusion at joints between waveguides is investigated in several works by Mencik, Ichchou and other co-authors [32, 40, 43, 51]. In their first work on this topic, Mencik and Ichchou [32] analyse the multimode wave propagation through waveguide by means of WFEM, thus they for-

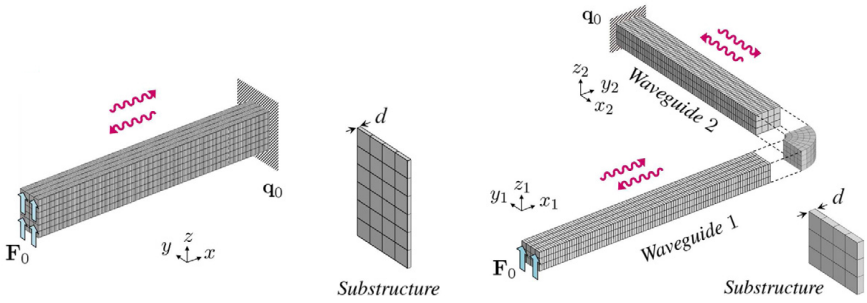

(a) *isolated beam* **(b)** *coupled beams*

Figure 1.2: FE models of one-dimensional structures [42, 45]

mulate the coupling, in terms of wave modes, between more waveguides at a joint. The coupling conditions at the joint interfaces are expressed through Lagrange multipliers. The so-called diffusion matrix, relating incident and reflected wavemodes, is obtained in a general way by applying the dynamical equilibrium at the interfaces. Several numerical tests are conducted on different connections between steel and aluminium waveguides, having rectangular cross-section. The diffusion matrix model is also applied to the analysis of damaged structures, wherein the damage is considered as a coupling element between two waveguides modelled with the WFEM: examples are reported for damaged straight [40] and curved beams [43] and for damaged stiffened panels [51].

Mencik [42, 45, 49] also focuses on the analysis of the forced response through the Wave and Finite Element Method. Firstly, he formulates the eigenproblem in one-dimensional finite structures [42], defining the positive and negative going waves as incident and reflected, respectively (formally, this is not correct, but this convention is clearly specified by the author and corrected in subsequent works). The presence of the boundaries, as well as external forces, is treated by the definition of a diffusion matrix, which is well suited for describing the Neumann and Dirichlet boundary conditions. The importance of definition of a reduced wave basis is remarked, showing the influence of the frequency response function in the case of an isotropic cantilevered beam excited at the free tip, as well as in the case of two isotropic beams connected through a joint. In the case of a layered beam, instead, a regularization strategy [39] is involved to take into account the different waves propagating in different layers. With the same approach, a hybrid technique based on the Component Mode Synthesis is introduced for analysing elastic joints [45].

On the other hand, Ichchou and other co-authors focus on the application of the Wave and Finite Element Method for the analysis of the wave propagation in random guided elastic media, by defining the so-called Stochastic Wave Finite Element (SWFE) approach [46, 54, 55]. It is an extension of the WFEM for uncertain periodic structures, using the first-order perturbation method. Within this technique, a Gaussian perturbation is applied to the dynamic stiffness matrix and to the force and displacement vectors. In their first work on this topic [46], the influence of the uncertain on elastic modulus, mass density and length cell on

longitudinal and flexural waves of simple waveguides is investigated, showing a good accordance with Monte Carlo simulations. Ben Souf et al. [54, 55] analysed uncertain coupled structures: first the effect of an uncertain Young's modulus on the forced response of two coupled Euler-Bernolli beam is analysed [54], then the variability of scattering properties in a stochastic coupling element is considered through a stochastic diffusion matrix [55], providing an expression for the uncertain coupling loss factors [80] between two deterministic waveguides.

Chronopoulos et al. [48, 53, 57] analysed the vibroacoustics of layered panels through the WFEM applied to two-dimensional waveguides. The sound transmission loss of curved composite panel is investigated [48, 57] in a SEA context by using the dispersion relations carried out through the WFEM, wherein the periodicity conditions on a four-noded plate element are imposed. Furthermore, it uses the dispersion relations to define a frequency-dependent dynamic stiffness matrix to evaluate the frequency response function of composite panels.

CONTRIBUTIONS FROM SOUTHAMPTON (UK)

Mace et al. [58] investigate the free wave propagation in simple waveguides (at the beginning the method is called waveguide-Finite Element) by using a commercial FE package for the modelling of an elementary cell. The method is formulated, providing also a description in terms of energy, power and group velocity. The dispersion curves estimated through WFEM, for a rod, a beam and a plate strip simply supported on two edges, well agree with analytical results; furthermore, the analysis of a sandwich beam highlights the high potential of this method if use in conjunction with FE software.

Duhamel et al. [59] study the formulation for calculating the forced response on a beam and on a simply supported plate using a recurrence relationship, based on the definition of propagating matrices.

Waki et al. [60, 61, 66] on the basis of previous works, perform a deep analysis on several waveguides and finite structures. In particular, firstly the flexural wave propagation in a plate strip with free boundaries is investigated, comparing the results with the analytical one [60]. Then, the forced vibration of a tyre is carried out [61], considering the tyre as a one-dimensional waveguide, uniform around the circumference. Differently by Duhamel et al. [59] and Mencik [42], the estimation of the forced response in finite structures is directly based on the wave propagation approach [81–84]. Also in this case, the use of a commercial FE package allows the modelling of the complicated cross section, involving different layer. The agreement with experimental results, completely reported in Waki's Ph. D. thesis [85] is very good. Finally, the numerical issues concerning the wave and finite element method for the analysis of one dimensional waveguide is investigate [66]. This work is the first concerning both finite element discretisation errors at low frequencies and the round-off ones in the high frequency range, providing suggestions to avoid them. The whole procedure for the evaluation of the forced response is formulated by steps. Illustrative results are presented for simply supported thin plate, highlighting the influence of the high-order wavemodes on the dynamic response.

In her Ph. D. thesis [86], Manconi is the first to formulate the Wave and Finite Element Method for the analysis of wave propagation in two-dimensional

structures, including isotropic, orthotropic and laminated plates [63, 65, 70, 71], as well as in axisymmetric structures such as curved panels, cylinders and fluid filled-pipes [62, 67–69, 79]. In particular, Mace and Manconi [63] investigate the wave propagation in plates by applying periodicity conditions to a four-noded quadrangular element, formulating the eigenvalue problems in terms of a reduced dynamic stiffness matrix. Compared to one dimensional waveguide, the eigenproblem has three parameters (the frequency and the propagation constants along the two in-plane directions), and hence the different forms of the problem are formulated. The presence of a viscoelastic material is taken into account simply supposing an hysteretic damping, i.e. by considering a complex stiffness matrix [65, 70, 71]. In the case of curved panels or cylinders [68, 69], a transformation matrix is defined into a system of cylindrical coordinates in order to express the mass and stiffness matrices of the curved elementary cell. Pre-stressed structures are investigated by calculating the effective loss factor through energy methods [79].

Renno's works focus on the analysis of the forced response of structures through the WFEM [72, 73, 77, 78] and on the calculation of reflection and transmission of joints [74, 76, 77]. On the basis of work by Waki et al. [66], Renno and Mace [72] investigate the forced response of a laminated beam, showing the good accordance with full Finite Element results. Besides these results, obtained for punctual excitation, they formulate for the first time the response of a waveguide to a convected harmonic pressure, leading to the analysis of the response to a general loading (for instance an arbitrary distributed load). This case is thus extended to homogeneous plates [73], investigate the response of a plate subject to an acoustic load, and cylinders [78]. At the same time, Renno and Mace start to investigate the scattering properties of joints between waveguides, in terms of reflection and transmission coefficients, modelling the joints through conventional FEM and the waveguides through WFEM [74, 77]. Furthermore, through consideration on the power flow between two SEA subsystems [80], reflection and transmission coefficients are used for evaluating the coupling loss factors two beams connected at a point joint [76].

2 THEORETICAL OVERVIEW

In this chapter, the theoretical fundamentals regarding the wave propagation in elastic solids are provided. The chapter starts with the definition of wave properties and parameters, introducing the dispersion relations which relate angular frequency and wavenumber. Then, the analysis of free wave propagation in infinite isotropic beam and plates is explained, remarking the several types of waves occurring. Before to introduce the propagation in finite one-dimensional structures, the difference between travelling waves and standing waves is highlighted. At the end, an introduction to the wave propagation in layered media, with particular attention to sandwich structures, is presented.

2.1 WAVES: PROPERTIES AND PARAMETERS

In general, a wave can be described as a disturbance that travels through a medium, transporting energy from one location (its source) to another location without transporting matter. A medium is intended as a material that carries the wave, and it should be considered as a collection of particles capable to interact with each other. When the wave travels in a medium, the single particles of the medium are temporarily displaced from their rest position, but there is always a force acting upon them that restore them to their original position. Hence there is not matter transportation, but only the energy is transmitted.

In order to characterise the wave motion in solid medium, the mathematical representation between time and space domains has to be explained. The basis of the representation considers the variation of a generic quantity q_i with time t and space; the simplest definitions of a one-dimensional travelling wave are in the form

$$q_1(x,t) = g(x-ct) \tag{2.1}$$

$$q_2(x,t) = f(x+ct) \tag{2.2}$$

where c is the speed of propagation of the wave, also called *phase speed*. The wave in Eq. (2.1) propagates in the positive x direction, whereas the one in Eq. (2.2) propagates in the negative direction. Since any time function can be described in the frequency domain as a superposition of harmonic components through

Fourier analysis, it is convenient to express the generic functions g and f in the form of harmonic waves:

$$g(x-ct) = \overline{g}\cos\left[\frac{2\pi}{\lambda_l}(x-ct)\right] \tag{2.3}$$

$$f(x+ct) = \overline{f}\cos\left[\frac{2\pi}{\lambda_l}(x+ct)\right] \tag{2.4}$$

where $\overline{g}$, $\overline{f}$ are the amplitudes of the waves, and λ_l is the wavelength of the wave, which indicates the spatial period of the harmonic wave. Defining the *wavenumber* k as the number of spatial wave per unit distance (i.e. the number of phase change per unit distance)

$$k = \frac{2\pi}{\lambda_l} \tag{2.5}$$

and the *circular frequency* ω as the number of phase change per unit time

$$\omega = \frac{2\pi c}{\lambda_l} = \frac{2\pi}{T}, \tag{2.6}$$

where T is the temporal period, it is possible to write the waves in usual form:

$$q_1(x,t) = \overline{g}\cos(kx-\omega t) = \mathrm{Re}\left[\overline{g}e^{i(kx-\omega t)}\right] \tag{2.7}$$

$$q_2(x,t) = \overline{f}\cos(kx+\omega t) = \mathrm{Re}\left[\overline{f}e^{i(kx+\omega t)}\right] \tag{2.8}$$

(Re indicates the real part and i is the imaginary unit).

The analogy between circular frequency ω and spatial frequency k is illustrated in Figure 2.1. Any form of spatial variation can be investigate through Fourier analysis into a spectrum of complex wavenumber components, just as any form of temporal signal can be analysed into a spectrum of complex frequency components. The relation between ω and k is defined as *dispersion relation*, depending on the type of wave, as well as the medium in which the wave travels. In particular, the waves are called *non-dispersive* if the dispersion relationship is linear, i.e. an arbitrary spatial form of disturbance is not modified during the propagation; differently, waves are named *dispersive*. Circular frequency and wavenumber are related by the phase velocity of the wave:

$$c = \frac{\omega}{k} = \frac{\lambda_l}{T}. \tag{2.9}$$

The *phase velocity of a wave* c is the rate at which the phase of the wave propagates through space. It should be not confused with the *group velocity of a wave* c_g, which is the velocity with which the overall shape of the waves' amplitudes (known as envelope of the wave) propagates through space, and it is defined as

$$c_g = \frac{\partial\omega}{\partial k}. \tag{2.10}$$

For non-dispersive wave, $c \equiv c_g$.

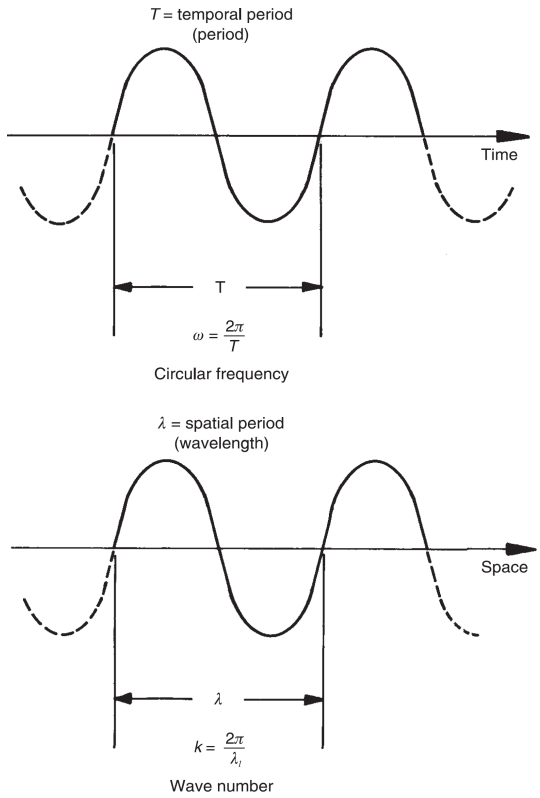

Figure 2.1: Analogy between circular frequency and wavenumber [87]

2.2 FREE WAVE PROPAGATION IN UNBOUNDED ISOTROPIC SOLIDS

The analysis of the wave propagation in unbounded media has been deeply treated in classical books [1, 2, 87, 88], wherein more details can be found. However, the goal of this section is providing to the reader all the information needed to understand the phenomena of wave propagation in waveguides. A waveguide is defined as a wave-bearing medium which extends in one (or two) of its dimensions (along which it is uniform) but confined within parallel boundaries in the other two (or one) dimensions (through which properties can vary). Therefore, bars and beams can be considered as one-dimensional waveguides since the waves travel along their longitudinal axis, whereas cylinders and plates are general examples of two-dimensional ones. However, in special special cases (i.e. simply-supported plate strip), two-dimensional structures can be assumed as one-dimensional waveguides since waves may travel in only one direction.

2.2.1 Longitudinal waves

In the case of longitudinal wave motion, classical books [2, 87] distinguish the pure longitudinal motion and the quasi-longitudinal motion.

By definition, in pure longitudinal wave motion, the direction of particle displacement is purely in the direction of wave propagation, causing a change in volume. The motion can be displayed by considering the motion of two planes, separated by a small distance δx, parallel to each other and perpendicular to the direction of propagation. In pure longitudinal motion, these planes exhibit absolute displacements from their position of equilibrium and their relative distance also change, as shown in Figure 2.2. The element may undergo a strain $\epsilon_{xx} = \partial\xi/\partial x$, where ξ is the displacement of the parallel planes in the x direction. According to Hooke's law, the longitudinal stress σ_{xx} is proportional to ϵ_{xx}.

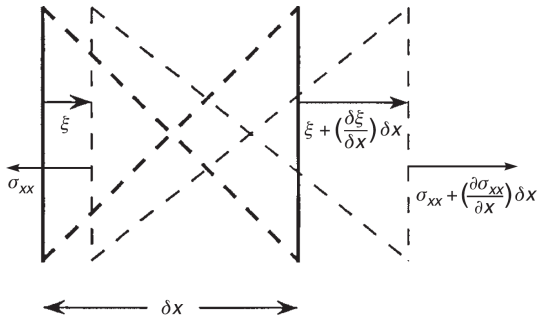

Figure 2.2: Displacements from equilibrium and stresses in a pure longitudinal wave [87]

In pure longitudinal motion, there can be no lateral strain and hence Poisson's contraction can be no allowed. In fact, this constraint, applied mutually by adjacent elements, creates lateral direct stress which determines that the constant of proportionality between longitudinal stress is not the Young's modulus of the material, but the bulk modulus B (which takes into account the constraint of the lateral motion [2]). The stress-strain relation for pure-longitudinal motion can be expressed as

$$\sigma_{xx} = B\frac{\partial\xi}{\partial x} = \frac{E(1-\nu)}{(1+\nu)(1-2\nu)}\frac{\partial\xi}{\partial x}, \tag{2.11}$$

where E is the Young's modulus and ν is the Poisson's ratio. The equation of motion of the element shown in Figure 2.2 is [18]

$$(\rho\delta x)\frac{\partial^2\xi}{\partial t^2} = \frac{\partial\sigma_{xx}}{\partial x}\delta x, \tag{2.12}$$

where ρ is the density of the material. Substituting Eq. (2.11) in Eq. (2.12), the wave equation for pure longitudinal waves is obtained:

$$\left(\frac{\rho}{B}\right)\frac{\partial^2\xi}{\partial t^2} = \frac{\partial^2\xi}{\partial x^2}. \tag{2.13}$$

Eq. (2.13) resembles the classical wave equation, and hence the ratio

$$c_l = \sqrt{B/\rho} \tag{2.14}$$

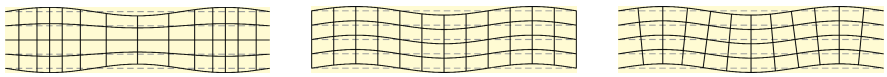

(a) *quasi-longitudinal* **(b)** *shear* **(c)** *bending*

Figure 2.3: Waves in beams [89]

represents the wave speed (i.e. the phase speed) of the longitudinal waves. It is worth to notice that, as highlighted by Fahy and Gardonio [87], this kind of motion can exist only in solid that extends in all directions to distance large compared to the wavelength. Known the phase velocity, it is possible to calculate the longitudinal wavenumber (according to Eq. (2.9)) as

$$k_l = \frac{\omega}{c_l}. \tag{2.15}$$

The proportional relation between circular frequency and wavenumber indicates that longitudinal waves are non-dispersive.

Quasi-longitudinal waves differ from the pure-longitudinal one because lateral stresses are not constrained. In the case of a bar, the cross-section dimensions can be comparable to the wavelength and the Poisson contraction must be included. In this case, the proportional relationship between longitudinal stress and strain in a bar is expressed by the Young's modulus E, and hence the phase speed velocity is

$$c_l'' = \sqrt{\frac{E}{\rho}}. \tag{2.16}$$

In the case of a plate, the in-plane dimensions can be assumed large compared to the wavelength: the phase velocity lies between the case of constrained media and the case of a bar. In fact, it can be expressed as [2]:

$$c_l' = \sqrt{\frac{E}{(1-\nu^2)\rho}}. \tag{2.17}$$

Note that the relation between the phase speed velocity above defined is $c_l < c_l' < c_l''$.

2.2.2 Transverse waves

A transverse wave is characterised by the motion of the particles of the medium in a direction perpendicular to the direction of energy transport, which causes a change in shape. The resistance in changing in shape comes about because a solid can support tangential stresses on any cutting plane, unlike a liquid or a gas. Because these tangential stresses oppose shearing displacements parallel to the cutting plane, they are called also shear stresses [2]. Considering again two planes, a distance δx apart, delimiting a rectangular element. Under the passing of a transverse wave, the transverse displacements of the two planes

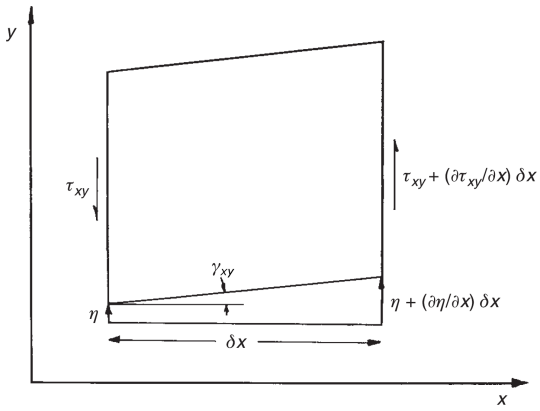

Figure 2.4: Displacements, shear strain and transverse shear stresses in transverse deformation [87]

differ by $\partial\eta/\partial x\delta x$, leading to the distortion of the rectangle into a parallelogram, as shown in Figure 2.4. The difference in vertical shear stresses causes the vertical acceleration $\partial^2\eta/\partial t^2$ of he element. The equation of the transverse motion, hence, results in

$$\rho\delta x\delta y\frac{\partial^2\eta}{\partial t^2} = \frac{\partial\tau_{xy}}{\partial x}\delta x\delta y \tag{2.18}$$

where τ_{xy} is the shear stress (the first subscript indicates the axis normal to the plane on which the stress acts, and the second indicates the direction of the stress). The stress-strain relationship is

$$\tau_{xy} = G\gamma_{xy} = G\frac{\partial\eta}{\partial x} \tag{2.19}$$

where γ_{xy} is the strain and G is the shear moduli ($G = E\ [2(1+\nu)]$). Thus the wave equation is

$$\frac{\rho}{G}\frac{\partial^2\eta}{\partial t^2} = \frac{\partial^2\eta}{\partial x^2}, \tag{2.20}$$

in which the phase velocity of the shear wave can be defined as

$$c_s = \sqrt{\frac{G}{\rho}} = \sqrt{\frac{E}{2\rho(1+\nu)}} \tag{2.21}$$

The following relations hold between shear and longitudinal phase velocities:

$$\frac{c_s}{c_l} = \sqrt{\frac{G}{B}} = \sqrt{\frac{1-2\nu}{2(1-\nu)}} \tag{2.22}$$

$$\frac{c_s}{c_l'} = \sqrt{\frac{G(1-\nu^2)}{E}} = \sqrt{\frac{1-\nu}{2}} \tag{2.23}$$

$$\frac{c_s}{c_l''} = \sqrt{\frac{G}{E}} = \sqrt{\frac{1}{2(1+\nu)}} \tag{2.24}$$

$$\tag{2.25}$$

The shear waves, similarly to the longitudinal ones, are non-dispersive.

Besides shear waves, also torsional waves in solid bars can be defined as transverse ones. In this case, the wave equation is [87]

$$\frac{\partial^2\theta}{\partial t^2} = \frac{GJ}{I_p}\frac{\partial^2\theta}{\partial x^2}, \tag{2.26}$$

where θ and I_p are, respectively, the rotation and the polar moment of inertia per unit length of the bar about its longitudinal axis; GJ is the torsional stiffness of the bar, depending on its cross-sectional shape. The phase velocity of torsional waves hence is

$$c_t = \sqrt{\frac{GJ}{I_p}} \tag{2.27}$$

and it approaches to the shear phase velocity for rotationally symmetric cross-sections. More details can be found in the book by Cremer et al. [2].

2.2.3 Flexural waves

Flexural waves involve both transverse and in-plane displacements: because of the large transverse deflection, one might think to include them into the class of transverse waves, but this would be wrong. In fact, stresses and strains act in the longitudinal direction, and the governing wave equation is completely different. The equation of bending wave is firstly obtained for a beam, and then for a plate.

2.2.3.1 *Beams*

It is calculated by imposing the equilibrium of a small element, undergoing to flexural wave. The primary assumption of pure bending theory is that plane cross sections remain plane during bending deformation of the element, according to the Kirchoff assumption. In this case, the in-plane displacements can be expressed as

$$\xi(x, y, t) = \xi(x, t) - y\beta(x, t) \tag{2.28}$$

$$\eta(x, y, t) = \eta(x, t) \tag{2.29}$$

where β is the in-plane rotation of the cross-section, whereas $\xi(x, t)$ and $\eta(x, t)$ are the displacements of the particle on the neutral axis ($y = 0$). Being $\epsilon_{xx} = \partial\xi/\partial x$, the strain distribution over the cross-section is

$$\epsilon_{xx} = \frac{\partial\xi}{\partial x} - z\frac{\partial\beta}{\partial x}. \tag{2.30}$$

The bending moment acting on the cross section can be expressed by employing the stress-strain relation as

$$M(x, t) = \int_A \sigma_{xx}(x, y, t) y dA = -EI\frac{\partial\beta}{\partial x} = -EI\frac{\partial^2\eta}{\partial x^2}, \tag{2.31}$$

being $\partial\beta/\partial x = \partial^2\eta/\partial x^2$. Similarly, the shear force acting on the cross section is

$$S(x,t) = \int_A \tau_{xy}(x,y,t)\,dA. \tag{2.32}$$

From the equation of motion in the transverse direction, it is obtained:

$$\frac{\partial S}{\partial x} = \rho A \frac{\partial^2 \eta}{\partial t^2}. \tag{2.33}$$

In the same way, imposing the moment equilibrium about the neutral axis of the cross-section, it can be written:

$$S = \frac{\partial M}{\partial x} + I\rho \frac{\partial^2 \beta}{\partial t^2}, \tag{2.34}$$

where I is the second moment of area of the section.

In conclusion, introducing Eq. (2.34) in Eq. (2.33), and considering the stress-strain (Eq. (2.30)) and the bending moment-curvature relations (Eq. (2.31)), leads to the following equation in terms of transverse displacements and in-plane rotation:

$$\frac{\partial^2}{\partial x^2}\left(EI\frac{\partial \beta}{\partial x}\right) + \rho A \frac{\partial^2 \eta}{\partial t^2} - \frac{\partial}{\partial x}\left(\rho I \frac{\partial^2 \beta}{\partial t^2}\right) = 0. \tag{2.35}$$

This equation can be simplified by employing different beam theories.

If Euler-Bernoulli beam theory is applied, the effects of rotary inertia (the third term on left-hand side) are negligible compared with those of the linear inertia, as well as the deformations associated with transverse shear. It is also assumed that deflections are small, leading to

$$\beta \cong \frac{\partial \eta}{\partial x}. \tag{2.36}$$

This assumption yield to the Euler-Bernoulli beam equation:

$$\frac{\partial^2}{\partial x^2}\left(EI\frac{\partial \beta}{\partial x}\right) + \rho A \frac{\partial^2 \eta}{\partial t^2} = 0. \tag{2.37}$$

which can be rewritten as

$$\frac{EI}{\rho A}\frac{\partial^4 \eta}{\partial x^4} = -\frac{\partial^2 \eta}{\partial t^2}. \tag{2.38}$$

This equation differs from those governing the previously considered forms of wave motion in that the spatial derivative is of fourth, and not second, order: the reason is that the bending wave is a hybrid between shear and longitudinal waves [87]. Fourier analysis is applicable such that any time dependence can be decomposed in pure tonal components and the propagation of those temporally sinusoidal components investigated. Substituting in Eq. (2.38) of the complex exponential expression for a harmonic waves in the form

$$\eta(x,t) = \overline{\eta} e^{i(kx-\omega t)}, \tag{2.39}$$

yields

$$k^4 = \frac{\rho A}{EI}\omega^2. \tag{2.40}$$

The wavenumbers solution of Eq. (2.40) are

$$k_e = \pm i k_b \tag{2.41}$$

$$k_p = \pm k_b \tag{2.42}$$

where k_b is the bending wavenumber

$$k_b = \sqrt[4]{\frac{\rho A}{EI}\omega^2} = \sqrt{\omega}\sqrt[4]{\frac{\rho A}{EI}} \tag{2.43}$$

The dependence of the wavenumber from the circular frequency indicates that flexural waves are dispersive. In Eq. (2.41), k_e wavenumbers are related to evanescent (near-field) waves, whose amplitudes decay exponentially with distance. On the other hand, k_p is associated to propagating (far-field) waves. The sign of the wavenumber is related to the direction (positive or negative) of the propagation. In terms of wave velocity, being in general the phase velocity $c = \omega/k$ and the group velocity $c_g = \partial\omega/\partial k$, it results:

$$c_b = \frac{\omega}{k_b} = \sqrt{\omega}\sqrt[4]{\frac{EI}{\rho A}} \tag{2.44}$$

$$c_{b_g} = 2c_b \tag{2.45}$$

When flexural wavelengths become short with respect to the beam thickness, shear deformation and rotary mass inertia become important, and hence the Euler-Bernoulli model is no longer valid. In this case, higher order theories must be employed, such as Rayleigh or Timoshenko beam ones [1, 88, 90]. Their derivation is beyond the scope of this thesis and can be found in classical books. According to the Timoshenko model, the wave equation for thick beam is [89]:

$$\frac{EI}{\rho A}\frac{\partial^4\eta}{\partial x^4} - \left(\frac{I}{A} + \frac{EI}{KAG}\right)\frac{\partial^2}{\partial x^2}\left(\frac{\partial^2\eta}{\partial t^2}\right) = -\frac{\partial^2\eta}{\partial t^2} - \frac{I\rho}{KAG}\frac{\partial^4\eta}{\partial t^4} \tag{2.46}$$

where G is the shear modulus and K is known as the Timoshenko shear coefficient. The phase velocity is again calculated by considering an harmonic wave, yielding

$$c_b = \sqrt{\frac{\sqrt{\left(\frac{EI}{KAG} - \frac{I}{A}\right)^2\omega^4 + 4\frac{EI}{\rho A}\omega^2} - \omega^2\left(\frac{EI}{KAG} + \frac{I}{A}\right)}{2\left(1 - \omega^2\frac{I\rho}{KAG}\right)}} \tag{2.47}$$

This expression is much more complicated of that obtained through Euler-Bernoulli theory. However, when shear resistance and rotary inertia are negligible (i.e. waves with long wavelengths with respect to thickness), the wave equation and

wave speed reduce to the simpler Euler-Bernoulli forms. Since long wavelengths imply low frequencies, thin beam theory is sometimes called a low frequency limit of the general thick beam theory. For very high frequencies, the shear resistance terms become dominant, so that the flexural wave equation simplifies to the shear wave equation, and the bending wave speed approaches the shear wave speed, with the only difference of the presence of the shear correction factor for finite structure.

2.2.3.2 *Plates*

Similarly to the beams, wave equation can be easily derived in the hypothesis of thin plate (i.e. thickness of the plate smaller than the minimum flexural wavelength), considering the assumption made by Kirchoff-Love for the plate. The procedure is quite the same as for the beam, and it is here omitted for sake of brevity and it can be found in several classic books [2, 91]. At the end, the wave equation for a plate element lying in the x-z plane is the classical equation of free vibration of a plate [92]:

$$D\nabla^4\eta + \rho h\frac{\partial^2\eta}{\partial t^2} = 0 \tag{2.48}$$

where

- $\nabla^4 = \nabla^2\nabla^2$ is the biharmonic differential operator, with $\nabla^2 = \partial^2/\partial x^2 + \partial^2/\partial z^2$;
- h is the thickness of the plate;
- D is the bending stiffness, or flexural rigidity, defined as

$$D = \frac{Eh^3}{12(1-\nu^2)}. \tag{2.49}$$

Explicitly specifying the biharmonic differential operator, Eq. (2.48) becomes

$$\frac{Eh^3}{12(1-\nu^2)}\left(\frac{\partial^4\eta}{\partial x^4} + 2\frac{\partial^4\eta}{\partial x^2\partial z^2} + \frac{\partial^4\eta}{\partial z^4}\right) = -\rho h\frac{\partial^2\eta}{\partial t^2}. \tag{2.50}$$

As done for the beam, consider a plane bending wave, propagating in any direction of the plane of the plate, and described by

$$\eta(x,z,t) = \overline{\eta}e^{i(\omega t - k_x x - k_z z)}. \tag{2.51}$$

(A certain disturbance propagates as a plane wave if its magnitude is constant along planes perpendicular to the direction of propagation.) Substitution in Eq. (2.50) leads to:

$$\left[\frac{Eh^3}{12(1-\nu^2)}\left(k_x^4 + 2k_x^2k_z^2 + k_z^4\right) - \rho h\omega^2\right]\overline{\eta} = 0 \tag{2.52}$$

$$\frac{Eh^3}{12(1-\nu^2)}\left(k_x^2 + k_z^2\right)^2 - \rho h\omega^2 = 0 \tag{2.53}$$

$$\frac{Eh^3}{12(1-\nu^2)}k_b^4 - \rho h\omega^2 = 0, \tag{2.54}$$

where the last relation is possible by considering $k_b^2 = k_x^2 + k_z^2$. Eq. (2.54) is the plane bending-wave equation for a wave travelling in the direction at angle $\theta = \arctan(k_z/k_x)$ to the x axis, i.e. the direction given by the vector sum of the wavenumber vector components $\mathbf{k}_x$ and $\mathbf{k}_z$. In Figure 2.5, plane waves, propagating in x-z plane, with different wave components are shown. In particular, in Figure 2.5a the wave propagates only in x direction, without amplitude variation along the z-axis, and hence the wave has only $\mathbf{k}_x$ vector component; instead, in Figure 2.5b the wave propagates in both x and z directions, with an angle $\theta = 19°$ respect to the x-axis.

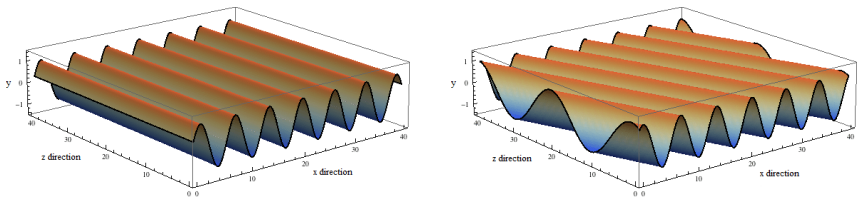

(a) $\theta = 0°$ **(b)** $\theta = 19°$

Figure 2.5: Plane waves with different wave components (images courtesy of Dr. Dan Russell [93])

In conclusion, a bending wavenumber vector can be defined by summing the vector $\mathbf{k}_b = \mathbf{k}_x + \mathbf{k}_z$, whose amplitude is the bending wavenumber

$$k_b = \sqrt{\omega}\sqrt[4]{\frac{12\rho(1-\nu^2)}{Eh^2}}. \tag{2.55}$$

Again, the phase speed velocity is

$$c_b = \frac{\omega}{k_b} = \sqrt{\omega}\sqrt[4]{\frac{Eh^2}{12\rho(1-\nu^2)}}. \tag{2.56}$$

As in the case of the beam, the phase speed velocity calculated for thin plate constitutes the low frequencies limit for the phase speed velocity calculated for thick beam, referring to Mindlin theory [94, 95], which can be expressed as [89]:

$$c_b = \sqrt{\frac{\sqrt{\left(\frac{D}{KhG} - \frac{h^2}{12}\right)^2 \omega^4 + 4\frac{D}{\rho h}\omega^2} - \omega^2\left(\frac{D}{KhG} + \frac{h^2}{12}\right)}{2\left(1 - \omega^2\frac{h^2\rho}{12KG}\right)}}. \tag{2.57}$$

At high frequencies, flexural waves in plates approach pure shear waves too.

2.2.4 Dispersion curves

In the previous sections, the dispersion relations for the three basic waves propagating in beams and plates are summarised. Usually, these relations are plotted,

in terms of k *vs.* f, c *vs.* f or c_g *vs.* f. This type of information is particularly useful in structure-acoustic problems, since it is fundamental recognizing the frequency, called critical, at which the flexural and the acoustic wavenumber are equal [2, 87]. Furthermore, dispersion curves are widely used also in the field of structural health monitoring (SHM), since the variation of wave speeds (compared to the initial configuration of the structure) might be due to a damage in the structure [91].

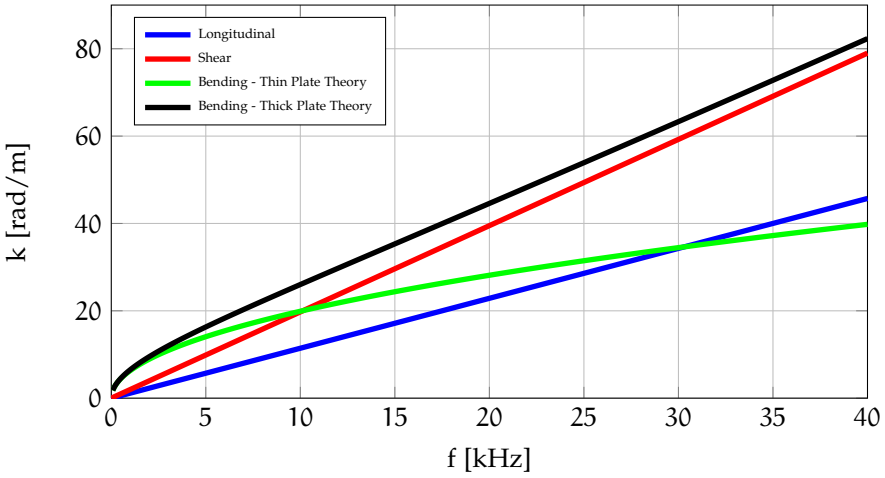

(a) *Wavenumber*

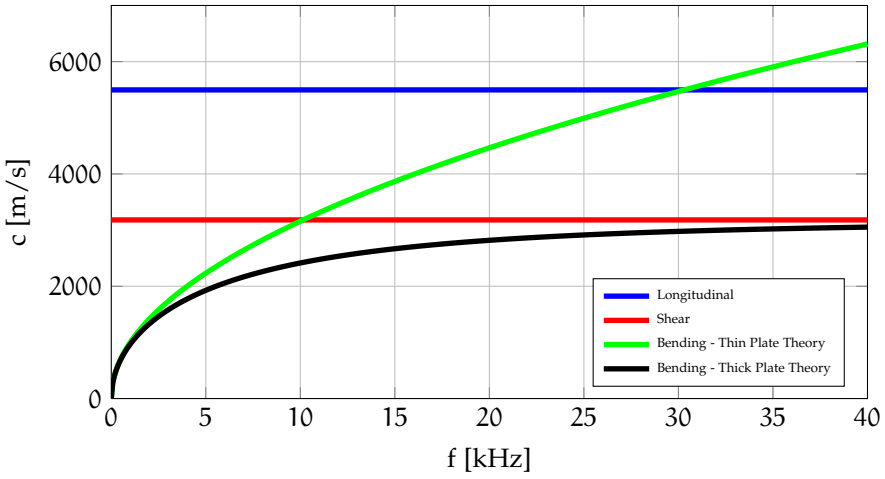

(b) *Phase velocity*

Figure 2.6: Dispersion relations for a steel plate 0.1 m thick

In Figure 2.6, the wavenumbers and the phase velocities of a steel plate 0.1 m thick are plotted against the frequency, according to the previous relations. As can be seen, the thin plate phase velocity becomes invalid at high frequencies, where rotary inertia and shear resistance are important; furthermore, at high frequencies the thick plate phase velocity approach the shear one.

2.2.5 Rayleigh and Lamb waves

Among the aforementioned waves, it seems that flexural waves is a combination of shear and longitudinal ones. Actually, other types of waves are obtained as sum of these two waves, mostly when the frequency increases and waves may propagate through the thickness too (i.e. the minimum wavelength is shorter than the minimum dimensions of the waveguide). In this case, waves propagate freely in all directions, and hence three-dimensional elasticity should be used.

It is proved [91] that any wave is the combination of:

- a *pressure wave* (or *compressional*, *axial*, *dilatational*, *longitudinal*, or *P-wave*), in which the particle motion is parallel to direction of wave propagation;
- two shear waves (or *transverse*, *distortional*, *S-waves*), in which the particle motion is perpendicular to the direction of wave propagation. These two waves travel with the same wave speed, expressed by Eq. (2.21), but they act in two perpendicular planes, being indicated as shear-horizontal (*SH-wave*) and shear-vertical (*SV-wave*) waves.

At this point, it can be useful to introduce new types of waves, Rayleigh and Lamb waves, belonging to the class of guided waves, used in SHM application. They are deeply described by Giurgiutiu [91].

Rayleigh waves, also called surface acoustic wave (SAW), are found in solids containing a free surface (e.g. the sea-waves). They travel close to the free surface with a little penetration in the depth of the solid (less than a wavelength), and they are mathematically obtained as a combination P and SV waves. The motion of particle of a Rayleigh wave is shown in Figure 2.7.

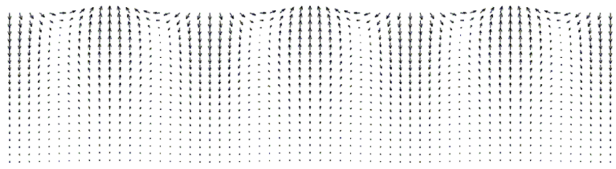

Figure 2.7: Rayleigh wave (SAW) [91]

Lamb wave, instead, are ultrasonic waves guided between two parallel free surfaces (i.e. upper and lower surfaces of a plate), and they are mathematically obtained as the simultaneously existence of P and SV waves. This type of guided waves are the most common used in SHM application. Two basic type of Lamb waves exist: symmetric (indicated with S_j) and antisymmetric (indicated with A_j) Lamb-waves modes, where the subscript indicates the order of the wave. Both types of Lamb wave are dispersive. The symmetric Lamb waves (Figure 2.8a) resembles the quasi-longitudinal one described above, whereas the antisymmetric ones (Figure 2.8b) are similar to the flexural ones. At lower frequencies, only the basic Lamb waves S_0 and A_0 exist, and they approach respectively the longitudinal and the flexural behaviour of a plate. At higher frequencies, instead, other Lamb waves propagates, and the basic S_0 and A_0 approach the Rayleigh wave confined to the plate surface. The trend of basic Lamb waves dispersion curves is

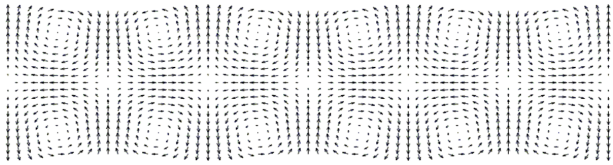

(a) *symmetric* S_0

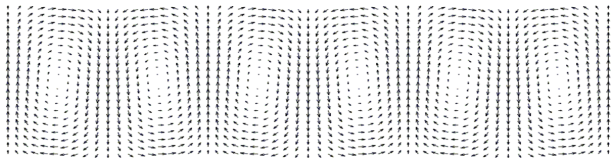

(b) *antisymmetric* A_0

Figure 2.8: Lamb waves [91]

shown in Figure 2.9, in which the wave speed dispersion curves obtained for an aluminium plate 1mm thick are reported.

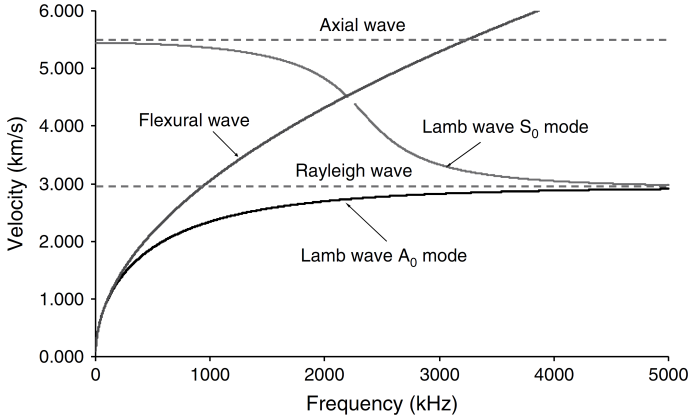

Figure 2.9: Wave speed dispersion curves for an aluminium plate 1 mm thick [91]

2.3 TRAVELLING WAVES, STANDING WAVES AND WAVES SUPERPOSITION

In order to investigate the forced response in finite structures through the wave approach, it is needed to introduce the concept of standing waves. The waves introduced so far are *travelling waves* since the wavefronts move in uninterrupted manner along the waveguide.

If two or more travelling waves propagate through a medium at the same time, the superposition principle may be applied to calculate the wave sum: the net displacement of the medium at any point in space or time is simply the sum of the individual wave displacement.

Now, let's consider a medium in which two sinusoidal waves y_1 and y_2, having the same frequency ω, wavelength k and amplitude $\overline{y}$, are travelling in opposite direction. The wave sum, y, can be expressed as:

$$y(x,t) = y_1(x,t) + y_2(x,t) = \overline{y}\cos(kx - \omega t) + \overline{y}\cos(kx + \omega t) = 2\overline{y}\cos(kx)\cos(\omega t). \tag{2.58}$$

It results that when the two waves are 180° out of phase with each other they cancel, whereas when they are exactly in phase with each other they add together. Hence, the net result alternates between location with zero displacements (*nodes*) and location with maximum displacements (*antinode*): this wave pattern oscillates in the time, but it does not travel to the left or the right, and hence it is called *standing wave*. From the mathematical point of view, this wave is no longer a travelling wave because the position and time dependence are separated in Eq. (2.58). In Figure 2.10, the standing wave pattern in three different times is shown.

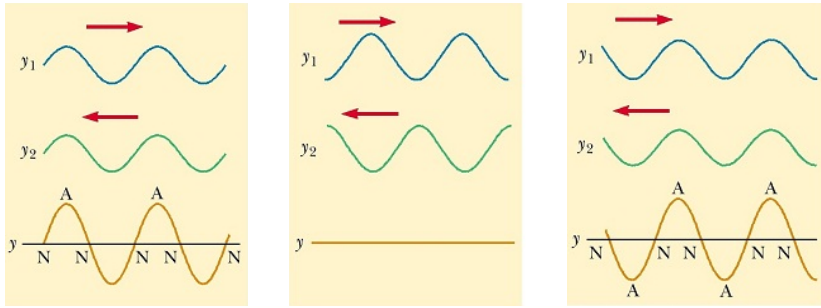

(a) $t = 0$ (b) $t = T/4$ (c) $t = T/2$

Figure 2.10: Standing wave pattern in three different times by two waves of equal amplitude traveling in opposite directions. N are nodes, A are antinodes

2.4 WAVES IN ONE-DIMENSIONAL FINITE STRUCTURES

Up to now, the wave propagation in infinite uniform waveguide has been investigated. However, physical structures are spatially limited by boundaries, which determine a changing in the wave, due to phenomena such as reflection, diffraction, refraction and scattering. In the analysis of the vibrational behaviour of structures, the reflection of the wave at the boundaries, as well as the refraction through the interface between two different media, are the most important aspects to be considered [2, 87]. In next chapter, the dynamic response of uniform finite beams is investigated, without take into account a possible variation of the properties of the structure along the longitudinal axis, i.e. no refraction occurs. On the other hand, the presence of elastic boundaries at the edge of the structure determines the reflection of the wave, which is here investigated.

The change in amplitude and phase of a reflected wave, compared to the incident one, depends on the type of constraint. Compatibility of displacement and equilibrium of forces must be satisfied at the constraint. Let's consider, for sake of simplicity, a bending positive-going wave travelling through an undamped semi-infinite beam, terminated by a simple support (Figure 2.11a) [87]. The incident wave displacement is

$$\eta_i^+(x,t) = \overline{\eta}_i e^{-ik_b x} e^{i\omega t} \tag{2.59}$$

The presence of the simple support suppresses transverse displacement and produce shear force reaction, without restriction of rotational displacement because it is not able to produce any moment reaction. The incident wave alone cannot satisfy the condition of zero transverse displacements at the support all the times. The incident wave, hence, determine negative-going propagating and near-field reflected waves, which together make it possible to satisfy the boundary conditions (Figure 2.11b). The solution of the Euler-Bernoulli beam equation Eq. (2.40), taking into account both propagating and evanescent components of the negative-going wave, is in the form

$$\eta_r^-(x,t) = \left[\overline{\eta}_{r_p} e^{ik_b x} + \overline{\eta}_{r_e} e^{k_b x}\right] e^{i\omega t} \tag{2.60}$$

The two unknowns $\overline{\eta}_{r_p}$ and $\overline{\eta}_{r_e}$ can be easily derived by applying the compatibility and equilibrium at the simple support, considering that there is no wave transmission [87]. In particular, it results

$$\overline{\eta}_{r_p} = \overline{\eta}_i; \qquad \overline{\eta}_{r_e} = 0 \tag{2.61}$$

Simply supports, hence, provide only the reflection of propagating waves, with zero near-field waves. This is not true for free ends or fully clamped support [96]. In conclusion, the beam displacement may be expressed as sum of the incident and the reflected waves (Figure 2.11c):

$$\eta(x,t) = \overline{\eta}_i \left[e^{-ik_b x} - e^{ik_b x}\right] e^{i\omega t} \tag{2.62}$$

The displacement fields of the incident, reflected and sum wave are shown in Figure 2.11. It is clear that the sum wave pattern has the form of a standing wave, in which spatial and temporal variations of displacement are independent.

If the beam is of finite length, the analysis of the free wave propagation leads to the determination of the natural modes of vibration of the structure. The analysis of free wave propagation in finite structure, the determination of vibration mode is based on the phase closure principle [97], which provides the condition for a propagating wave to formulate a standing wave. The principle states that, in order to give rise to a standing wave (i.e. a vibration mode), a propagating wave must return to its starting point after completing one complete circuit of the system with the same amplitude and phase, i.e. it close on itself [96]. Let's consider a finite beam, simply supported on both ends, through which a wave with a given wavenumber is travelling in the positive direction after reflection on left support (Figure 2.12a): this wave is incident upon the right support and, as in the case of semi-infinite beam, is reflected with a change in phase equal to π (Figure 2.12b).

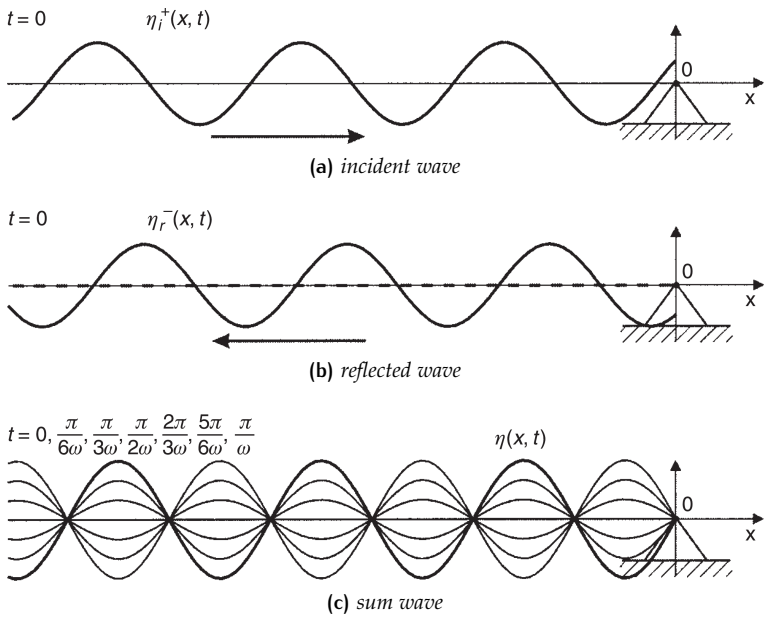

Figure 2.11: Wave fields generated in a simply supported semi-infinite beam (Faint solid line: propagating incident and reflected wave components; dashed line: near-field reflected wave component; thick solid line: sum wave (propagating + near-field) [87]

This reflected wave is negative-going, therefore it is reflected again on the left support, returning along the path of the original wave (Figure 2.12c). The relative phase in change between the original wave and the returning one depends on the free wavenumber and the length of the beam. In order to have phase coincidence, and hence phase closure, it is required that the phase change over one return journey is equal to $2\pi n$, with n integer number. Since the wavenumber is defined as the phase change per unit length, phase coincidence occurs when [87]

$$k_b(2l) = n(2\pi) \Longrightarrow k_b = \frac{n\pi}{l} \tag{2.63}$$

($2l$ is the total length through which the wave travels). When phase coincidence happen, a pure standing wave fields exists in the finite structure, and the frequencies at which phase coincidence occurs are called *natural or characteristics frequencies of the structure*. The corresponding spatial distributions of vibration amplitudes are known as *natural modes of the structure*. In the case of bending waves, substituting the expression of the bending wavenumber (Eq. (2.43)) in Eq. (2.63) yields

$$\omega = \frac{n^2\pi^2}{l^2}\sqrt{\frac{EI}{\rho A}}. \tag{2.64}$$

An example of phase coincidence is shown in Figure 2.12 for $k_b l = 5\pi$. Natural frequencies depend only on the material properties and geometrical attributes of the beam and play a fundamental role within the analysis dynamic response of a

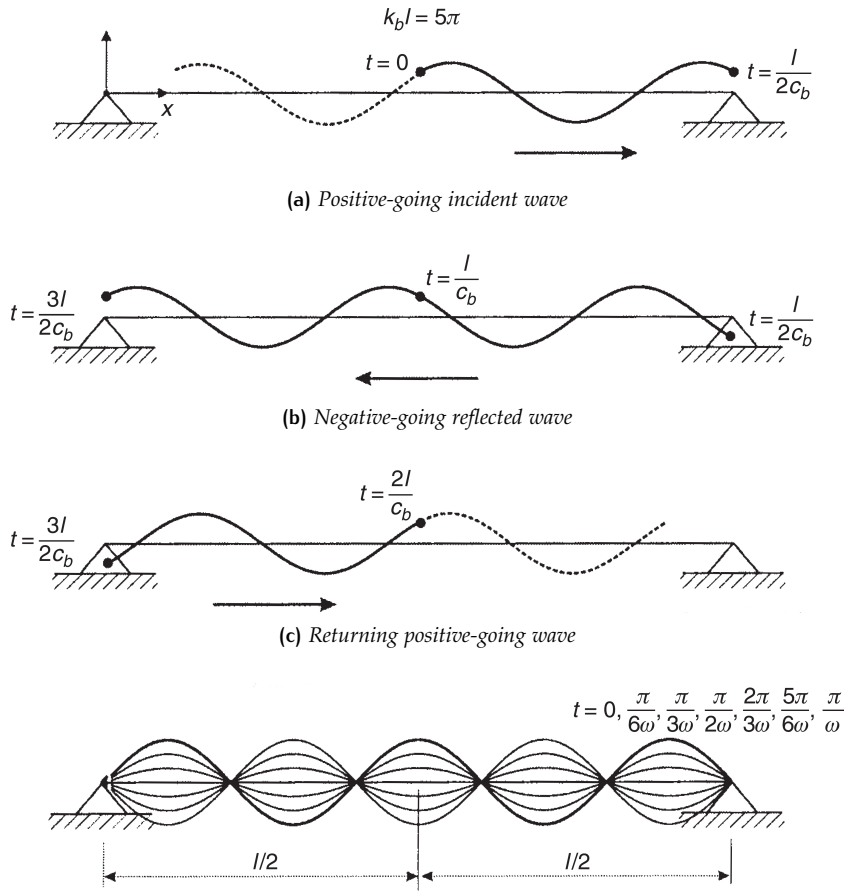

Figure 2.12: Wave fields generated in a finite beam simply supported on both edges for $k_b l = 5\pi$ (bullet dots represents the wave fronts) [87]

system. In absence of damping, natural frequencies coincide with resonant ones, and hence if the system is excited with a small amplitude harmonic force with an angular frequency equal to a natural frequency of the system, this last exhibits a very large response (theoretically infinite). In the case the system is excited by an impulsive force, having an infinite frequency content, the Frequency Response Function (FRF) of the system presents peaks in correspondence of all natural frequencies [98].

Fahy and Gardonio [87] deeply describe the evaluation of the forced response of a beam, based on the wave propagation approach. The calculation is based on the application of the propagation laws to the waves directly excited by an harmonic force acting on the structure, obviously taking into account the effect of the constraints at the boundary. Since propagation laws and boundary effects

have been previously treated, let's consider the effect of a harmonic force onto an infinite beam in terms of waves. Th equation of free motion in undamped beam

$$EI\frac{\partial^4\eta}{\partial x^4} + \rho A\frac{\partial^2\eta}{\partial t^2} = 0 \tag{2.65}$$

applies to all points of the beam not subject to external forces. Suppose that a harmonic point force acts in $x = 0$: in this case, the equation of motion in this point is

$$EI\frac{\partial^4\eta}{\partial x^4} + \rho A\frac{\partial^2\eta}{\partial t^2} = F_0\delta(x-0)e^{i\omega t} \tag{2.66}$$

(where $\delta(x-0)$ id the Dirac delta function). The two equation of motion are equivalent at each point, except at the driving point, where the force is applied. The complex solution, again, contains both positive and negative going waves, but at $x = 0$ the wave amplitude must satisfy the conditions of equilibrium in order to take into account the effect of the force. By imposing these conditions [87], the complex transverse displacements generated by the complex point force are

$$\eta(x,t) = \begin{cases} -\dfrac{jF_0}{4EIk_b^3}\left[e^{-ik_b x} - ie^{-k_b x}\right]e^{-i\omega t} & \text{if } x > 0 \\ -\dfrac{jF_0}{4EIk_b^3}\left[e^{ik_b x} - ie^{k_b x}\right]e^{-i\omega t} & \text{if } x < 0 \end{cases} \tag{2.67}$$

and the time dependence of the vibration field is shown in Figure 2.13. If the beam is terminated by constraints, then the positive and negative going waves interact at the boundary according to the relations previously investigated.

2.5 WAVE PROPAGATION IN LAYERED MEDIA

Layered media are obtained by superposing layers made by different material and/or with different orientation. This is usually made in order to obtain a media with improved mechanical properties (compared to those of the individual components). The analysis of wave propagation in layered media is much more complicated compared to isotropic ones, mostly at high frequencies: when the wavelength becomes of the same order of magnitude of the layers thickness, repeated reflections and refractions between the layers occur [99, 100]. For this reason, the analytical theory employed to model the layered media should be chosen accurately, depending on the frequency range of interest.

For what concerns laminated composite plates, the Equivalent Single Layer (ESL) theories, within the composite is homogenised, are extension into composite field of theories dedicate to isotropic material. Basically, the most used methods belonging to this class are:

- the Classical Laminate Plate Theory (CLPT) [101], which is an extension of the Kirchoff-Love theory;

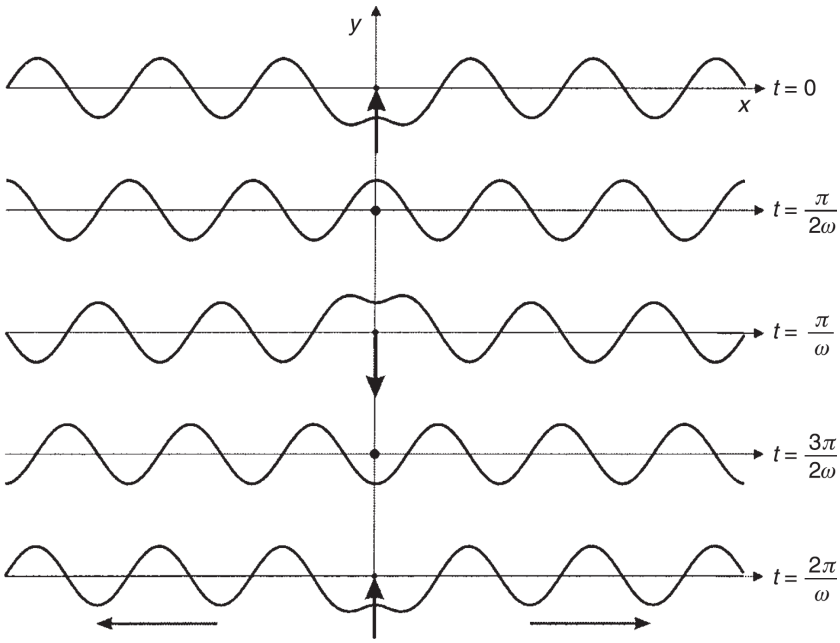

Figure 2.13: Bending vibration field generated by a harmonic point force acting on an infinite beam [87]

- the First order Shear Deformation Theory (FSDT) [102], which revise the basic assumptions of the first order theory proposed by Mindlin, and hence it takes into account deformations associated with transverse shear and rotational inertia of the cross section.

Both theories are suitable for analysing very thin plate in the low frequency range. For thick layered plates and/or for high frequencies, high-order theories lead to better results than ESL theories, as demonstrated by Carrera [103]. For instance, Layer-Wise (LW) theory [11, 104] removes the homogenisation of the laminate by considering each layer independently, leading on the other hand to an increased computational effort.

Even more refined models are required for sandwich panel. In fact, a sandwich panel is a layered structure, constituted by two relatively thin and stiff face sheets enclosing a low-density, thick and soft core. In this case, the shear deformation within the core must be taken into account, and hence Higher order Shear Deformation Theories (HSDT) are required [11, 105, 106]. However, the analysis of wave propagation in sandwich structures has been widely investigated, mostly for their vibroacoustic characterisation [107]. In fact, sandwich panels have lower sound transmission loss than homogeneous traditional panels with similar stiffness because of their lower weight. Furthermore, sandwich structures are strongly characterised by the coexistence of both anti-symmetric and symmetric (or dilatational) wave modes, also at low frequencies, which determines the presence of two coincident frequencies. (The coincidence frequency, in general, is defined as the frequency at which the bending wavelength λ_b in

the structure equals the wavelength of the acoustic wave λ_a of the surrounding air. At this frequency, the structure is transparent to the incident acoustic wave.)

The first study concerning the vibroacoustics of sandwich was made by Kurtze and Watters [6] who developed the so-called *Shear Wall* in 1959. In their work, the possibility to shift the coincidence frequency out of the range of interest is investigated, in order to avoid the dip in the transmission loss curve and to extend the validity of the mass law [2, 107]. The developed theoretical model assumes that face sheets respond as thin elementary plates in bending, whereas the core acts simply as an incompressible spacer and the dilatational motion is not considered. Shear effects are included in the core. The analysis of propagation speed of both flexural and shear waves suggests that the use of an incompressible, soft in shear core can favour the propagation of shear rather than bending waves in sandwich panel, increasing the coincidence frequency: the behaviour of the sandwich panel gradually transforms from a global bending (the whole panel) to a local one (the single face sheets) when the core is subjected to pure shear. An update of Kurtze and Watters' model is the one developed by Ford et al. [108], which includes the dilatational modes since the core is considered compressible. Although this model is not supported by physical reasons [8], it can be considered as a milestone in the vibroacoustic analysis of multi-layered structures since it will be corrected and improved in several subsequent studies [8, 109]. In particular, Dym and Lang [8] were the first to consolidate the principal points of sandwich behaviour into a single, formal model (further improved in 1976 [110]) for the theoretical prediction of the transmission loss in unidirectional symmetric sandwich panels based on the analysis of wave propagation, highlighting the inconsistencies of the previous works [6, 108, 109] and the possibility to analyse separately flexural and dilatational modes of vibrations for a symmetric sandwich panel, which is no longer possible for an asymmetric one [9]. Moore and Lyon [7, 111] extended all the previous work to the analysis of symmetric sandwich panels with orthotropic cores, evaluating the impedance of the structure through the wave propagation approach. Their studies led to the patenting of the so-called *Mode Cancelling Panel* [112], having a core very soft in compression which moves the symmetric coincidence frequency to low frequencies. Nilsson [10] investigates dynamic and acoustic properties of isotropic sandwich plates through the wave propagation, obtaining results very similar to those of Kurtze and Watters [6]. In his work, the displacements of the skins are described by means of the theory for thin plates; instead, the displacements of the core are derived by superposition of the transverse and the longitudinal waves propagating in the core, expresses as function of a scalar stream function and a velocity potential, respectively. The continuity at the interfaces between the core and the skins is imposed, and at the end the wave equations and the applied boundary conditions lead to the determination of the overall propagation constant by means of an iteration chain. A consistent Higher order Shear Deformation Theory (HSDT) is proposed by Sokolinsky and Nutt [5] and used by Wang et al. [113], wherein the thin face sheets are modelled as Euler-Bernoulli beam and the core as a two dimensional medium in which both longitudinal and transverse displacements vary non-linearly through the thickness.

3 WAVE AND FINITE ELEMENT METHOD FOR 1-DIMENSIONAL PROBLEMS

In this chapter, the Wave and Finite Element Method (WFEM) for the analysis of uniform one-dimensional waveguides is introduced. This method is based on the Finite Element analysis of a short segment of the waveguide (eventually using a commercial package) under investigation. Once the stiffness and mass finite element matrices are known, it is possible to formulate an eigenvalue problem based on the transfer matrix of the elementary cell, which is obtained through the application of periodicity conditions, continuity of displacements and equilibrium of forces at the interface between two adjacent cells. Thus, wavenumbers and wavemodes are calculated as solutions of this eigenproblem.

Furthermore, once the dispersion curves of an infinite waveguide are known, it is also possible to describe the dynamic behaviour of a finite structure having the same characteristics by using the wave approach: the motion can be described as the superposition of several travelling waves.

The chapter is basically divided in three sections. In the first one, the Wave and Finite Element Method is formulated, together with the wave approach for the estimation of the forced response of finite structures. Then, the developed code is briefly explained. At the end, the results, both in terms of dispersion curves and Frequency Response Functions, are shown for different types of structure.

3.1 WFEM FOR 1-DIMENSIONAL WAVEGUIDES

3.1.1 Dynamic stiffness matrix

Consider a one-dimensional waveguide, having infinite extension. The application of the Wave and Finite Element Method (WFEM) [31, 32, 58, 59, 66, 72] for the prediction of its dispersion relations starts with modelling a *small* segment of length Δ of the waveguide under investigation, as shown in Figure 3.1. The waveguide is homogeneous along its axis x, but its properties can vary in an arbitrary manner over its cross-section.

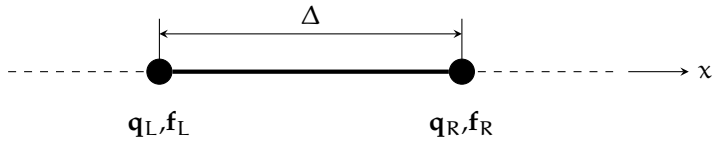

Figure 3.1: A segment of a uniform waveguide

The length of the segment Δ, as specified later in the text, should be enough small compared to the minimum wavelength in the frequency range of interest.

The finite element model of the elementary *cell* can be obtained by using the analytical formulation [21, 22] or through a commercial FE package. The only condition is that there must be the same number of nodes and degrees of freedom (DOFs) on each side of the segment, and they must be numbered in the same order.

The discrete dynamic equation of the cell obtained from the FE model at a given circular frequency ω is given by (time harmonic dependence of the form $e^{i\omega t}$ is assumed throughout this work, and it is suppressed for sake of brevity) [72]

$$\left(\mathbf{K} + i\omega\mathbf{C} - \omega^2\mathbf{M}\right)\mathbf{q} = \mathbf{f} + \mathbf{e} \tag{3.1}$$

where $\mathbf{q}$, $\mathbf{f}$ and $\mathbf{e}$ are $2n \times 1$ vectors of nodal DOFs, internal nodal forces and external nodal forces, respectively. $\mathbf{K}$, $\mathbf{C}$ and $\mathbf{M}$ are the stiffness, viscous damping and mass matrices. Damping can be included both by considering a viscous damping matrix $\mathbf{C}$ or by $\mathbf{K}$ being complex (taking into account the structural damping coefficient). Eq. (3.1) can be written in a different form by introducing the dynamic stiffness matrix, defined as

$$\tilde{\mathbf{D}} = \mathbf{K} + i\omega\mathbf{C} - \omega^2\mathbf{M}. \tag{3.2}$$

Nodal forces and DOFs can be decomposed into sets associated with the left (L) and right (R) boundaries and interior (I) nodes. In this case, assuming there are not external forces on the interior nodes, Eq. (3.1) turns into [59]

$$\begin{bmatrix} \tilde{\mathbf{D}}_{II} & \tilde{\mathbf{D}}_{IL} & \tilde{\mathbf{D}}_{IR} \\ \tilde{\mathbf{D}}_{LI} & \tilde{\mathbf{D}}_{LL} & \tilde{\mathbf{D}}_{LR} \\ \tilde{\mathbf{D}}_{RI} & \tilde{\mathbf{D}}_{RL} & \tilde{\mathbf{D}}_{RR} \end{bmatrix} \begin{Bmatrix} \mathbf{q}_I \\ \mathbf{q}_L \\ \mathbf{q}_R \end{Bmatrix} = \begin{Bmatrix} \mathbf{0} \\ \mathbf{f}_L \\ \mathbf{f}_R \end{Bmatrix}. \tag{3.3}$$

Any interior DOFs can be removed by condensation [59, 66]. In fact, from the first row of the Eq. (3.3)

$$\mathbf{q}_I = -\tilde{\mathbf{D}}_{II}^{-1}\left(\tilde{\mathbf{D}}_{IL}\mathbf{q}_L + \tilde{\mathbf{D}}_{IR}\mathbf{q}_R\right). \tag{3.4}$$

This leads to

$$\begin{bmatrix} \tilde{\mathbf{D}}_{LL} - \tilde{\mathbf{D}}_{LI}\tilde{\mathbf{D}}_{II}^{-1}\tilde{\mathbf{D}}_{IL} & \tilde{\mathbf{D}}_{LR} - \tilde{\mathbf{D}}_{LI}\tilde{\mathbf{D}}_{II}^{-1}\tilde{\mathbf{D}}_{IR} \\ \tilde{\mathbf{D}}_{RL} - \tilde{\mathbf{D}}_{RI}\tilde{\mathbf{D}}_{II}^{-1}\tilde{\mathbf{D}}_{IL} & \tilde{\mathbf{D}}_{RR} - \tilde{\mathbf{D}}_{RI}\tilde{\mathbf{D}}_{II}^{-1}\tilde{\mathbf{D}}_{IR} \end{bmatrix} \begin{Bmatrix} \mathbf{q}_L \\ \mathbf{q}_R \end{Bmatrix} = \begin{Bmatrix} \mathbf{f}_L \\ \mathbf{f}_R \end{Bmatrix}, \tag{3.5}$$

which can be easily written as

$$\begin{bmatrix} \mathbf{D}_{LL} & \mathbf{D}_{LR} \\ \mathbf{D}_{RL} & \mathbf{D}_{RR} \end{bmatrix} \begin{Bmatrix} \mathbf{q}_L \\ \mathbf{q}_R \end{Bmatrix} = \begin{Bmatrix} \mathbf{f}_L \\ \mathbf{f}_R \end{Bmatrix}. \tag{3.6}$$

The new dynamic stiffness matrix is thus obtained after elimination of the interior degrees of freedom. The partitions are of size $n \times n$, where n is the number of

DOFs at the left-hand (and right-hand) of the segment. Since $\mathbf{D}$ is symmetric, the following relations hold:

$$\mathbf{D}_{LL}^{T} = \mathbf{D}_{LL}, \tag{3.7}$$

$$\mathbf{D}_{RR}^{T} = \mathbf{D}_{RR}, \tag{3.8}$$

$$\mathbf{D}_{LR}^{T} = \mathbf{D}_{RL}, \tag{3.9}$$

where the superscript T indicates the transpose matrix.

3.1.2 Wave analysis in a cell

The study of the wave propagation through the waveguide can be reduced to the analysis of a single cell, by applying the periodicity conditions together with continuity of displacements and equilibrium of forces at the interfaces between two consecutive cells.

3.1.2.1 *Periodicity conditions: the Bloch theorem*

The possibility to investigate a periodic structure modelling just its representative cell is based on the Bloch theorem (or Floquet-Bloch theorem), which gives a rigorous and well-posed problem representing wave dispersion in undamped media [17].

Figure 3.2 represents an infinite one-dimensional waveguide, obtaining by replicating along its axis the elementary cell (green coloured), with length Δ. Each point P in the structure can be expressed with respect to a corresponding point U in the elementary cell, translated n_{cell} along the x axis. Hence:

$$\mathbf{r}_p = \mathbf{r}_u + n_{cell}\Delta\mathbf{i}, \tag{3.10}$$

being $\mathbf{i}$ a unit vector directed along x axis.

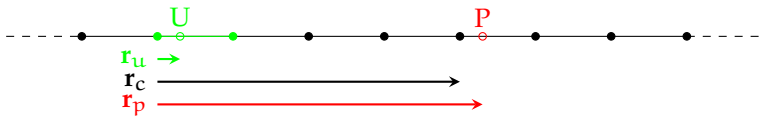

Figure 3.2: Schematic representation of an infinite periodic waveguide. Green cell is the considered unit cell

According to the Bloch theorem [17], the displacement $u(\mathbf{r}_p, \omega)$ in a generic point P of the periodic system can be expressed in terms of the displacement $u(\mathbf{r}_u, \omega)$ of the corresponding point in the reference unit cell, multiplied by an exponential term defining amplitude and phase change as the wave propagates from the reference cell to the considered one, which is function only on the number of cells between them (and hence is independent on the cell location within the waveguide). The relation between the displacements of the two points is

$$u(\mathbf{r}_p, \omega) = u(\mathbf{r}_u, \omega)e^{-i\mathbf{k}\cdot(n_{cell}\Delta\mathbf{i})}, \tag{3.11}$$

where the symbol $\cdot$, in the exponent, indicates a scalar product. Hence, the amplitude and phase change are determined by the wavenumber vector $\mathbf{k}$. Given the one-directionality of the problem, and considering two adjacent cells ($n_{cell} = 1$), Eq. (3.11) becomes

$$u(\mathbf{r}_p, \omega) = u(\mathbf{r}_u, \omega) e^{-ik\Delta} = u(\mathbf{r}_u, \omega)\lambda, \tag{3.12}$$

where λ is the propagation constant associated to the wavenumber k, defined as

$$\lambda = e^{-ik\Delta}. \tag{3.13}$$

It describes the amplitude and the phase change over a distance Δ of the wave characterised by the wavenumber k.

3.1.2.2 *Continuity of displacements and equilibrium of forces: the transfer matrix*

Once the primitive irreducible cell is identified, the boundary conditions at the interfaces must be imposed. Suppose that no external forces are applied to the structure, and consider two adjacent elementary cells of a waveguide, as shown in Figure 3.3.

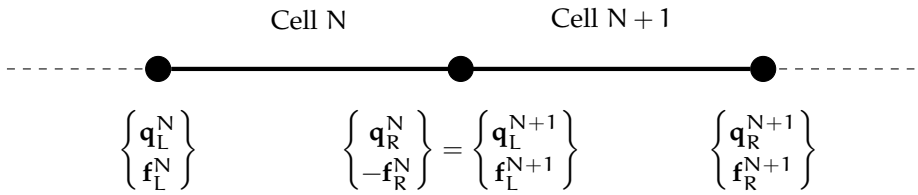

Figure 3.3: Two adjacent elementary cells of a waveguide

From continuity of displacements and equilibrium of forces at the interface between the cell N and $(N+1)$, it follows that [58]

$$\mathbf{q}_L^{N+1} = \mathbf{q}_R^N, \tag{3.14}$$

$$\mathbf{f}_L^{N+1} = -\mathbf{f}_R^N. \tag{3.15}$$

These relations can be expressed in matrix form as

$$\mathbf{T} \begin{Bmatrix} \mathbf{q}_L^N \\ \mathbf{f}_L^N \end{Bmatrix} = \begin{Bmatrix} \mathbf{q}_R^N \\ -\mathbf{f}_R^N \end{Bmatrix} = \begin{Bmatrix} \mathbf{q}_L^{N+1} \\ \mathbf{f}_L^{N+1} \end{Bmatrix}. \tag{3.16}$$

$\mathbf{T}$ is the transfer matrix, relating the nodal displacements and forces (evaluated on the left side) between two adjacent cells. The terms of the transfer matrix can be easily derived by exploiting the relation between nodal displacements and forces expressed through the dynamic stiffness matrix in Eq. (3.6). In fact, from the first row (no interior DOFs or, if present, already condensed)

$$\mathbf{q}_L^{N+1} = \mathbf{D}_{LR}^{-1} \left(\mathbf{f}_L^N - \mathbf{D}_{LL} \mathbf{q}_L^N \right) \tag{3.17}$$

Substituting Eq. (3.17) in the second row Eq. (3.6) gives

$$\left(\mathbf{D}_{RL} - \mathbf{D}_{RR}\mathbf{D}_{LR}^{-1}\mathbf{D}_{LL}\right)\mathbf{q}_L^N + \mathbf{D}_{RR}\mathbf{D}_{LR}^{-1}\mathbf{f}_L^N = -\mathbf{f}_L^{N+1} \tag{3.18}$$

Eqs. (3.16), (3.17) and (3.18) finally provide the transfer matrix

$$\mathbf{T} = \begin{bmatrix} -\mathbf{D}_{LR}^{-1}\mathbf{D}_{LL} & \mathbf{D}_{LR}^{-1} \\ -\mathbf{D}_{RL} + \mathbf{D}_{RR}\mathbf{D}_{LR}^{-1}\mathbf{D}_{LL} & -\mathbf{D}_{RR}\mathbf{D}_{LR}^{-1} \end{bmatrix}. \tag{3.19}$$

It is worth to highlight that the transfer matrix $\mathbf{T}$ depends only on the dynamic stiffness of one cell of the waveguide.

3.1.3 Free wave propagation: the eigenvalue problem

Under the passage of a wave of the form $\sim e^{j(\omega t - kx)}$ along the waveguide, the relation between the nodal displacements and forces on the left and on the right sides of the elementary cell can be expressed through:

- the Bloch theorem, for which

$$\mathbf{q}_R = \lambda \mathbf{q}_L, \tag{3.20}$$
$$\mathbf{f}_R = -\lambda \mathbf{f}_L, \tag{3.21}$$

  where λ depends on the cell length Δ;

- the transfer matrix defined in Eq. (3.19).

Thus, from Eqs. (3.16), (3.20) and (3.21), it is possible describing the free wave propagation through the formulation of an eigenvalue problem in the form

$$\mathbf{T}\begin{Bmatrix} \mathbf{q}_L \\ \mathbf{f}_L \end{Bmatrix} = \lambda \begin{Bmatrix} \mathbf{q}_L \\ \mathbf{f}_L \end{Bmatrix}. \tag{3.22}$$

wherein the propagation constants λ are the eigenvalue of the transfer matrix.

3.1.3.1 *Properties of eigenvalues and eigenvectors*

The eigenproblem of Eq. (3.22) has $2n$ eigenvalues. In particular, the generic eigenvalue λ_j ($j = 1, 2, \cdots, 2n$) is related to the phase change (or decay) over the length Δ of the elementary cell, and hence it represents the propagation constants. The associated eigenvector (or basis wave vector, or eigenwave) $\mathbf{\Phi}_j$ represents a wavemode containing information about both the displacements and the internal forces over the cross-section. (Again, here n indicates the number of nodal DOFs on each side of the cell.)

The eigenvector can be partitioned in two $n \times 1$ vectors, associated with the nodal DOFs and the nodal forces, i.e.

$$\mathbf{\Phi}_j = \begin{Bmatrix} \mathbf{\Phi}_j^q \\ \mathbf{\Phi}_j^f \end{Bmatrix}, \tag{3.23}$$

where the superscript q and f indicate the vectors related to DOFs and forces, respectively.

It is worth to remark that the $2n$ eigenvalues of the eigenproblem come in n independent pairs [59]. In fact, the first row of Eq. (3.22) leads to

$$\mathbf{f}_L = (\mathbf{D}_{LL} + \lambda \mathbf{D}_{LR})\, \mathbf{q}_L. \tag{3.24}$$

Combining this with the second row of Eq. (3.22) gives

$$\left(\mathbf{D}_{LL} + \mathbf{D}_{RR} + \lambda \mathbf{D}_{LR} + \frac{1}{\lambda}\mathbf{D}_{RL}\right) \mathbf{q}_L = 0. \tag{3.25}$$

From Eq. (3.25), it results that the eigenvalues are the roots of the determinant

$$\left|\mathbf{D}_{LL} + \mathbf{D}_{RR} + \lambda \mathbf{D}_{LR} + \frac{1}{\lambda}\mathbf{D}_{RL}\right| = 0, \tag{3.26}$$

but by taking the transpose of Eq. (3.25) and applying the symmetric properties of the dynamic stiffness matrix, it can be also obtained that they are the roots of

$$\left|\mathbf{D}_{LL} + \mathbf{D}_{RR} + \lambda \mathbf{D}_{RL} + \frac{1}{\lambda}\mathbf{D}_{LR}\right| = 0. \tag{3.27}$$

This leads to the fundamental properties that if λ is an eigenvalue, $1/\lambda$ is also an eigenvalue for any shape or properties of the cell. The eigensolutions therefore come in two sets whose eigenvalues and eigenvectors are $(\lambda_j, \mathbf{\Phi}_j^+)$ and $(1/\lambda, \mathbf{\Phi}_j^-)$, which represent n positive-going and n negative-going waves, respectively. In order to identify the two groups of waves, the positive-going waves are those for which the magnitude is less than 1, or the carried power is positive going, i.e.

$$\begin{aligned} &|\lambda_j| \leqslant 1 \\ &\mathrm{Re}\left\{\mathbf{f}_L^H \dot{\mathbf{q}}_L\right\} = \mathrm{Re}\left\{i\omega \mathbf{f}_L^H \mathbf{q}_L\right\} < 0, \text{ if } |\lambda_j| = 1 \end{aligned} \tag{3.28}$$

where the superscript H represent the Hermitian operator. Eq. (3.28) implies that either the amplitude of a wave decreases in the direction of propagation or that, if the amplitude remains constant, there is time average power transmission in the direction of propagation.

From Eqs. (3.26) and (3.27), it results that $\mathbf{q}_L$ is both a right eigenvector associated with the eigenvalue λ (Eq. (3.26)) and a left eigenvector associated with the eigenvalue $1/\lambda$ (Eq. (3.27)).

The right eigenvector (vector $2n \times 1$, partitioned in two vectors $n \times 1$) of the eigenproblem of Eq. (3.22) for the eigenvalue λ_j is given by

$$\mathbf{\Phi}_j = \begin{Bmatrix} \mathbf{\Phi}_j^q \\ \mathbf{\Phi}_j^f \end{Bmatrix} = \begin{Bmatrix} \mathbf{q}_L(\lambda_j) \\ (\mathbf{D}_{LL} + \lambda_j \mathbf{D}_{LR})\, \mathbf{q}_L(\lambda_j) \end{Bmatrix}, \tag{3.29}$$

whereas the left eigenvector (vector $1 \times 2n$) associated with λ_j is given by

$$\mathbf{\Psi}_j = \begin{Bmatrix} \mathbf{\Psi}_j^f & \mathbf{\Psi}_j^q \end{Bmatrix} = \left\{ {}^T\mathbf{q}_L\left(\frac{1}{\lambda_j}\right)(\mathbf{D}_{RR} + \lambda_j \mathbf{D}_{LR}) \quad {}^T\mathbf{q}_L\left(\frac{1}{\lambda_j}\right) \right\}. \tag{3.30}$$

However, for our purposes, the left eigenvector is rearranged as

$$\boldsymbol{\Psi}_j = \left\{ \boldsymbol{\Psi}_j^q \quad \boldsymbol{\Psi}_j^f \right\} \tag{3.31}$$

Summarising, it is possible to write the right and left eigenproblems as follows:

$$\mathbf{T}\boldsymbol{\Phi}_j = \lambda_j \boldsymbol{\Phi}_j \tag{3.32}$$

$$\boldsymbol{\Psi}_j \mathbf{T} = \lambda_j \boldsymbol{\Psi}_j \tag{3.33}$$

Obviously, the right and left eigenproblems provide the same eigenvalues, while the orthogonality relations between the left and right eigenvector can be expressed as

$$\boldsymbol{\Psi}_i \boldsymbol{\Phi}_j = d_i \delta_{ij} \tag{3.34}$$

where δ_{ij} is the Kronecker delta and d_i is arbitrary. The normalization may involve either the displacement part of the eigenvector (i.e. $\mathbf{q}(\lambda_j)$, $\mathbf{q}(1/\lambda)$ [59] or the whole eigenvector in a such a way that $d_i = 1$ [66, 72]. In the second case, which is the normalisation adopted in this work, the wavemodes are normalised so that

$$\boldsymbol{\Psi}\boldsymbol{\Phi} = \mathbf{I}, \tag{3.35}$$

where $\mathbf{I}$ is the identity matrix. A consequence of this normalisation is that

$$\boldsymbol{\Psi}\mathbf{T}\boldsymbol{\Phi} = diag(\lambda_j) \tag{3.36}$$

where $diag(\cdot)$ represents a diagonal matrix.

3.1.3.2 *Type of waves: propagating, evanescent and attenuating*

In general, the j-th eigenvalue, which is the propagation constant of the corresponding wave, can be written as

$$\lambda_j = e^{-ik_j\Delta} = e^{-\mu_j\Delta} e^{-ik'_j\Delta} \tag{3.37}$$

where the wavenumber $k_j = k'_j - i\mu_j$ (with $k'_j, \mu_j \in \mathbb{R}$) may be complex. The imaginary μ_j and real k'_j parts of the wavenumber k_j are equal, respectively, to the attenuation and the phase change per unit length associated with the j-th wave. In Eq. (3.37), the signs of μ_j and k'_j have been chosen in a such a way that they are positive for positive-going waves.

The waves can be classified depending on the nature (real, imaginary, complex) of the eigenvalue. In the absence of damping, those eigenvalue having $|\lambda_j| = 1$, with $\lambda_j = e^{-ik'_j\Delta}$ (i.e. $\mu_j = 0$) represent freely propagating waves with wavenumber k'_j, while those for which λ_j is real (i.e. $k'_j = 0$) represent evanescent waves. Under certain circumstances (e.g. damped system, hence complex dynamic stiffness matrix), there may be a pair of complex conjugate eigenvalues for which λ_j is complex and $|\lambda_j| < 1$: these represent decaying but oscillatory waves. The different types of waves are summarized in Table 3.1 and Figure 3.4 [114]. In the

Table 3.1: Properties of eigenvalues and associated waves [114]

λ	$\lvert\lambda\rvert$	μ	k'	Wave	Direction
imaginary	1	0	>0	propagating	Positive
real	<1	>0	0	evanescent	
complex	<1	>0	>0	attenuating	
imaginary	1	0	<0	propagating	Negative
real	>1	<0	0	evanescent	
complex	>1	<0	<0	attenuating	

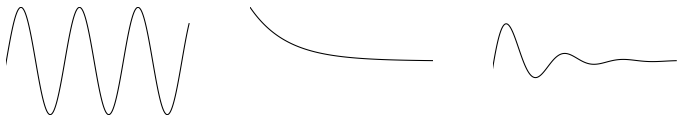

(a) *propagating* **(b)** *evanescent* **(c)** *attenuating*

Figure 3.4: Different types of waves [114]

general case, a wave is either a slowly decaying propagating wave or a rapidly attenuating, but slightly oscillatory, evanescent wave.

Numerical results are usually presented in terms of k'_j and μ_j (or, which is the same, as $\mathrm{Re}\{k_j\}$ and $\mathrm{Im}\{k_j\}$). For this reason, Eq. (3.37) can be rewritten as

$$k'_j - i\mu_j = -\frac{\ln \lambda_j}{i\Delta}. \tag{3.38}$$

3.1.3.3 *The wave motion and the wave basis*

According to the Bloch theorem, propagation over a distance L is such that, for motion given by the j-th wavemode, nodal displacement and forces at location x and $x + L$ are related by

$$\mathbf{q}(x + L) = \lambda_j \mathbf{q}(x) \qquad \mathbf{f}(x + L) = \lambda_j \mathbf{f}(x). \tag{3.39}$$

However, in general the motion of the waveguide is a sum of wave components, therefore it is necessary to calculate the contribution of each wave. For this purpose, the left and right eigenvectors can be grouped by partitioning the positive- and negative-going waves, as follows

$$\begin{aligned} \boldsymbol{\Phi}^+ &= \begin{bmatrix} \boldsymbol{\Phi}_1^+ & \cdots & \boldsymbol{\Phi}_n^+ \end{bmatrix} \\ \boldsymbol{\Phi}^- &= \begin{bmatrix} \boldsymbol{\Phi}_1^- & \cdots & \boldsymbol{\Phi}_n^- \end{bmatrix} \\ \boldsymbol{\Phi} &= \begin{bmatrix} \boldsymbol{\Phi}^+ & \boldsymbol{\Phi}^- \end{bmatrix} \end{aligned} \tag{3.40}$$

$$\boldsymbol{\Psi}^{+} = \begin{bmatrix} \boldsymbol{\Psi}_1^{+} \\ \vdots \\ \boldsymbol{\Psi}_n^{+} \end{bmatrix} \qquad \boldsymbol{\Psi}^{-} = \begin{bmatrix} \boldsymbol{\Psi}_1^{-} \\ \vdots \\ \boldsymbol{\Psi}_n^{-} \end{bmatrix} \qquad \boldsymbol{\Psi} = \begin{bmatrix} \boldsymbol{\Psi}^{+} \\ \boldsymbol{\Psi}^{-} \end{bmatrix} \tag{3.41}$$

Since the number of positive- and negative- going waves are equal to the number of DOFs on each side of the cell, in their original sense $\boldsymbol{\Phi}^{+}$ and $\boldsymbol{\Phi}^{-}$ are $2n \times n$ matrices, whereas $\boldsymbol{\Psi}^{+}$ and $\boldsymbol{\Psi}^{-}$ are $n \times 2n$.

These partitions of the left and right eigenvector can be further partitioned in order to isolate the part of the eigenwaves related to the nodal DOFs and the one containing to the nodal forces, e.g.

$$\boldsymbol{\Phi}_q^{+} = \begin{bmatrix} \boldsymbol{\Phi}_{q,1}^{+} & \cdots & \boldsymbol{\Phi}_{q,n}^{+} \end{bmatrix}, \qquad \boldsymbol{\Psi}_q^{+} = \begin{bmatrix} \boldsymbol{\Psi}_{q,1}^{+} \\ \vdots \\ \boldsymbol{\Psi}_{q,n}^{+} \end{bmatrix}. \tag{3.42}$$

Obviously, in the same way the matrices $\boldsymbol{\Phi}_q^{-}$, $\boldsymbol{\Psi}_q^{-}$, $\boldsymbol{\Phi}_f^{\pm}$ and $\boldsymbol{\Psi}_f^{\pm}$ can be defined, and all of them have dimensions $n \times n$ since no considerations have been done yet on the number of waves to be retained. These matrices, together with the orthogonality relation of Eq. (3.35), define the transformation between the physical domain and the wave domain. In the physical domain, the motion is simply described in terms of $\mathbf{q}$ and $\mathbf{f}$; in the wave domain, instead, each wave belonging to the basis, formed by the right (left) eigenvectors matrix $\boldsymbol{\Phi}$ ($\boldsymbol{\Psi}$), contributes to the motion with an amplitude $\mathbf{a}^{+}$ or $\mathbf{a}^{-}$, depending on the direction of the travelling wave.

In particular, the transformation between the two domains can be written as

$$\mathbf{q}_L = \boldsymbol{\Phi}_q^{+}\mathbf{a}^{+} + \boldsymbol{\Phi}_q^{-}\mathbf{a}^{-}, \tag{3.43}$$

$$\mathbf{f}_L = \boldsymbol{\Phi}_f^{+}\mathbf{a}^{+} + \boldsymbol{\Phi}_f^{-}\mathbf{a}^{-}, \tag{3.44}$$

or, in matrix form

$$\begin{Bmatrix} \mathbf{q}_L \\ \mathbf{f}_L \end{Bmatrix} = \boldsymbol{\Phi} \begin{Bmatrix} \mathbf{a}^{+} \\ \mathbf{a}^{-} \end{Bmatrix}, \tag{3.45}$$

where $\mathbf{a} = \begin{Bmatrix} \mathbf{a}^{+} \\ \mathbf{a}^{-} \end{Bmatrix}$ is the vector of the waves' amplitudes.

3.1.4 Model reduction

Once the wave basis is defined, it is possible to consider only a limited number of waves m to reconstruct to motion of the waveguide (as in modal analysis a limited number of modes is considered). In this case, the matrices $\boldsymbol{\Phi}_{q,f}^{\pm}$ and $\boldsymbol{\Psi}_{q,f}^{\pm}$ (and similar) are $n \times m$ and $m \times n$, respectively. The choice of the number of waves to be retained is still a complicated task, since it can strongly affect the

calculation of the motion of the waveguide. However, as a rule of thumb, all the propagating waves (having $|\lambda_j| = 1$) must be retained, together with the slowest attenuating waves (i.e. with $|\lambda_j| < 1$, but μ_j small). The reasons for the reduction of the size of the wave basis are basically two:

- the high-order wavemodes, i.e. the waves which decay very rapidly with distance, have a negligible contribution to the response, and hence can be neglected in order to reduce the computational cost;
- the calculation of high-order wavemodes is very prone to poor numerical conditioning [66].

3.1.5 Numerical issues

The use of the Wave and Finite Element Method for the numerical calculation of free wave propagation is characterised by various numerical issues, deeply discussed by Waki et al. [66] and here briefly summarised. These issues are due both to the finite element discretisation of a periodic structures (at high frequencies) and to the resolution of an eigenproblem based on the Dynamic Stiffness Matrix (in the low frequency range).

DISCRETISATION

This type of issue occurs in general at high frequencies when the dynamic behaviour of a continuous structure is described by means of a discrete model. In the case of Finite Element, the length of the element must be chosen as a function of the minimum wavelength: as a rule of thumb, at least six element per wavelength should be considered in order to reconstruct correctly the wave. These errors also depend on the aspect ratio of the element used.

PERIODIC STRUCTURE EFFECTS

Periodic structures exhibit two own effects due to the periodicity. First of all, their dynamic behaviour is characterised by pass-band (in which the waves are free to propagate) and stop-band (in which the waves decay with distance) frequency regions [25, 115]. The problem is that the bounds of the pass- and stop- bands depend on the natural frequencies of the elementary cell under several boundary conditions [116, 117]. On the other hand, at high frequencies an aliasing effect occurs when the segment length becomes comparable to the wavelength: if $k\Delta$ is a (dimensionless) wavenumber, solution of the eigenvalue problem, then also $k\Delta + 2n\pi$ yields to the same solution for any integer n. Hence, the eigenwaves and frequencies are periodic functions of the propagation constant. Both the periodic structure effects described can be overcome by properly choosing the length of the cell.

TRUNCATION OF INERTIA TERMS IN THE DSM

The numerical issues described above occur mostly at high frequencies and can be solved by ensuring the length of the cell is enough shorter than the minimum wavelength. However, if the size of the element is too small, round-off errors can occur at low frequencies, due to truncation of inertia terms in the Dynamic Stiff-

ness Matrix, defined in Eq. (3.2). Neglecting the damping for sake of simplicity, the generic term of the matrix is $D_{ij} = K_{ij} - \omega^2 M_{ij}$. At very low frequencies, the stiffness term can be very large compared to the inertia term, determining to the truncation of some digits of this last because of computer finite precision arithmetic.

Obviously, round-off errors can be reduced by using a higher precision arithmetic (if available) and/or by considering a longer cell, determining a decrease of the stiffness, as well as an increase of the mass (i.e. the inertia term).

MATRIX INVERSION IN THE DSM AND NUMERICAL CONDITIONING

The eigenproblem described by Eq. (3.22) can suffer from poor numerical conditioning, because the transfer matrix defined in Eq. (3.19) implies $\mathbf{D}_{LR}$ is inverted. This problem can be solved by conditioning the eigenvalue problem. Zhong et al. [118, 119] reformulated the Eq. (3.22) only in terms of the displacement vectors, leading to

$$\begin{bmatrix} (\mathbf{D}_{LR} - \mathbf{D}_{RL}) & -(\mathbf{D}_{LL} + \mathbf{D}_{RR}) \\ (\mathbf{D}_{LL} + \mathbf{D}_{RR}) & (\mathbf{D}_{LR} - \mathbf{D}_{RL}) \end{bmatrix} \begin{Bmatrix} \mathbf{q} \\ \lambda\mathbf{q} \end{Bmatrix} = \frac{1}{\lambda + 1/\lambda} \begin{bmatrix} \mathbf{o} & \mathbf{D}_{LR} \\ -\mathbf{D}_{LR} & \mathbf{o} \end{bmatrix} \begin{Bmatrix} \mathbf{q} \\ \lambda\mathbf{q} \end{Bmatrix} \quad (3.46)$$

Eq. (3.46) has repeated eigenvalues $(\lambda + 1/\lambda)^{-1}$. Hence, propagation constants can be easily determined, overcoming the numerical issues. However, the calculation of the eigenvectors of the original eigenproblem is not trivial [66], being based on singular value decomposition.

3.1.6 Examples: dispersion curves

In this section, some simple examples are reported in order to allow the comprehension of the previous sections.

3.1.6.1 *Infinite rod*

The dispersion relation of the longitudinal waves travelling in an infinite rod are calculated by applying the WFEM, and then compared to the analytic solution [1, 2].

Consider a rod element of length Δ, as shown in Figure 3.5, having two degrees of freedom. This element constitutes the elementary cell of the one-dimensional waveguide under investigation.

Figure 3.5: Rod element

The analytic stiffness and mass finite element matrices for the rod element are [22]:

$$\mathbf{K} = \frac{EA}{\Delta}\begin{bmatrix} 1 & -1 \\ -1 & 1 \end{bmatrix} \quad ,\mathbf{M} = \frac{\rho A\Delta}{6}\begin{bmatrix} 2 & 1 \\ 1 & 2 \end{bmatrix}, \tag{3.47}$$

where E and ρ are Young's modulus and density of the material, respectively; A is the cross-sectional area. The damping is taken into account by assuming a hysteretic damping η, leading to a complex Young's modulus $E_c = (1 + i\eta)E$. These matrices lead to the following dynamic stiffness matrix [120]

$$\mathbf{D} = \begin{bmatrix} 1 - \dfrac{\rho\Delta^2\omega^2}{3E_c} & -1 - \dfrac{\rho\Delta^2\omega^2}{6E_c} \\ \\ -1 - \dfrac{\rho\Delta^2\omega^2}{6E_c} & 1 - \dfrac{\rho\Delta^2\omega^2}{3E_c} \end{bmatrix}. \tag{3.48}$$

Given the expression of the propagation speed of longitudinal waves in solid media (Eq. (2.16)), the corresponding wavenumber is

$$k_l = \frac{\omega}{c_l''} = \omega\sqrt{\frac{\rho}{E_c}} = \sqrt{\frac{\rho\omega^2}{E_c}}. \tag{3.49}$$

It is worth to remark that the propagation velocity of longitudinal waves does not depend on the frequency, i.e. the relation between the wavenumber and the frequency is linear, therefore they are non-dispersive waves. Once the wavenumber of longitudinal wave in thin rod is defined, it is possible to express the dynamic stiffness matrix as a function of a dimensionless wavenumber $k_l\Delta$,; in fact, substituting Eq. (3.49) in the expression of the dynamic stiffness matrix (Eq. (3.48), this last can be rewritten as

$$\mathbf{D} = \begin{bmatrix} 1 - \dfrac{(k_l\Delta)^2}{3} & -1 - \dfrac{(k_l\Delta)^2}{6} \\ \\ -1 - \dfrac{(k_l\Delta)^2}{6} & 1 - \dfrac{(k_l\Delta)^2}{3} \end{bmatrix}, \tag{3.50}$$

which leads to the transfer matrix (according to Eq. (3.19))

$$\mathbf{T} = \frac{1}{1 + \dfrac{(k_l\Delta)^2}{6}}\begin{bmatrix} 1 - \dfrac{(k_l\Delta)^2}{3} & -1 \\ \\ (k_l\Delta)^2 - \dfrac{(k_l\Delta)^4}{12} & 1 - \dfrac{(k_l\Delta)^2}{3} \end{bmatrix}. \tag{3.51}$$

The eigenvalues of this matrix are given by

$$\begin{aligned} \lambda^{\pm} &= \frac{1}{1 + \dfrac{(k_l\Delta)^2}{6}}\left(1 - \frac{(k_l\Delta)^2}{3} \pm ik_l\Delta\sqrt{1 - \frac{(k_l\Delta)^2}{12}}\right) = \\ &= 1 \pm ik_l\Delta - \frac{(k_l\Delta)^2}{2} + O\left((k_l\Delta)^3\right). \end{aligned} \tag{3.52}$$

As expected, since there is one DOF on each side of the rod element, one pair of eigenvalues is identified, representing propagating waves in the positive and negative directions. It is possible to verify that, in absence of damping, $|\lambda^{\pm}| = 1$ for $(k\Delta)^2 < 12$, which represent the cut-off wavenumber for the FE model, i.e. the frequency at which the stop-band begins.

Suppose that the waveguide has a cross-sectional area $A = 10^{-6}\,m^2$ and it is made of aluminium ($E = 70\,GPa$, $\rho = 2700\,kg/m^3$). The elementary cell is long $\Delta = 0.001\,m$. No damping is included.

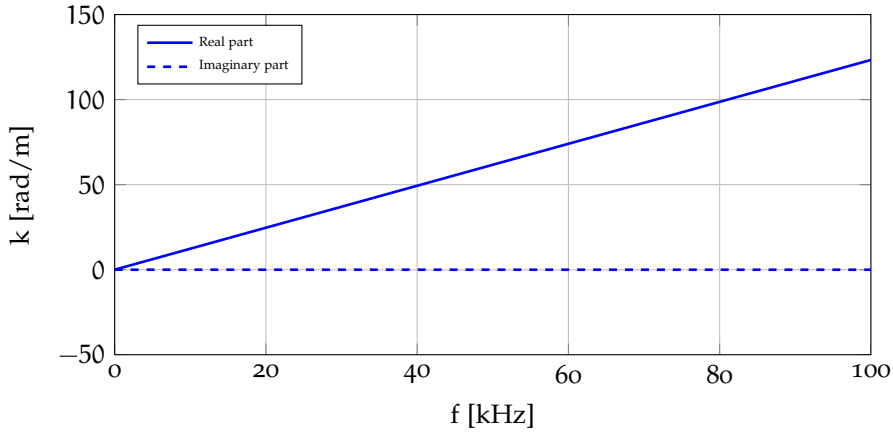

(a) *positive-going wave*

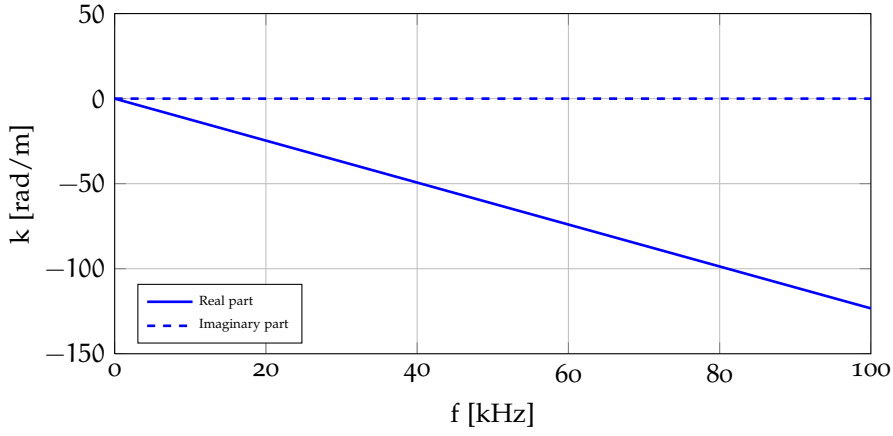

(b) *negative-going wave*

Figure 3.6: Dispersion curves for thin aluminium rod cell

In Figure 3.6, the dispersion curves (wavenumber k as a function of the frequency f) of the aluminium rod cell are plotted. On the top, the positive wavenumber is reported; on the bottom, the negative one. The two dispersion curves (positive and negative) are the same, except for the sign of both the real and imaginary parts. Hence, it is possible to consider only one of the two dispersion graph, related to the positive-going wave. In Figure 3.7, the longitudinal wavemode is

represented at $f = 10\,Hz$ for a portion of the waveguide (the cross-sectional dimensions are enlarged to improve the comprehension). The color bar indicates the displacement along the axis x of the waveguide.

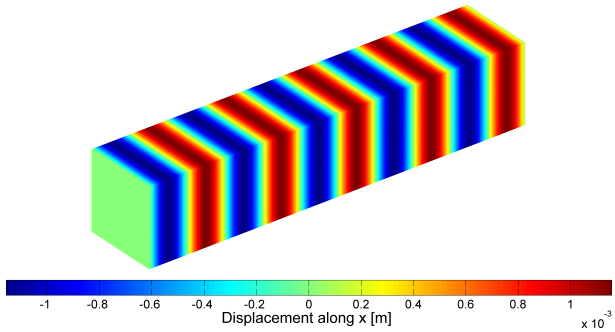

Figure 3.7: Longitudinal eigenwave at $f = 10Hz$ in thin aluminium rod

In Figure 3.8, the numerical solution, obtained through WFEM, for the positive-going wave is compared to the analytical one, showing that for this value of Δ the numerical results are identical to the analytical ones in the whole considered frequency range.

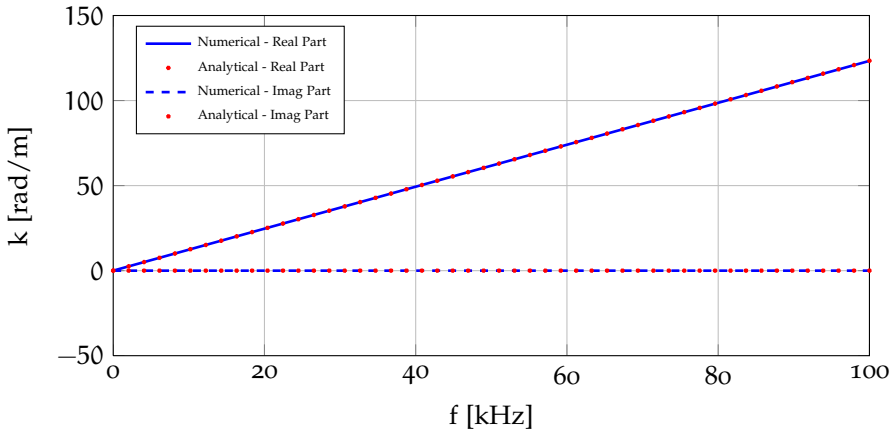

Figure 3.8: Numerical-analytical comparison of dispersion curves of thin aluminium rod

In Figure 3.9, the dimensionless wavenumber $k\Delta$ (numerically estimated) is plotted against the dimensionless frequency $\Omega = k_l\Delta = \omega\Delta\sqrt{\rho/E}$ (analytically calculated). It is possible to observe that in the low frequency range the numerical solution is identical to the numerical one. When the aliasing effect occurs, the numerical values move away from the numerical ones because of the discretisation error. However, waves propagate freely up to $\Omega_c = k\Delta < \sqrt{12}$, since the imaginary part is zero. Ω_c is the cut-off frequency of the model, and it defines the end of the first pass-band region. For higher frequencies, the stop-band region begins, therefore the finite element model predicts a pair of attenuating waves ($Im\{k\} < 0$, i.e. $\mu > 0$): this means that waves are no longer free to propagate, and decay with distance.

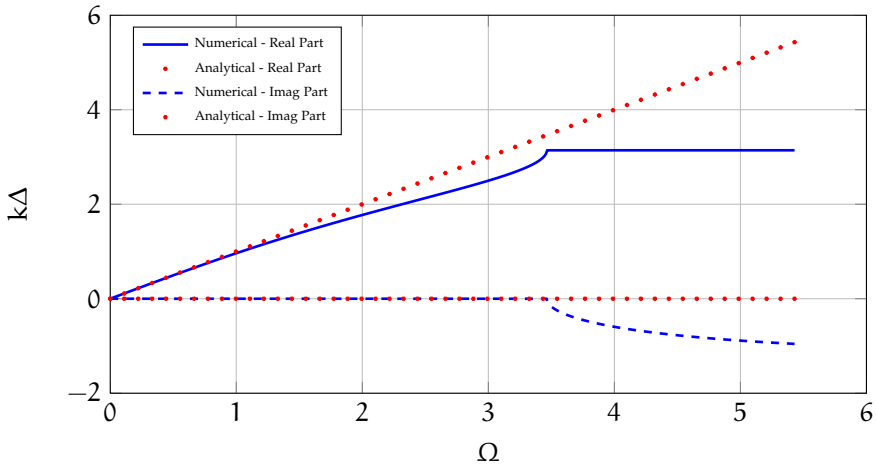

Figure 3.9: Dimensionless dispersion curves of thin aluminium rod

3.1.6.2 *Infinite beam*

Consider now an infinite uniform Euler-Bernoulli beam, undergoing the bending vibration. As explained in Section 2.2.3.1, four dispersive waves are present in the waveguide, grouped in two pairs of propagating and evanescent waves going in the positive and in the negative directions.

Similarly to the previous example for the rod, in this section the numerical dispersion curves of an Euler-Bernoulli beam, obtained through WFEM, are compared to the analytical ones. Consider a small segment Δ of the beam, being the elementary cell of the waveguide. The finite element model of the cell has two nodes, and at each node there are two DOFs, displacement and rotation, and correspondingly two nodal forces, shear and bending moment. The beam element is shown in Figure 3.10.

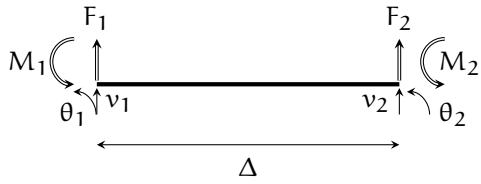

Figure 3.10: Beam element

The analytic stiffness and mass finite element matrices for the beam element are [22]:

$$\mathbf{K} = \frac{EI_z}{\Delta^3}\begin{bmatrix} 12 & 6\Delta & -12 & 6\Delta \\ 6\Delta & 4\Delta^2 & -6\Delta & 2\Delta^2 \\ -12 & -6\Delta & 12 & -6\Delta \\ 6\Delta & 2\Delta^2 & -6\Delta & 4\Delta^2 \end{bmatrix}, \tag{3.53}$$

$$\mathbf{M} = \frac{\rho A \Delta}{420} \begin{bmatrix} 156 & 22\Delta & 54 & -13\Delta \\ 22\Delta & 4\Delta^2 & 13\Delta & -3\Delta^2 \\ 54 & 13\Delta & 156 & -22\Delta \\ -13\Delta & -3\Delta^2 & -22\Delta & 4\Delta^2 \end{bmatrix}. \tag{3.54}$$

The cell is made of aluminium, and the cross-section have the following characteristics: $A = 10^{-6}\,\mathrm{m}^2$, $I_z = 8.33 \times 10^{-14}\,\mathrm{m}^4$. The length of the segment is $\Delta = 0.001\,\mathrm{m}$. A damping coefficient $\eta = 0.01$ is considered.

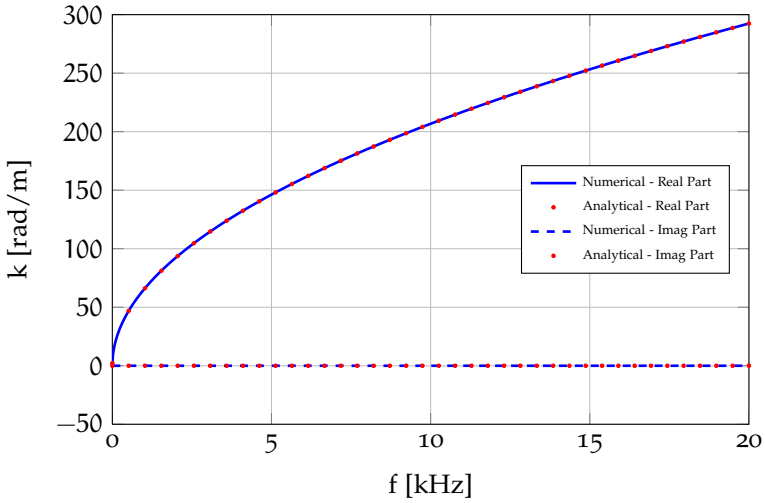

(a) *propagating wavenumber*

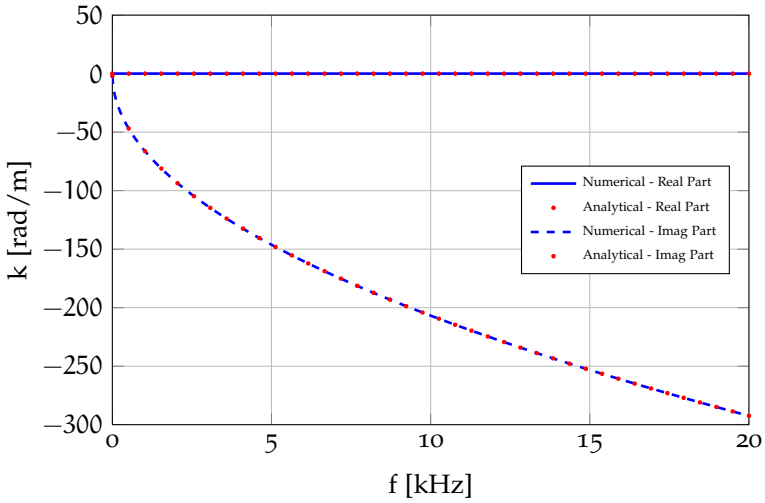

(b) *evanescent wavenumber*

Figure 3.11: Dispersion curves for aluminium Euler-Bernoulli beam

The dispersion curves for the pairs of positive-going waves are shown in Figure 3.11. Analytical and numerical curves coincide in the considered frequency range. Furthermore, according to Table 3.1, Figure 3.11a reports the dispersion relation for the propagating wave, whereas Figure 3.11b shows that of the evanescent one. The corresponding eigenwaves at $f = 10\,\text{Hz}$ are shown in Figure 3.12. In particular, the bending wave is represented on the left (Figures 3.12a-3.12c), whereas on the right the evanescent wave is shown (Figures 3.12b-3.12d). For both the eigenwaves, the surface of the beam are coloured in terms of displacement along y axis and in terms of rotation about z axis, in order to provide a complete information since they are not visible from the graphical deformation of the waveguide. As mentioned before, the evanescent wave vanishes soon with the distance.

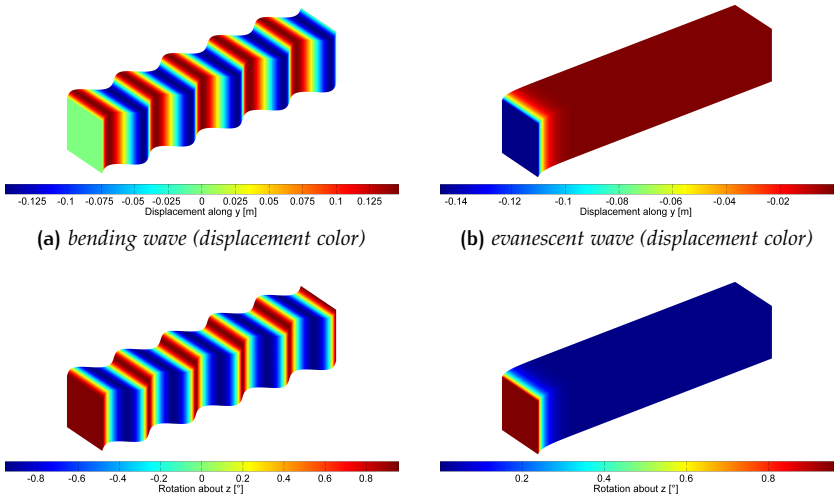

(a) *bending wave (displacement color)*

(b) *evanescent wave (displacement color)*

(c) *bending wave (rotation color)*

(d) *evanescent wave (rotation color)*

Figure 3.12: Wavemodes at $f = 10\text{Hz}$ for aluminium Euler-Bernoulli beam

3.2 VIBRATION ANALYSIS USING WAVE APPROACH

The dynamic response of a one-dimensional periodic structure can be derived through the wave approach, i.e. calculating the motion as the superposition of the travelling waves [87]. In this sense, the dispersion relations, estimated by means of the WFEM for free wave propagation, can be used to calculate the amplitudes of the waves.

The work by Duhamel et al. [59] is the first concerning the evaluation of the forced response through the WFEM, using a recursive technique based on the number of cells used to discretise the structure. More recent formulations [42, 66, 72], instead, focus on the analysis of a single cell, exploiting the wave propagation laws to evaluate the response in a given point of the structure [81, 121].

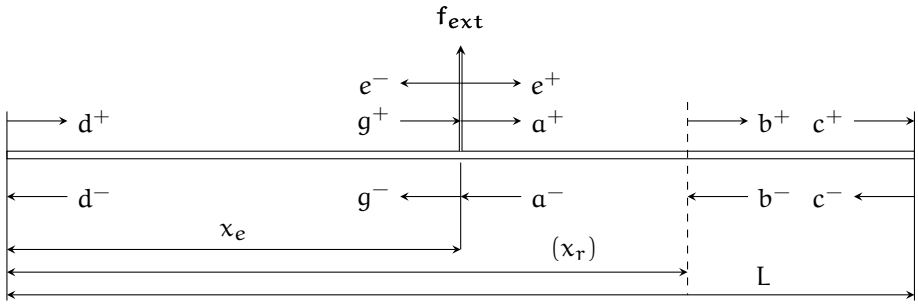

Figure 3.13: Waves in a finite structure excited by point load [66]

In general, the forced response is calculated by projecting the equation of motion onto the wave basis defined in Eqs. (3.43),(3.44). Typically, the wave approach involves the following steps [81, 121, 122]:

- calculation of the amplitudes of the direct excited waves in an infinite waveguide, excited by a punctual excitation;
- calculation of the reflection matrices at boundaries or other discontinuities;
- calculation of the propagating waves in the waveguide;
- sum of all the involved waves, due to excitation, propagation and reflection;
- determining of the physical response by superimposing waves' amplitudes at a desired response point.

The problem is schematically represented in Figure 3.13. The force f_{ext} generates n pairs of directly excited waves propagating in positive ($\mathbf{e}^+$) and negative ($\mathbf{e}^-$) directions. The travelling waves propagate toward the boundaries. The incident waves ($\mathbf{c}^+$ and $\mathbf{d}^-$) impinge on the boundaries, and then they are reflected ($\mathbf{c}^-$ and $\mathbf{d}^+$). Hence, in the steady state condition, at the excitation point, the sum waves ($\mathbf{a}^+$ and $\mathbf{g}^-$) are obtained as the sum of the directly excited waves and the waves propagating from the boundaries ($\mathbf{g}^+$ and $\mathbf{a}^-$). In next paragraphs, the amplitudes of all the involved waves are calculated.

DIRECTLY EXCITED WAVES

Consider a point on an infinite one-dimensional waveguide excited by a harmonic point force f_{ext}. Waves are then induced, propagating outwards from the excitation point in both the positive and negative directions. In order to calculate their amplitudes $\mathbf{e}^+$ and $\mathbf{e}^-$, continuity and equilibrium conditions at the excitation point are projected onto the wave basis through the transformation defined in Eq. (3.45). The transformation on the wave domain can be expressed in extended form as:

$$\begin{Bmatrix} \mathbf{q} \\ \mathbf{f} \end{Bmatrix} = \begin{bmatrix} \mathbf{\Phi}_q^+ & \mathbf{\Phi}_q^- \\ \mathbf{\Phi}_f^+ & \mathbf{\Phi}_f^- \end{bmatrix} \begin{Bmatrix} \mathbf{e}^+ \\ \mathbf{e}^- \end{Bmatrix}. \tag{3.55}$$

Applying the continuity of displacements ($\mathbf{q}^+ = \mathbf{q}^-$) and the equilibrium of the force ($\mathbf{f}^+ - \mathbf{f}^- = \mathbf{f}_{ext}$) at the excitation point [84], it follows that

$$\boldsymbol{\Phi}_q^+ \, \mathbf{e}^+ - \boldsymbol{\Phi}_q^- \, \mathbf{e}^- = \mathbf{0}, \tag{3.56}$$

$$\boldsymbol{\Phi}_f^+ \, \mathbf{e}^+ - \boldsymbol{\Phi}_f^- \, \mathbf{e}^- = \mathbf{f}_{ext}, \tag{3.57}$$

and in matrix form

$$\begin{bmatrix} \boldsymbol{\Phi}_q^+ & -\boldsymbol{\Phi}_q^- \\ \boldsymbol{\Phi}_f^+ & -\boldsymbol{\Phi}_f^- \end{bmatrix} \begin{Bmatrix} \mathbf{e}^+ \\ \mathbf{e}^- \end{Bmatrix} = \begin{Bmatrix} \mathbf{0} \\ \mathbf{f}_{ext} \end{Bmatrix}. \tag{3.58}$$

In the case that all the n wavemodes are considered for the wave basis, the amplitudes of the directly excited waves can be determined from Eq. (3.58) as

$$\begin{Bmatrix} \mathbf{e}^+ \\ \mathbf{e}^- \end{Bmatrix} = \begin{bmatrix} \boldsymbol{\Phi}_q^+ & -\boldsymbol{\Phi}_q^- \\ \boldsymbol{\Phi}_f^+ & -\boldsymbol{\Phi}_f^- \end{bmatrix}^{-1} \begin{Bmatrix} \mathbf{0} \\ \mathbf{f}_{ext} \end{Bmatrix}. \tag{3.59}$$

However, the inversion of the matrix can lead to numerical errors since it could be ill-conditioned, especially for complicated structures. As specified in Section 3.1.4, the highest order wavemodes are usually excluded from the wave basis, leading to the matrix in Eq. (3.58) being no longer square: in this case, a pseudo-inverse could be calculated, or singular value decomposition used [66]. A solution to avoid this kind of problem is exploiting the orthogonality of the left and right eigenvectors, expressed by Eq. (3.35). In fact, premultiplying Eq. (3.58) by the matrix of left eigenvectors properly rearranged (in this work, the left eigenvectors are partitioned differently from how is described by Waki et al. [66]), provides

$$\begin{bmatrix} \boldsymbol{\Psi}_q^+ & \boldsymbol{\Psi}_f^+ \\ \boldsymbol{\Psi}_q^- & \boldsymbol{\Psi}_f^- \end{bmatrix} \begin{bmatrix} \boldsymbol{\Phi}_q^+ & -\boldsymbol{\Phi}_q^- \\ \boldsymbol{\Phi}_f^+ & -\boldsymbol{\Phi}_f^- \end{bmatrix} \begin{Bmatrix} \mathbf{e}^+ \\ \mathbf{e}^- \end{Bmatrix} = \begin{bmatrix} \boldsymbol{\Psi}_q^+ & \boldsymbol{\Psi}_f^+ \\ \boldsymbol{\Psi}_q^- & \boldsymbol{\Psi}_f^- \end{bmatrix} \begin{Bmatrix} \mathbf{0} \\ \mathbf{f}_{ext} \end{Bmatrix}, \tag{3.60}$$

from which,

$$\begin{Bmatrix} \mathbf{e}^+ \\ -\mathbf{e}^- \end{Bmatrix} = \begin{bmatrix} \boldsymbol{\Psi}_q^+ & \boldsymbol{\Psi}_f^+ \\ \boldsymbol{\Psi}_q^- & \boldsymbol{\Psi}_f^- \end{bmatrix} \begin{Bmatrix} \mathbf{0} \\ \mathbf{f}_{ext} \end{Bmatrix}. \tag{3.61}$$

In conclusion, the amplitudes of the directly excited waves are calculated as

$$\begin{Bmatrix} \mathbf{e}^+ \\ \mathbf{e}^- \end{Bmatrix} = \begin{Bmatrix} \boldsymbol{\Psi}_f^+ \, \mathbf{f}_{ext} \\ -\boldsymbol{\Psi}_f^- \, \mathbf{f}_{ext} \end{Bmatrix}, \tag{3.62}$$

which is always well-conditioned.

BEHAVIOUR OF WAVES AT BOUNDARIES

As a wave travels through a finite structure, it will reach the end of the medium and/or encounter an obstacle or perhaps another medium through which it could travel. Waves incident upon discontinuities are reflected and transmitted (if not absorption is considered). Instead, in the case of elastic boundary conditions, an incident wave is only reflected, without any transmission. In this work, only classic boundary conditions (force-free, clamped, simply supported) are considered.

(Refer to works made by Mencik [32, 42] and Renno and Mace [77] for the calculation of scattering properties for general boundaries.)

When a generic wave $\mathbf{h}^+$, travelling in the positive direction, impinges on an elastic boundary on the right end side, a reflected wave $\mathbf{h}^-$, travelling in the opposite direction, is generated such that

$$\mathbf{h}^- = \mathbf{R}\mathbf{h}^+ \tag{3.63}$$

where $\mathbf{R}$ is the matrix of reflection coefficients, which depends on the type of constraint.

In general, each boundary condition can always be expressed in the form

$$\mathbf{A}\mathbf{f} + \mathbf{B}\mathbf{q} = \mathbf{o}. \tag{3.64}$$

Projecting the DOFs and force onto the wave domain through Eq. (3.55) gives

$$\begin{aligned} &\mathbf{A}\left(\mathbf{\Phi}_f^+ \mathbf{h}^+ + \mathbf{\Phi}_f^- \mathbf{h}^-\right) + \mathbf{B}\left(\mathbf{\Phi}_q^+ \mathbf{h}^+ + \mathbf{\Phi}_q^- \mathbf{h}^-\right) = \\ &= \mathbf{h}^+\left(\mathbf{A}\,\mathbf{\Phi}_f^+ + \mathbf{B}\,\mathbf{\Phi}_q^+\right) + \mathbf{h}^-\left(\mathbf{A}\,\mathbf{\Phi}_f^- + \mathbf{B}\,\mathbf{\Phi}_q^-\right) = \mathbf{o}, \end{aligned} \tag{3.65}$$

from which

$$\mathbf{h}^- = -\left(\mathbf{A}\,\mathbf{\Phi}_f^- + \mathbf{B}\,\mathbf{\Phi}_q^-\right)^{-1}\left(\mathbf{A}\,\mathbf{\Phi}_f^+ + \mathbf{B}\,\mathbf{\Phi}_q^+\right)\mathbf{h}^+ = \mathbf{R}\mathbf{h}^+. \tag{3.66}$$

Hence, in general, the reflection matrix $\mathbf{R}$ can be expressed as

$$\mathbf{R} = -\left(\mathbf{A}\,\mathbf{\Phi}_f^- + \mathbf{B}\,\mathbf{\Phi}_q^-\right)^{-1}\left(\mathbf{A}\,\mathbf{\Phi}_f^+ + \mathbf{B}\,\mathbf{\Phi}_q^+\right). \tag{3.67}$$

An analogous expression can be found for waves reflected from the left boundaries, such as $\mathbf{h}^+ = \mathbf{L}\mathbf{h}^-$, i.e.

$$\mathbf{L} = -\left(\mathbf{A}\,\mathbf{\Phi}_f^+ + \mathbf{B}\,\mathbf{\Phi}_q^+\right)^{-1}\left(\mathbf{A}\,\mathbf{\Phi}_f^- + \mathbf{B}\,\mathbf{\Phi}_q^-\right). \tag{3.68}$$

The elements of the matrices $\mathbf{A}$ and $\mathbf{B}$ are in general complex and frequency dependent. They can be expressed in terms of the dynamic stiffness matrix [84, 121], but simple expression exists for the most common boundary conditions.

- For fixed boundary, $\mathbf{A} = \mathbf{o}$ and $\mathbf{B} = \mathbf{I}$, leading to

$$\mathbf{R} = -\left(\mathbf{B}\,\mathbf{\Phi}_q^-\right)^{-1}\left(\mathbf{B}\,\mathbf{\Phi}_q^+\right), \qquad \mathbf{L} = -\left(\mathbf{B}\,\mathbf{\Phi}_q^+\right)^{-1}\left(\mathbf{B}\,\mathbf{\Phi}_q^-\right). \tag{3.69}$$

- For force-free boundary, $\mathbf{A} = \mathbf{I}$ and $\mathbf{B} = \mathbf{o}$, leading to

$$\mathbf{R} = -\left(\mathbf{A}\,\mathbf{\Phi}_f^-\right)^{-1}\left(\mathbf{A}\,\mathbf{\Phi}_f^+\right), \qquad \mathbf{L} = -\left(\mathbf{A}\,\mathbf{\Phi}_f^+\right)^{-1}\left(\mathbf{A}\,\mathbf{\Phi}_f^-\right). \tag{3.70}$$

- For simply-supported boundary,

$$\mathbf{R} = -\mathbf{I}, \qquad \mathbf{L} = -\mathbf{I}. \tag{3.71}$$

The reflection coefficient matrix $\mathbf{R}$ and $\mathbf{L}$ gives the amplitudes of the reflected waves in terms of those of the incident waves. If $\mathbf{R}$ is a diagonal matrix, each wavemode reflects at the boundary without wavemode conversion. Finite, perhaps complex, off-diagonal terms in the reflection matrix represent wavemode conversion such that one type of incident wave will be scattered to other wavemodes.

PROPAGATING WAVES

The amplitude of all the waves changes as they propagating, depending on their own wavenumbers and the distance to be covered. Their variations can be derived by applying the definition of propagation constant. According to Figure 3.14, for instance, if the waveguide has n wave components, the waves' amplitudes at two points a distance x apart are given by

$$\mathbf{s}^+ = \mathbf{T}(x)\mathbf{h}^+, \tag{3.72}$$

where $\mathbf{T}(x)$ is the wave propagation matrix. It can be expressed as

$$\mathbf{T}(x) = diag\left(e^{-ik_1 x}, e^{-ik_2 x}, \cdots, e^{-ik_n x}\right). \tag{3.73}$$

All the elements of the wave propagation matrix have a magnitude less or equal to the unity, with the elements corresponding to the high order wavemodes being approximately zero.

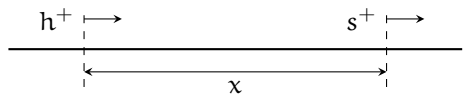

Figure 3.14: Waves propagation over a distance x

SUM OF WAVES

Once the amplitudes of directly excited, reflected and propagating waves are known, it is possible to calculate the waves' amplitudes at a given response point by considering the excitation and reflection relations together with the wave propagation laws.

First of all, the sum waves must be evaluated at a reference point, e.g. the driving point. Consider the finite waveguide represented in Figure 3.13. At the excitation point, the amplitudes of the waves $\mathbf{a}^+$ and $\mathbf{g}^-$ are given by the sum of the directly excited waves and the incident waves (which are the waves coming from the reflection at the boundaries), i.e.

$$\mathbf{a}^+ = \mathbf{e}^+ + \mathbf{g}^+ \tag{3.74}$$
$$\mathbf{g}^- = \mathbf{e}^- + \mathbf{a}^-. \tag{3.75}$$

At the right and left boundaries, the following reflection relations can be written:

$$\mathbf{c}^- = \mathbf{R}\mathbf{c}^+ \tag{3.76}$$
$$\mathbf{d}^+ = \mathbf{L}\mathbf{d}^-. \tag{3.77}$$

Along the waveguide, the following propagation relations hold:

$$\mathbf{g}^+ = \mathbf{T}(x_e)\mathbf{d}^+ \tag{3.78}$$
$$\mathbf{d}^- = \mathbf{T}(x_e)\mathbf{g}^- \tag{3.79}$$
$$\mathbf{a}^- = \mathbf{T}(L - x_e)\mathbf{c}^- \tag{3.80}$$
$$\mathbf{c}^+ = \mathbf{T}(L - x_e)\mathbf{a}^+ \tag{3.81}$$

According to Eqs. (3.74)-(3.81), it is possible to evaluate the unknown amplitudes $\mathbf{a}^+$ and $\mathbf{a}^-$. In particular, they are given by

$$\begin{aligned}
\mathbf{a}^+ &= \mathbf{e}^+ + \mathbf{g}^+ = \\
&= \mathbf{e}^+ + \mathbf{T}(x_e)\mathbf{d}^+ = \\
&= \mathbf{e}^+ + \mathbf{T}(x_e)\mathbf{L}\mathbf{d}^- = \\
&= \mathbf{e}^+ + \mathbf{T}(x_e)\mathbf{L}\mathbf{T}(x_e)\mathbf{g}^- = \\
&= \mathbf{e}^+ + [\mathbf{T}(x_e)\mathbf{L}\mathbf{T}(x_e)]\left(\mathbf{e}^- + \mathbf{a}^-\right) = \\
&= \mathbf{e}^+ + \mathbf{T}(x_e)\mathbf{L}\mathbf{T}(x_e)\mathbf{e}^- + \mathbf{T}(x_e)\mathbf{L}\mathbf{T}(x_e)\mathbf{T}(L-x_e)\mathbf{c}^- = \\
&= \mathbf{e}^+ + \mathbf{T}(x_e)\mathbf{L}\mathbf{T}(x_e)\mathbf{e}^- + \mathbf{T}(x_e)\mathbf{L}\mathbf{T}(L)\mathbf{R}\mathbf{c}^+ = \\
&= \mathbf{e}^+ + \mathbf{T}(x_e)\mathbf{L}\mathbf{T}(x_e)\mathbf{e}^- + \mathbf{T}(x_e)\mathbf{L}\mathbf{T}(L)\mathbf{R}\mathbf{T}(L-x_e)\mathbf{a}^+
\end{aligned} \tag{3.82}$$

$$\begin{aligned}
\mathbf{a}^- &= \mathbf{T}(L-x_e)\mathbf{c}^- = \\
&= \mathbf{T}(L-x_e)\mathbf{R}\mathbf{c}^+ = \\
&= \mathbf{T}(L-x_e)\mathbf{R}\mathbf{T}(L-x_e)\mathbf{a}^+ = \\
&= \mathbf{T}(L-x_e)\mathbf{R}\mathbf{T}(L-x_e)\left[\mathbf{e}^+ + (\mathbf{T}(x_e)\mathbf{L}\mathbf{T}(x_e))\left(\mathbf{e}^- + \mathbf{a}^-\right)\right] = \\
&= \mathbf{T}(L-x_e)\mathbf{R}\mathbf{T}(L-x_e)\mathbf{e}^+ + [\mathbf{T}(L-x_e)\mathbf{R}\mathbf{T}(L)\mathbf{L}\mathbf{T}(x_e)]\left(\mathbf{e}^- + \mathbf{a}^-\right)
\end{aligned} \tag{3.83}$$

In conclusion:

$$\mathbf{a}^+ = [\mathbf{I} - \mathbf{T}(x_e)\mathbf{L}\mathbf{T}(L)\mathbf{R}\mathbf{T}(L-x_e)]^{-1}\left[\mathbf{e}^+ + \mathbf{T}(x_e)\mathbf{L}\mathbf{T}(x_e)\mathbf{e}^-\right] \tag{3.84}$$

$$\mathbf{a}^- = [\mathbf{I} - \mathbf{T}(L-x_e)\mathbf{R}\mathbf{T}(L)\mathbf{L}\mathbf{T}(x_e)]^{-1}\left[\mathbf{e}^- + \mathbf{T}(L-x_e)\mathbf{R}\mathbf{T}(L-x_e)\mathbf{e}^+\right] - \mathbf{e}^- \tag{3.85}$$

The adopted approach allows numerical stability. In fact, the above solutions are well-conditioned because the matrices being inverted are diagonally dominant and the element of the wave propagation matrices are less than or equal to the unity.

RESPONSE CALCULATION

In order to calculate the response at a desired point of the structure, the waves' amplitudes must be calculated in this point. Considering the response point with coordinate x_r, as shown in Figure 3.13. Since the sum waves are calculated in a reference point (in this case the driving point x_e) their amplitude at x_r depends only on the relative distance from x_e and can be easily evaluated by applying propagation laws. In fact:

- if $x_r > x_e$, then

$$\mathbf{b}^+ = \mathbf{T}(x_r - x_e)\mathbf{a}^+ \tag{3.86}$$

$$\mathbf{b}^- = \mathbf{T}(L-x_r)\mathbf{R}\mathbf{T}(L-x_r)\mathbf{b}^+ \tag{3.87}$$

- if $x_r < x_e$, then

$$\mathbf{b}^- = \mathbf{T}(x_e - x_r)\mathbf{g}^- \tag{3.88}$$

$$\mathbf{b}^+ = \mathbf{T}(x_r)\mathbf{L}\mathbf{T}(x_r)\mathbf{b}^- \tag{3.89}$$

- if $x_r = x_e$ (driving point), then

$$\mathbf{b}^+ = \mathbf{a}^+ \tag{3.90}$$
$$\mathbf{b}^- = \mathbf{a}^- \tag{3.91}$$

Finally, the response in the physical domain can be obtained by substituting the expression for the amplitudes of the waves $\mathbf{b}^+$ and $\mathbf{b}^-$ in the Eq. (3.55).

3.2.1 Examples: forced response

Using the analytic definition of mass and stiffness matrices for rod and beam elements, defined in Section 3.1.6, the forced response of analogous one-dimensional finite structures is estimated through WFEM, and then compared to theoretical results.

3.2.1.1 *Rod*

Consider a rod, $L = 2\,\text{m}$ long, obtained by replicating the rod cell described in Section 3.1.6.1, and suppose it is clamped on the left side and free on the other one. On the rod, a harmonic axial force with magnitude $F = 1\,\text{N}$ acts on the free edge. A damping coefficient $\eta = 0.02$ is considered. The cell length is $\Delta = 0.001\,\text{m}$.

The analytical solution for this problem is provided by [123]

$$u(x) = \frac{F}{k_l A E_c} \frac{\sin(k_l x_r)}{\cos(k_l L)} = \frac{F}{\frac{2\pi f}{c_l} A E_c} \frac{\sin\left(\frac{2\pi f}{c_l} x_r\right)}{\cos\left(\frac{2\pi f}{c_l} L\right)}. \tag{3.92}$$

In Figure 3.15, the Frequency Response Functions (FRFs) calculated at the free edge (driving point) and at the half-length of the rod are represented, showing that the numerical-theoretical correlation is perfect since the marks (theoretical calculation) lie on the solid line (numerical estimation).

3.2.1.2 *Beam*

Consider now a beam, $L = 1\,\text{m}$ long, modelled according the Euler-Bernoulli theory. The structure is obtained by replicating along the longitudinal axis a beam cell $0.001\,\text{m}$ long, as described in Section 3.1.6.2. The structure is damped, with a hysteretic damping coefficient $\eta = 0.02$. Suppose the beam is simply supported on both side, i.e. only rotations allowed. At $x_f = 0.75L$ (starting from the left side), a harmonic vertical point force with magnitude $F = 1\,\text{N}$ is applied.

The theoretical solution for calculation of the vertical displacement at a given point of the beam can be obtained by superimposing an infinite number of natural mode shapes [123]

$$v(x) = \frac{2F}{\rho A L} \sum_{j=1}^{\infty} \frac{1}{\omega^2 - \omega_j^2} \sin\left(\frac{j\pi x_f}{L}\right) \sin\left(\frac{j\pi x_r}{L}\right), \tag{3.93}$$

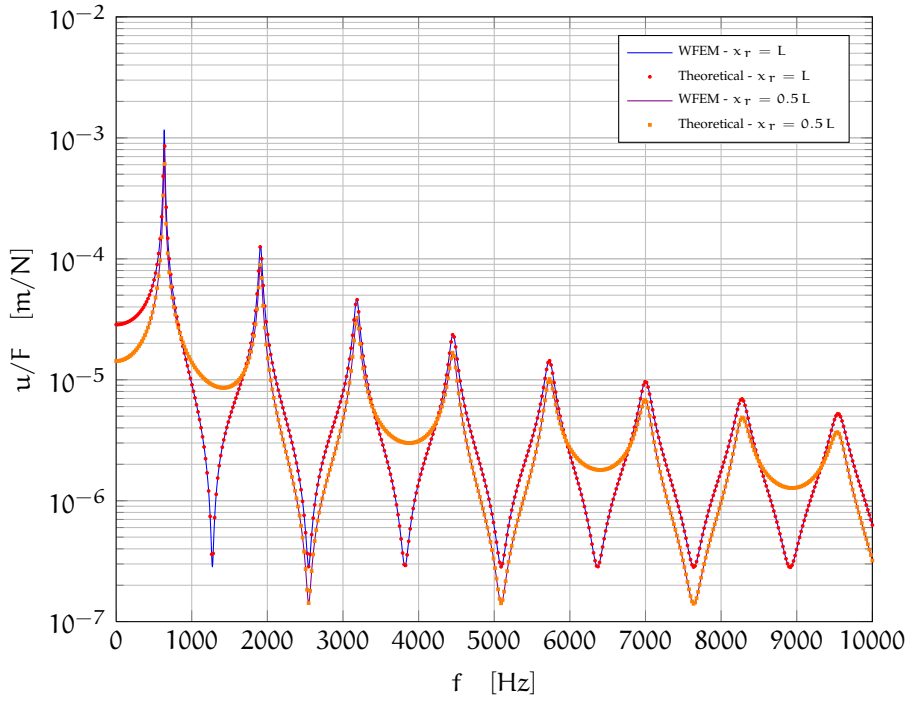

Figure 3.15: FRFs of longitudinal displacements a clamped-free rod excited at the free edge calculated through WFEM and theoretical approach

where the natural circular frequencies ω_j are given by

$$\omega_j = (j\pi)^2 \sqrt{\frac{E_c I_z}{\rho A L^4}} \tag{3.94}$$

As known, depending on the maximum frequency at which the dynamic response is calculated, a finite number of modes can be taken into account since the contribution of higher modes towards the response is negligible.

In Figure 3.16, FRFs of the vertical displacements calculated at the driving point and at the half-length of the beam are shown. For the analytic response, 150 modes have been retained. As in the case of the rod, the correlation is perfect. It is worth to remark that the accuracy of the WFEM calculation depends, as expected, on the length of the cell. At the same time, the analytic response depends on the number of natural modes taken into account. The great advantage of the WFEM over the modal approach is that the decrease of the cell length does not affect the computational time, whereas the increase of the number of modes determines a longer computation. Furthermore, the WFE model, based on a beam element 0.001 m long, has only 2 degree of freedom: if the beam was analysed by means of a FE analysis, meshed using beam elements with the same length of the WFE elementary cell, it should have 2000 DOFs.

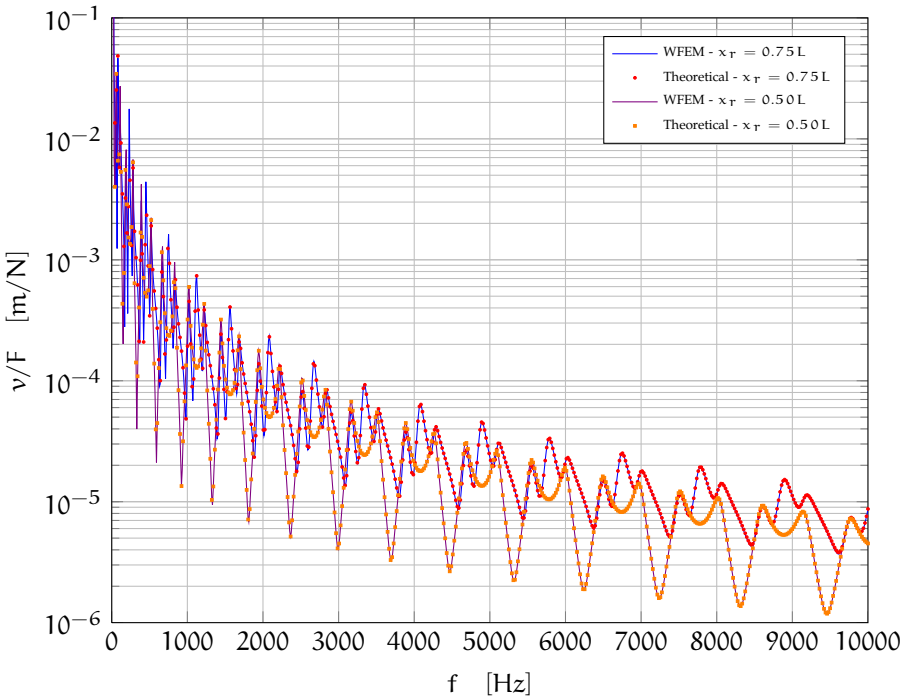

Figure 3.16: FRFs of vertical displacements of a simply-supported beam excited at 3/4L calculated through WFEM and theoretical approach

3.3 THE CODE FOR 1D-WFEM

A software package has been written in MATLAB® for the numerical analysis of wave propagation and forced response in periodic one-dimensional structures by means of the Wave and Finite Element Method. The code *WFEM1D.m* is here briefly described, according to the flow chart shown in Figure 3.17.

Before running the code *WFEM1D.m*, mass and stiffness matrices of the cell under investigation must be defined in a pre-processor phase. This can be done:

- by analytically definition, as done in Sections 3.1.6, if the waveguide cell can be modelled using simple finite elements;
- by importing the matrices from commercial finite element packages.

In the second case, the software ANSYS® is used as pre-processor to model the cell, and then to export the matrices into a text file in order to allow the importing in MATLAB® workspace. An example of the command list for ANSYS® is reported in Appendix A. Besides the commands needed to create the model, inserting material properties, nodes and elements, ANSYS® allows the exportation onto a text file of mass and stiffness matrices through the substructuring analysis, performed with the command:

```
ANTYPE,SUBSTR
```

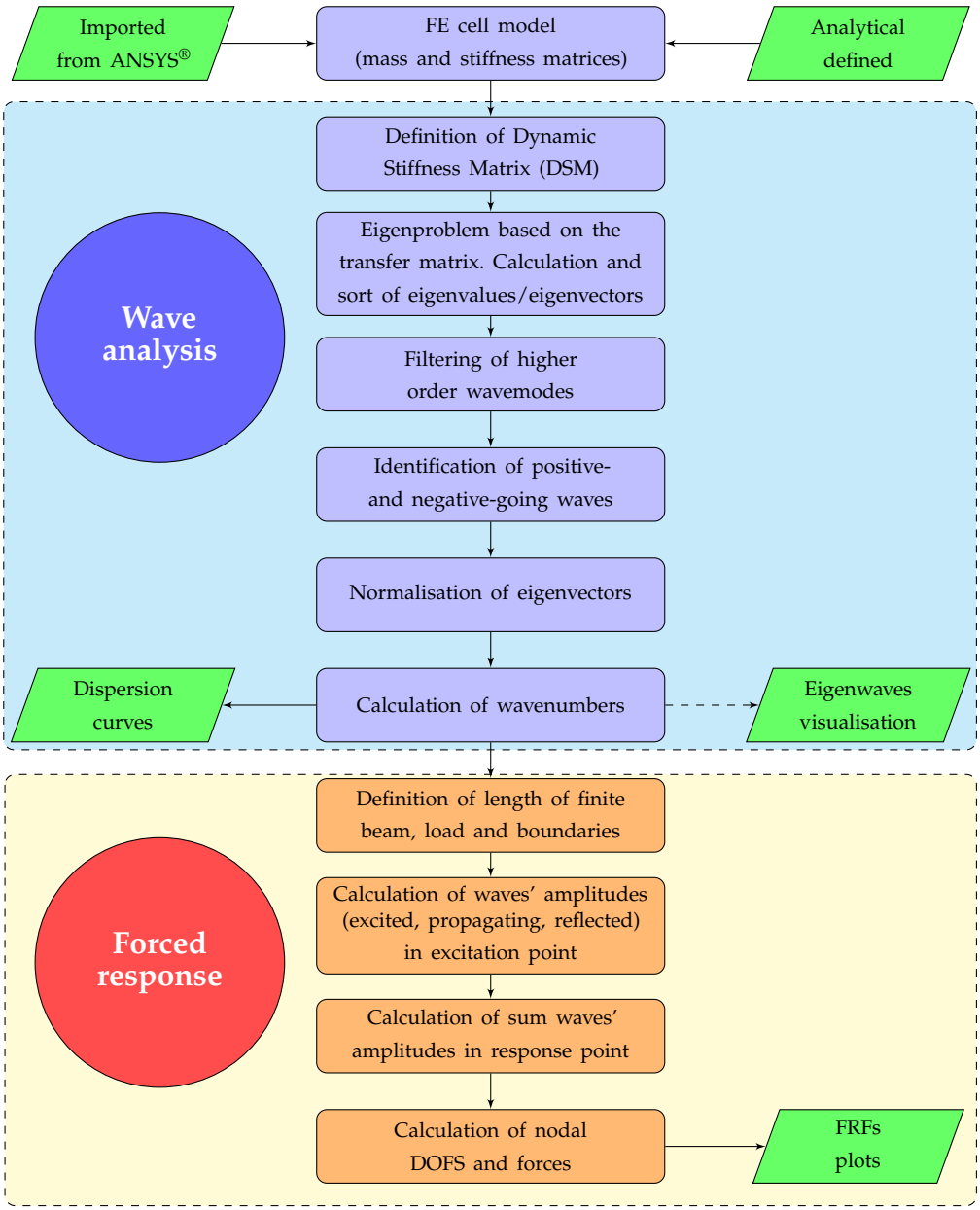

Figure 3.17: Flow chart of the code *WFEM1D.m*

.

The substructure analysis, in general, is used to reduce the system matrices to a smaller set of degrees of freedom through condensation techniques [124, 125]. With the command

```
SEOPT,MATRICES_NAMES,3,1
```

both mass and stiffness matrices are carried out, whereas

```
M,ALL,ALL
```

defines the master nodes and DOFs on which the matrices must be projected. In this case, all the nodes and relative DOFs are defined as master. Once the matrices are written into text file, another MATLAB® function (*readansys.m*) is used to import them in MATLAB® workspace.

After mass and stiffness matrices of the cell have been imported, the code *WFEM1D.m* can be start. First of all, the frequency range, in which the analysis must be performed, is defined. The Dynamic Stiffness Matrix is calculated (Eq. (3.6)), and then the transfer matrix can be written according to Eq. (3.19). At each frequency of interest, the eigenvalue and the eigenvectors of the transfer matrix are calculated and sorted.

The sorting of the eigenvalues is a time consuming task, performed through the calculation of the Modal Assurance Criterion (MAC) between the sets of eigenvectors carried out at two consecutive frequencies. The MAC is a mathematical tool used to compare two vectors [98]. The MAC between two mode shapes $\boldsymbol{\Phi}_{\omega 1}$ and $\boldsymbol{\Phi}_{\omega 2}$, calculated at the two frequencies ω_1 and ω_2, is defined as:

$$MAC\left(\boldsymbol{\Phi}_{\omega 1}, \boldsymbol{\Phi}_{\omega 2}\right) = \frac{\left|\boldsymbol{\Phi}_{\omega 1}^{*\mathrm{T}}\, \boldsymbol{\Phi}_{\omega 2}\right|^2}{\left(\boldsymbol{\Phi}_{\omega 1}^{*\mathrm{T}}\, \boldsymbol{\Phi}_{\omega 2}\right)\left(\boldsymbol{\Phi}_{\omega 1}^{*\mathrm{T}}\, \boldsymbol{\Phi}_{\omega 2}\right)}. \tag{3.95}$$

A MAC value close to 1 indicates a high degree of correlation between the two mode shapes. The time needed for the sort of the eigenvalues depends on the number of DOFs of the model and on the number of frequency considered.

Once eigensolutions are obtained and sorted, the wave analysis continues following the steps described in Section 3.1.

- The higher order wavenumbers are filtered (see Section 3.1.3.3) in order to define the reduced wave basis.
- Positive- and negative-going waves are identified (Eq. (3.28)).
- Right eigenvectors are normalised (Eq. (3.35)).
- The wavenumbers are calculated as a function of the frequency (Eq. (3.38)).
- The dispersion curves (and eventually the eigenwaves) are plotted.

Once the wave analysis is performed, the forced response starts, following the steps listed in Section 3.2. The length of the finite structure must be defined, together with the position of the force along the structure and the position of the response point. The load is hence set, according to the DOFs of the cell. Then, the boundary condition matrices are defined (Eqs. (3.67) and (3.68)) and the amplitudes of directly excited, propagating and reflected waves are calculated in the

driving point. At the end, the amplitudes of the sum waves are evaluated at the response point, and then transformed in the physical domain to calculate nodal displacement and force to plot FRFs.

CODE RESTRICTIONS

The code presents some limitations.

- The use of substructuring analysis in ANSYS® determines that the elements must have constant stiffness, damping, and mass effects (e.g. material properties do not change with temperature).
- The filtering of higher order eigenvalues is still user-based, since it is not possible yet to establish a general criterion.
- The structure can be excited only at one point, and the response can be evaluated in one point as well.
- Only the classical elastic boundary conditions (free, clamped and simply supported) can be applied to the sides of the structure.

3.4 RESULTS

In this section, the wave propagation and the dynamic response of different types of one-dimensional waveguides and finite structures are investigated through the Wave and Finite Element Method. Besides the examples reported in Sections 3.1.6 and 3.2.1, showing the perfect agreement with analytical solution for simple waveguides, the goal of this section is to validate this approach comparing the results with full FEM results, as well as with analytical, numerical and experimental ones available in literature. At the end, the forced response of a hybrid sandwich beam is estimated through WFEM and compared to those of performed experimental test.

3.4.1 Effect of the Finite Element discretisation on dispersion curves

Consider a steel infinite beam, whose material properties and geometrical attributes are reported in Table 3.2.

For this type of waveguide, different eligible finite elements are available in the commercial package ANSYS®. Herein, four different elements are considered (BEAM3, BEAM4, BEAM188, SOLID45 [126]) in order to analyse the influence of the chosen finite element for modelling the cell, as well as the length of the cell, on the results obtained through WFEM.

BEAM ELEMENTS

The use of three different linear (2-node) beam elements, to model the elementary cell, is investigated.

BEAM3 is a uni-axial element with tension, compression, and bending capabilities. The element has three degrees of freedom at each node: translations in the

Table 3.2: Characteristics of the elementary cell

Young modulus E	2.1e11	GPa
Poisson ratio ν	0.33	
Density ρ	7800	kg/m^3
Section	Square	
Cross-section area A	$1e{-}6$	m^2
Moment of inertia I_z	$8.33e-14$	m^4

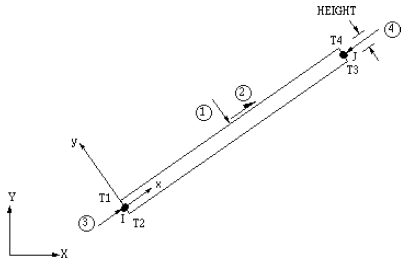

(a) *BEAM3*

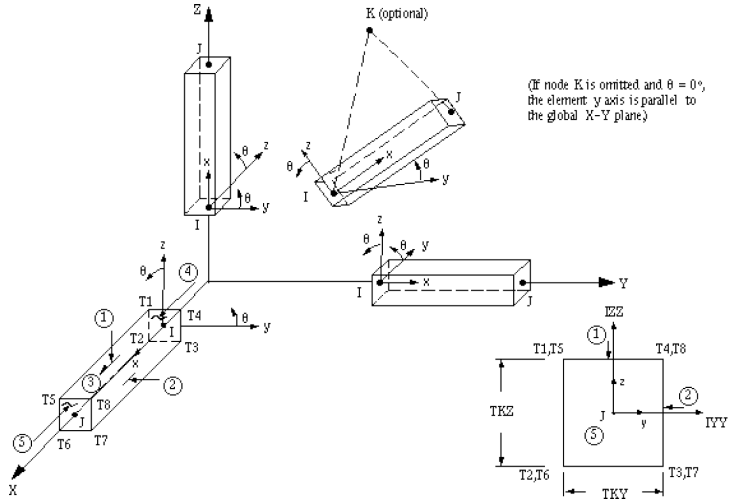

(b) *BEAM4*

Figure 3.18: BEAM3 and BEAM4 elements [126]

nodal x and y directions and rotation about the nodal z-axis. Hence, it is able to describe the motion only in the plane x-y.

BEAM4 is the same as BEAM3, but the motion is described in three dimensions. In fact, it considers also the torsion capability and has six degrees of freedom at each node: translations in the nodal x, y, and z directions and rotations about the nodal x, y, and z axes.

Usually, BEAM3 and BEAM4 (shown in Figure 3.18 [126]) are based on the Euler-Bernoulli beam model, i.e. the effect of shear deformation is neglected. These elements are usually used for analysing slender beams.

BEAM188 is a beam element in three dimensions with six degree of freedom at each node, as BEAM4. The main difference is that this element is based on Timoshenko beam theory, and hence it is suitable for analysing slender to moderately thick beam structures.

In Figure 3.19, the dispersion curves (related to the positive-going waves) obtained by using the three beam elements are shown. No damping is considered. As can be observed, the three elements lead to the same results, corresponding to the analytical ones as well. Obviously, since the element BEAM3 has only vertical displacement and rotation as nodal DOFs, the dispersion curve related to the shear wave cannot be predicted. Furthermore, elements BEAM4 and BEAM188 describe the motion in three dimensions, and hence they are able to describe the wave motion involving both cross-section displacements. In this case, since a square cross-section is considered, the wavenumbers corresponding to the bending in the two flexural planes are coincident. The effect of the length of the el-

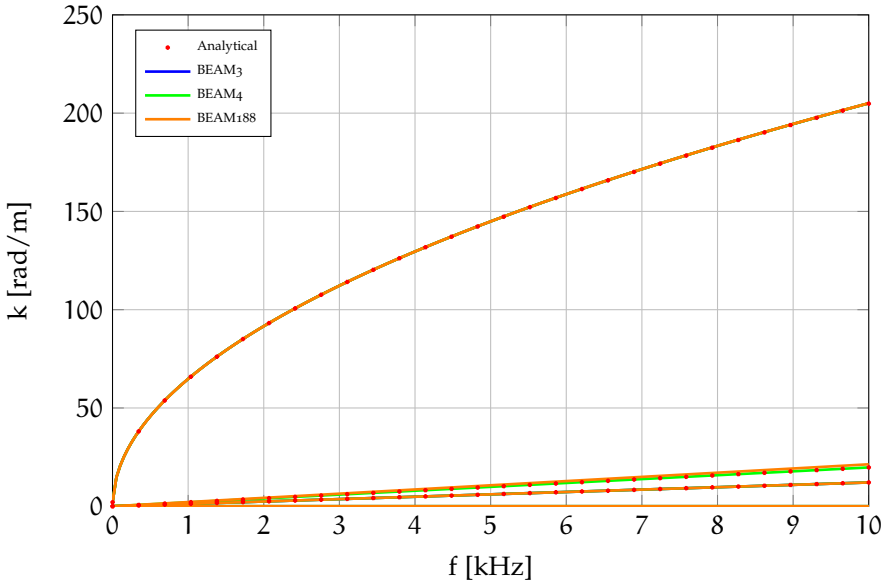

Figure 3.19: Effect of different ANSYS® beam elements on the dispersion curves ($\Delta = 0.001$ m)

ementary cell is also investigated. In Figure 3.20, the dispersion curves for the steel cell are plotted for three different lengths. The cell is modelled by using a BEAM4 element. The results show that the calculation of the longitudinal and the shear wavenumbers does not depend, in this frequency range, on the cell length. These wavenumbers, in fact, correspond to wavelength which can be well discretised even using the longest elementary cell ($\Delta = 0.01$ m). For what concerns the bending wavenumbers, instead, in the high frequency range the dispersion curve obtained with the longest cell deviates from the analytical solution, predicting

lower wavenumbers. In Figure 3.21, the zoom in the high frequency range allows to appreciate the difference between the curves, due exclusively to the finite element discretisation. Furthermore, it can be also observed that the curves obtained with the two shortest cells are overlaid, which means that the solution converges to the analytical one. However, the use of very small cell length can lead to numerical errors.

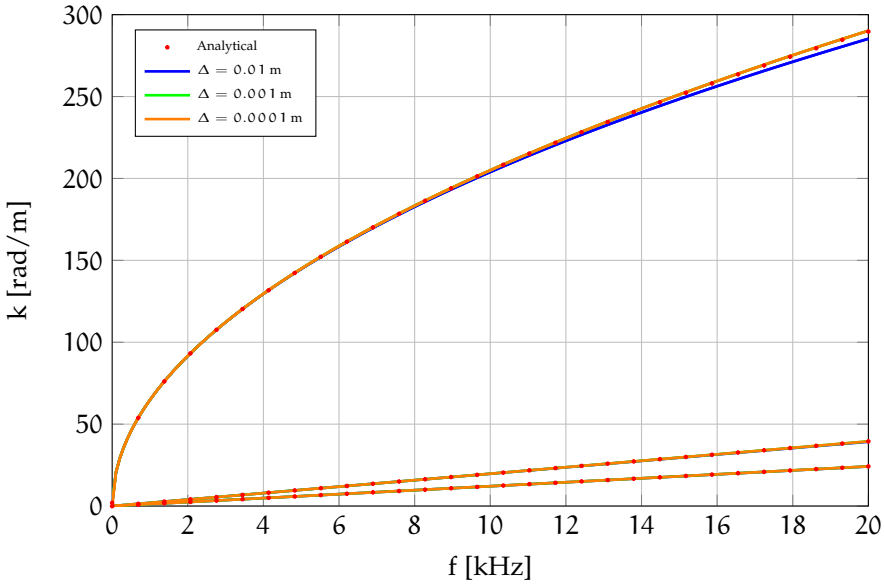

Figure 3.20: Influence of the length of the cell on dispersion relations (BEAM4)

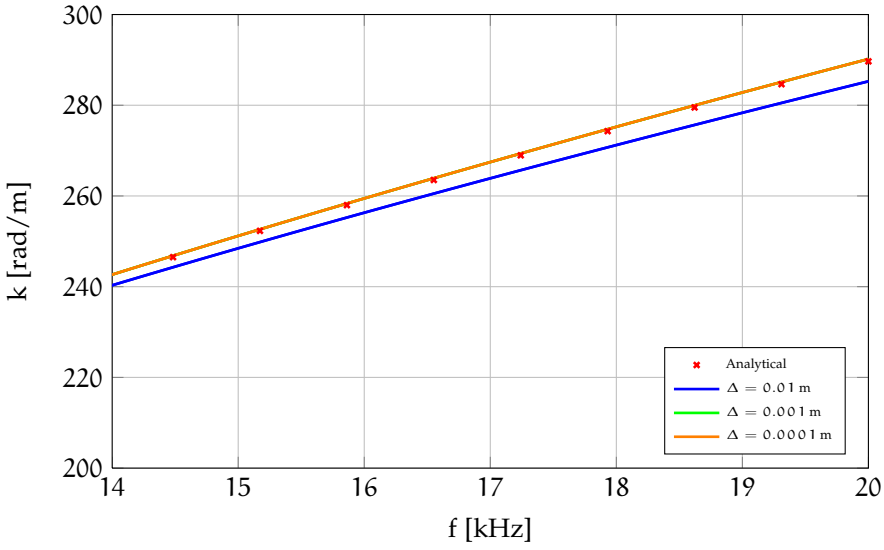

Figure 3.21: Influence of the length of the cell on dispersion relations - Zoom at high frequencies (BEAM4)

SOLID ELEMENTS

The use of beam elements does not allow to get information about the deformation of the cross-section, since both stiffness and matrix are projected on the neutral axis of the structures. Sometimes, the modelling of the waveguide by using brick elements can be very useful, as in the case of complex shape sections or when the beam is layered (as in the case of composite or sandwich beams). Besides the brick elements offered by ANSYS®, the use of the element SOLID45 is here investigated. SOLID45 is a 8-nodes element, with three degrees of freedom at each node, corresponding to the translations in x, y, and z directions (Figure 3.22).

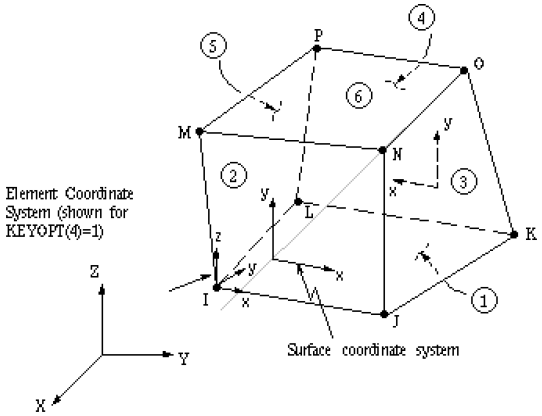

Figure 3.22: SOLID45 element [126]

The use of a solid element generally leads to an increasing of the number of degree of freedom of the model compared to the beam ones. In fact, beam elements have only two nodes (and maximum six DOFs per node). Instead, using solid elements, at least eight nodes must be taken into account if the waveguide is meshed with only one brick. Obviously, the number of DOFs increases as the number of solid elements used for discretise the section. First of all, similarly to the sensitivity analysis performed on the beam elements in the previous section, the effect of the length of the cell described in Table 3.2 is investigated. One solid element is used to model the cross-section. An example, obtained for $\Delta = 0.001$ m, is shown in Figure 3.23: the violet colour indicates the defined master degrees of freedom.

In Figure 3.24, the dispersion curves for two different lengths of the cell are shown. A damping coefficient $\eta = 0.01$ is included. In this case, the shortest cell is not able to describe the bending wavenumber at high frequency (as for the beam element), because the length of the cell is comparable to that of the wave. Furthermore, the use of SOLID45 leads to a wrong prediction of the bending wavenumber at low frequencies for both the lengths.

The error at low frequencies is due to the truncation of inertia terms in the Dynamic Stiffness Matrix, described in Section 3.1.5. This issue strongly depends on the material of the waveguide under investigation (among the length of the cell), in particular on the elastic modulus. Only with the goal to demonstrate that, it is possible to investigate how the accuracy of the numerical dispersion curves

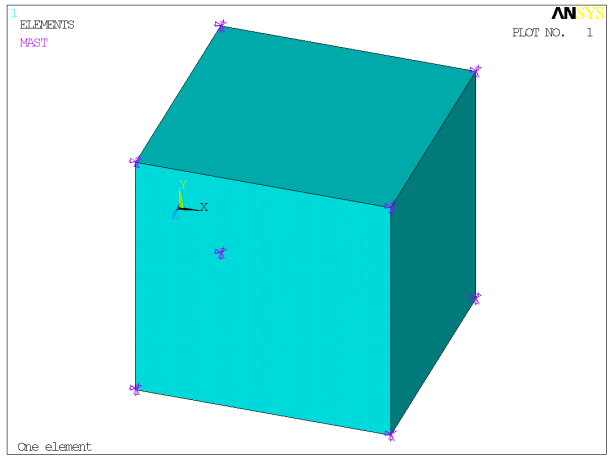

Figure 3.23: Waveguide cell modelled using one SOLID45

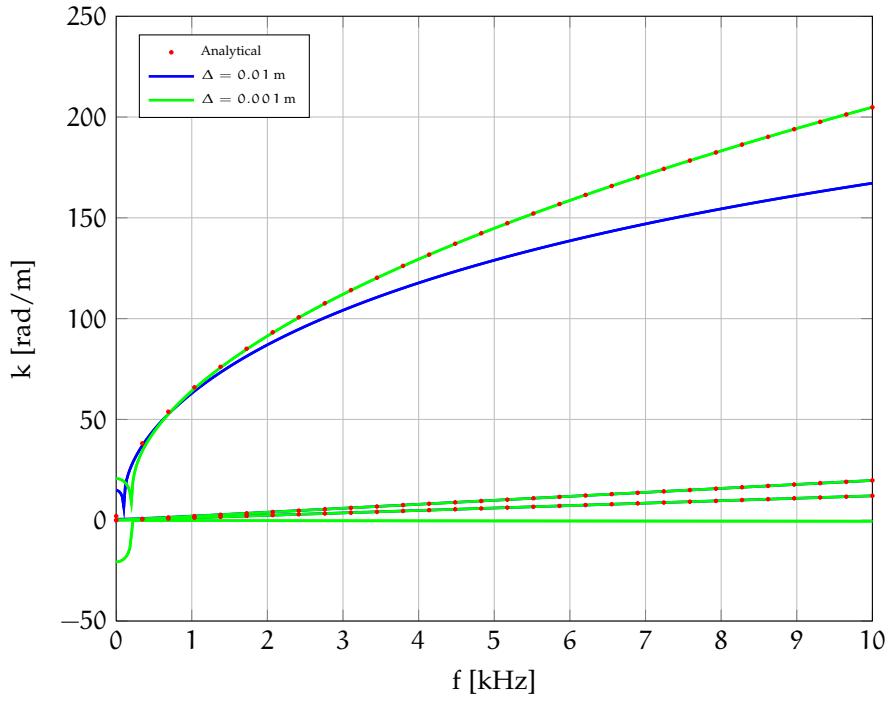

Figure 3.24: Influence of the length of the cell modelled using a SOLID45 element

respect to the analytical ones changes at low frequencies (range $0 - 500\,\text{Hz}$) as a function of Young modulus. Let's consider the same cubic cell of Figure 3.23, having a density $\rho = 7800\,\text{kg/m}^3$. In Figure 3.25, the dispersion curves are plotted for different elastic moduli (continuous curves: WFEM solution; only marks: analytic solution). It is evident that low values of Young modulus guarantee the convergence of the numerical solution to the analytical one. Instead, numerical errors occurs starting from $E = 1 \times 10^9\,\text{Pa}$.

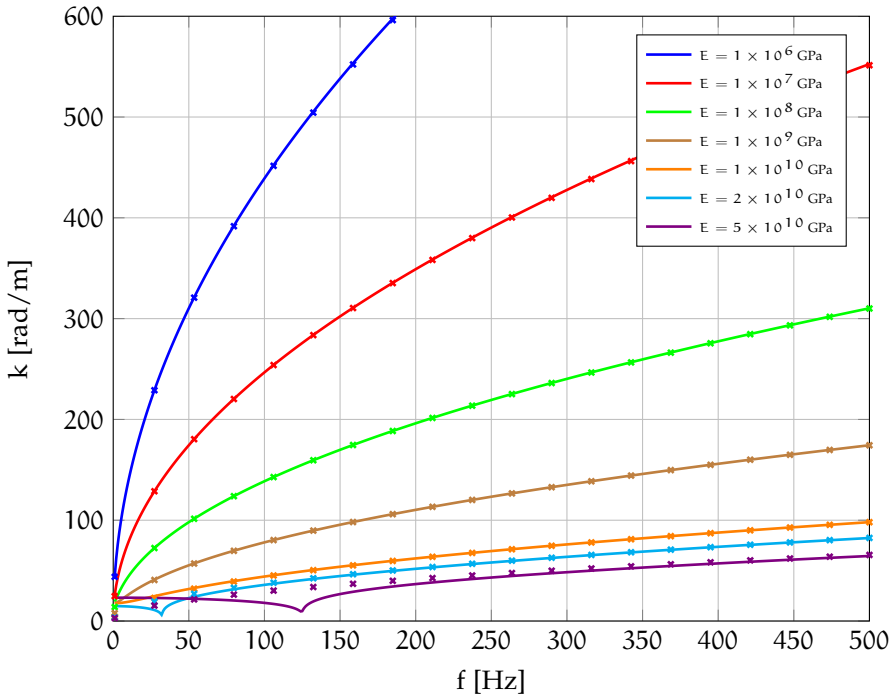

Figure 3.25: Influence of the elastic modulus on the bending wavenumber obtained through WFEM using SOLID45 element

Obviously, the material properties are fixed and they are not design variables, hence the round-off errors must be reduced in other ways. Waki et al. [66] suggest the use of finite element models with internal nodes, and then condense them. This technique is adopted in the case of the cubic cell under investigation, introducing an increasing number of internal nodes (in Figure 3.26, the FE model of the cell with 36 internal nodes is shown) by projecting the finite element matrices only onto the nodes on the edges of the cell. The dispersion curves of the steel cubic cell are reported for different number of condensed nodes in Figure 3.27. The number of condensed nodes strongly influences the numerical solution. Starting from the cell modelled without internal nodes, there is a reduction of the error by increasing the number of condensed nodes up to 12 (3 rows of internal nodes). However, condensing more nodes can lead to other numerical errors at low frequencies.

In conclusions, it can be highlighted that if solid elements are used to model the waveguide cross-section, the number of design variables further increases, because the round-off errors of the Dynamic Stiffness Matrix must be taken into account in the low frequency range. This issue must be addressed by the analyst, since it depends on the computer on which the code is working and its precision. As the frequency increases, the numerical solution of the bending wavenumber converges to the analytical one if the length of the cell is enough small compared to the wavelength (as in the case of the beam).

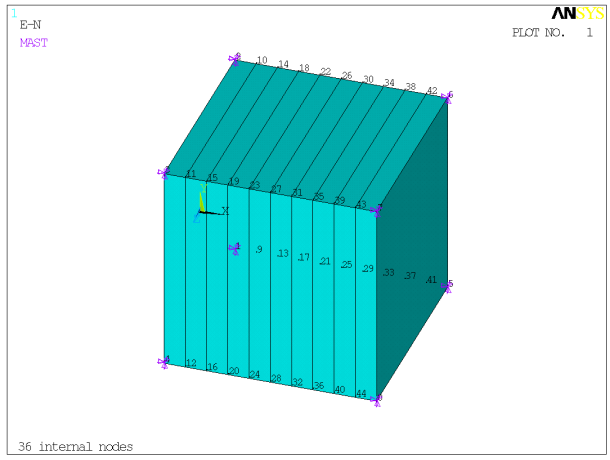

Figure 3.26: Waveguide cell modelled with 36 internal nodes

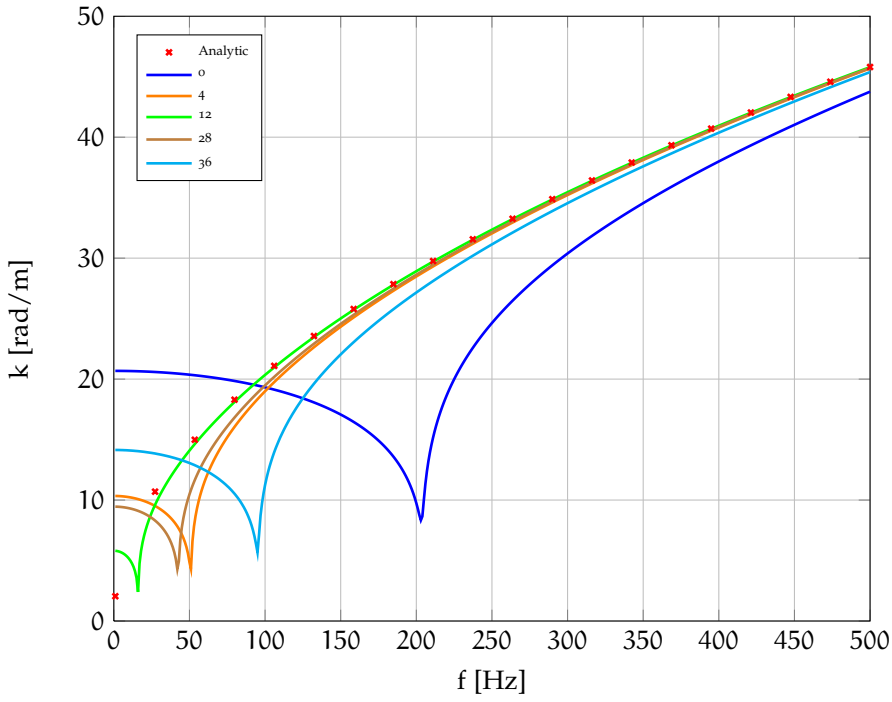

Figure 3.27: Influence of the number of condensed nodes on the bending wavenumber obtained through WFEM using SOLID45 element

During this work, using a double precision arithmetic, it has been possible the identification of given lengths, which guarantee the convergence of the solution at low frequencies on the computer used, but no criteria can be fixed since they depend on the type of computer machine and on the FE model of the waveguide section under investigation. For instance, if the steel waveguide with square cross-section is modelled by using one element, a length $\Delta = 0.0015\,\mathrm{m}$ guarantees a

good agreement at low frequencies, but if the waveguide is modelled using 2×2 element then the best length is $\Delta = 0.001\,71\,\text{m}$.

3.4.2 Forced response: first comparisons with full Finite Element Method

A cantilever aluminium beam, subject to different loads, is investigated through WFEM and FEM. The geometry is shown in Figure 3.28, where $L = 0.2\,\text{m}$, $b = 0.02\,\text{m}$ and $h = 0.004\,\text{m}$. A damping $\eta = 0.01$ is included. The goal is to compare the WFE and FE results using different element, such as BEAM3, BEAM4 and SOLID45.

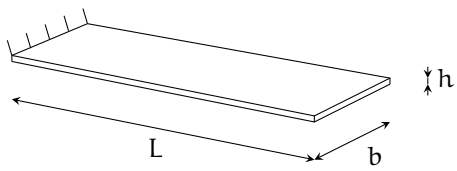

Figure 3.28: Clamped beam

BEAM3

A vertical load of magnitude $F_y = 1\,\text{N}$ and a bending moment $M_z = 1\,\text{Nm}$ are applied at the half length of the beam. For the WFE model, the elementary cell is long $\Delta = 0.002\,\text{m}$ and it is modelled using a BEAM3 element. The FE model of the beam is carried out in ANSYS®, using the same spatial mesh (leading to 100 beam elements).

In Figure 3.29, vertical displacement and rotation at the free side of the beam are plotted. The results obtained through WFEM and FEM are the same. Of course, the FE model presents 202 DOFs, whereas the WFEM only 2 with a corresponding reduction of the computational cost.

BEAM4

The same beam is modelled using BEAM4 elements, both for the ANSYS® model and for the elementary cell for the WFE model, in order to obtain the motion of the beam along the three principal axes x, y, z. The same spatial mesh, as in the previous case with BEAM3, is used. Thus, in this case the FE model has 606 DOFs, against the 6 of the WFE. Three unit forces, (F_x, F_y, F_z) are applied at the free tip of the beam, and corresponding displacements are estimated at $x_r = 3/4L = 0.15\,\text{m}$. Also in this case, the accordance between FE and WFEm results is perfect, since the curves in Figure 3.30 are overlapped.

SOLID45

The beam, subject to the same load conditions of the case modelled with BEAM4, is now modelled using SOLID45 elements. Depending of the number of elements used to discretise the cross-section, this kind of modelling can be attractive for more complex structures, where detailed information could be required. The elementary cell, shown in Figure 3.31a, is modelled by using 20 SOLID45 elements

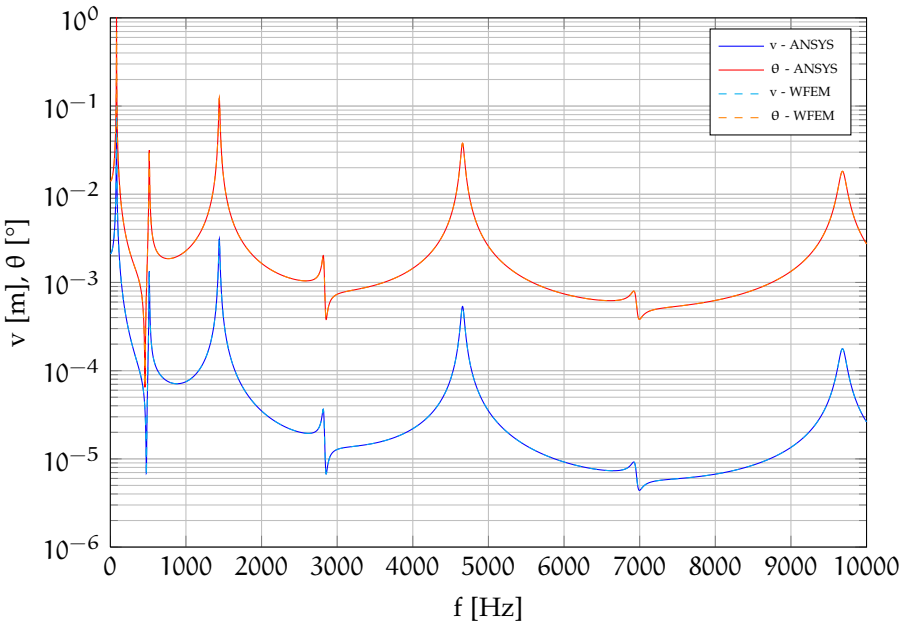

Figure 3.29: Vertical displacement and rotation about z direction at the free tip of a cantilever beam, excited at half length, modelled with BEAM3

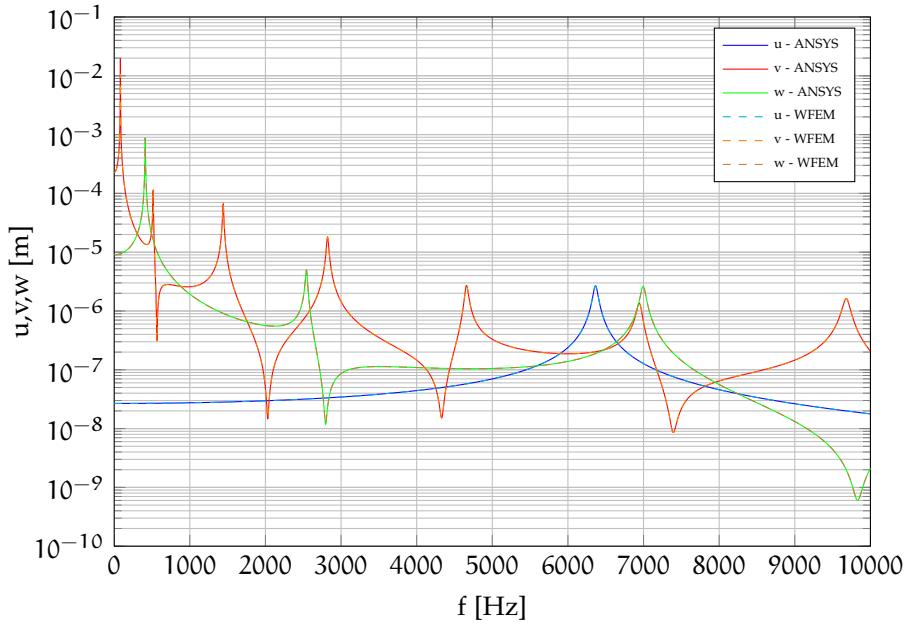

Figure 3.30: Displacements along x, y and z directions in the response point $x_r = 3/4L$ for a cantilever beam modelled with BEAM4, excited on the free tip

(i.e. 2×10 elements). The whole cantilever beam, modelled using the same el-

ement and same spatial discretisation, is shown in Figure 3.31b, constituted by 2000 brick elements.

In this case, Timoshenko theory is assumed to be valid, and the including of the shear deformation effects determines a variation of the previous results, as can be highlighted by comparing Figures 3.30 and 3.32. However, the FEM-WFEM comparison shows a very good accordance on the three displacement curves.

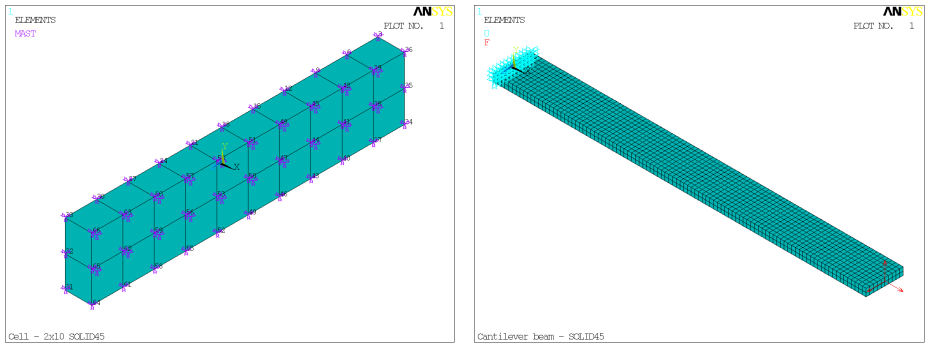

(a) *SOLID45 cell* ($\Delta = 0.002\,\mathrm{m}$) **(b)** *Cantilever beam - SOLID45*

Figure 3.31: Elementary cell and cantilever beam modelled using SOLID45 elements

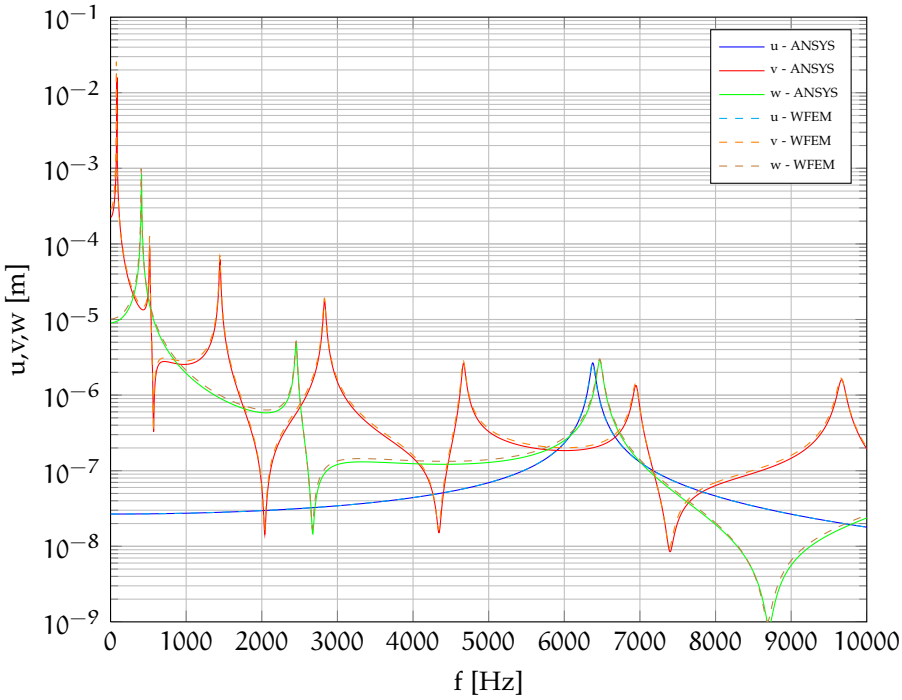

Figure 3.32: Displacements along x, y and z directions in the response point $x_r = 3/4L$ for a cantilever beam modelled with SOLID45, excited on the free tip

3.4.3 Comparison with literature results

In this section, the results obtained through the code *WFEM1D.m* are compared to those available in literature in terms of dispersion curves and forced response, providing an overview of the potential of the implemented method for different type of one-directional structures.

3.4.3.1 *Dispersion curves of a thin walled tubular waveguide*

In the previous sections, the results concern the analysis of solid beam structures. However, the method is also suitable to investigate thin walled structures. Consider, for instance, a steel waveguide ($E = 210\,GPA$, $\rho = 7850\,kg/m^3$, $\nu = 0.3$), having a tubular cross-section $40\,mm \times 60\,mm$, with a wall thickness $2\,mm$. Ichchou et al. [34] investigate through the WFEM the aliasing effect, providing also indication about the post-processing for the estimation of group velocities and energy velocities. In that work, the walls of the waveguide are modelled using thin shell elements. In this case, the elementary cell is modelled using SOLID45 elements. Each element has a square cross-section (length of the side $l = 2\,mm$) in order to uniformly mesh the waveguide cell. The length of the elementary cell is $\Delta = 1.2\,mm$. The finite element model, realised in ANSYS®, is shown in Figure 3.33.

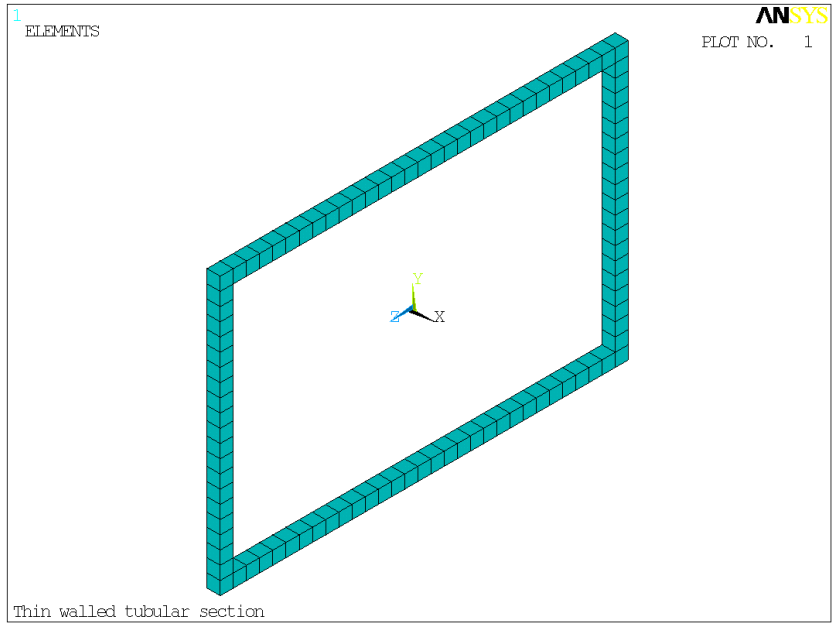

Figure 3.33: Thin walled tubular section modelled using SOLID45

In Figure 3.34, the dispersion curves of this waveguide are plotted, showing the good agreement with results available in literature. The small difference appreciable starting from 2500 Hz is probably due to the different finite element chosen for the discretisation.

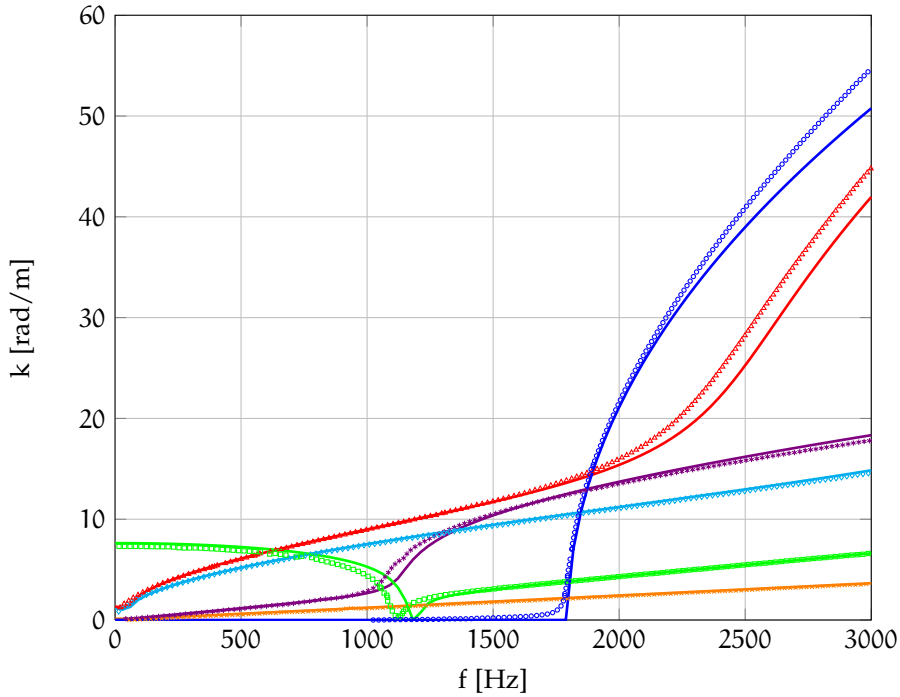

Figure 3.34: Dispersion curve for a tubular structure. Continuous curves: own WFEM code. Only marks: literature results [34]

3.4.3.2 *Dispersion curves of a simply supported plate strip*

Using the one-dimensional WFEM, it is also possible to investigate the bending waves travelling along a simply supported plate strip [58, 87], like that shown in Figure 3.35.

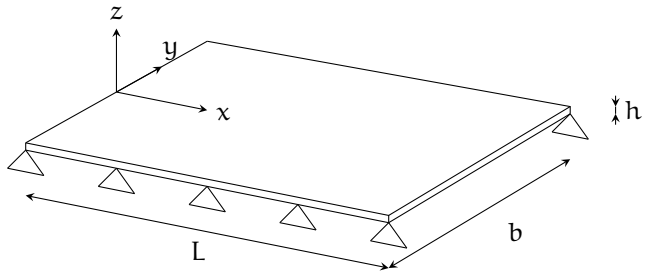

Figure 3.35: Simply supported plate strip

It is known that, for this kind of boundary conditions, propagating waves have a y dependence of sinusoidal form, whereas the variation along the longitudinal axis for the j-th wave can be expressed as [58]

$$k_{p,n}^2 = k_p^2 - \left(\frac{n\pi}{b}\right)^2 \quad k_{e,n}^2 = k_p^2 + \left(\frac{n\pi}{b}\right)^2, \tag{3.96}$$

where $k_p = \sqrt{\rho h \omega^2 / D}$ is the free plate wavenumber, with $D = \sqrt{Eh^3/12(1-\nu^2)}$ being the bending stiffness. Results are obtained for a steel strip, having thickness $h = 0.001\,m$ and width $b = 1\,m$. Since the strip is very thin, compared to the width, a plane element is suggested for FE modelling. In this case, SHELL63 element is used. This element has six degrees of freedom at each node: nodal translations in x, y, and z directions and rotations about the x, y, and z axes. The segment of the plate, with $\Delta_x = 0.02m$, is modelled in ANSYS® using 50 rectangular SHELL63 elements along y direction. Only the in-plane DOFs are considered in order to reduce the computational cost, and hence the model has 149 DOFs (considering also the boundary conditions). In Figure 3.36, analytical and numerical dispersion curves are shown for the first five positive-going waves. It is evident that for frequencies for which $k_p > n\pi/L$, the wavenumber $k_{p,n}$ represents a propagating wave, otherwise it is evanescent. The accordance of WFE results with the analytical ones (Eq. (3.96)) is quite good.

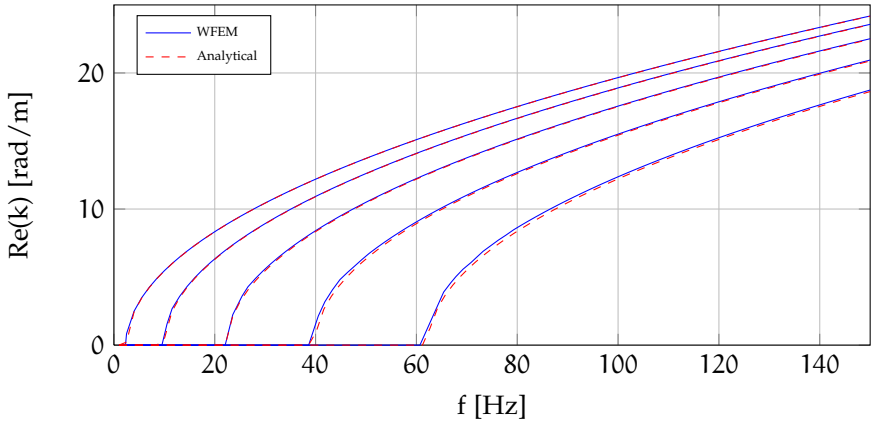

(a) *Real part of wavenumbers*

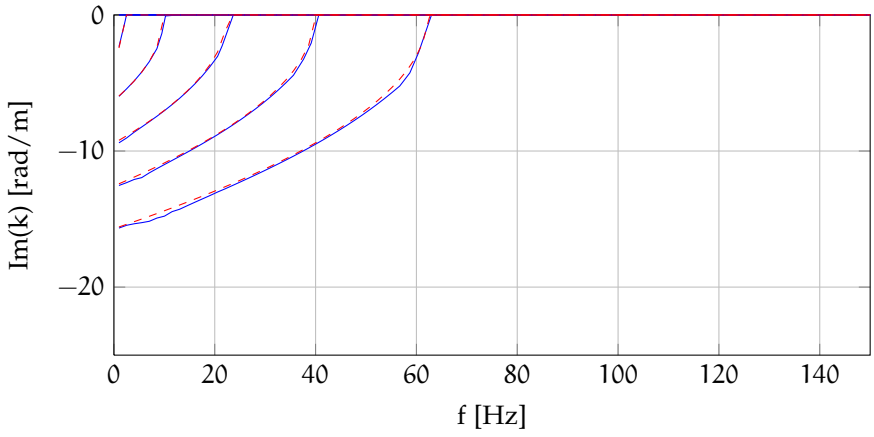

(b) *Imaginary part of wavenumbers*

Figure 3.36: Dispersion curves for a plate strip modelled using SHELL63 elements

3.4.3.3 *Forced response of laminated beam*

In the previous test-cases, only structures made of isotropic materials are investigated, but WFEM is suitable to analyse laminated and sandwich beams as well. For example, a cantilevered laminated beam is here investigated, as made by Renno and Mace [72]. The beam is made of four orthotropic layers of 1 mm thick glass-epoxy, having a density $\rho = 2000\,\mathrm{kg/m^3}$, with a stacking sequence $[0/45/-45/0]$ degrees.

Table 3.3: Mechanical properties of a glass/epoxy ply [72]

Young's moduli [GPa]			Shear moduli [GPa]			Poisson's ratios		
$E_{x'}$	$E_{y'}$	$E_{z'}$	$G_{x'y'}$	$G_{x'z'}$	$G_{y'z'}$	$\nu_{x'y'}$	$\nu_{x'z'}$	$\nu_{y'z'}$
54	4.8	54	1.78	3.16	2.33	0.313	0.06	0.028

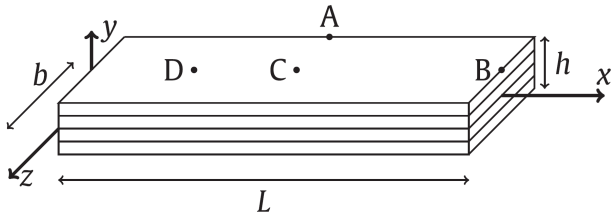

(a) *Beam dimensions [72]*

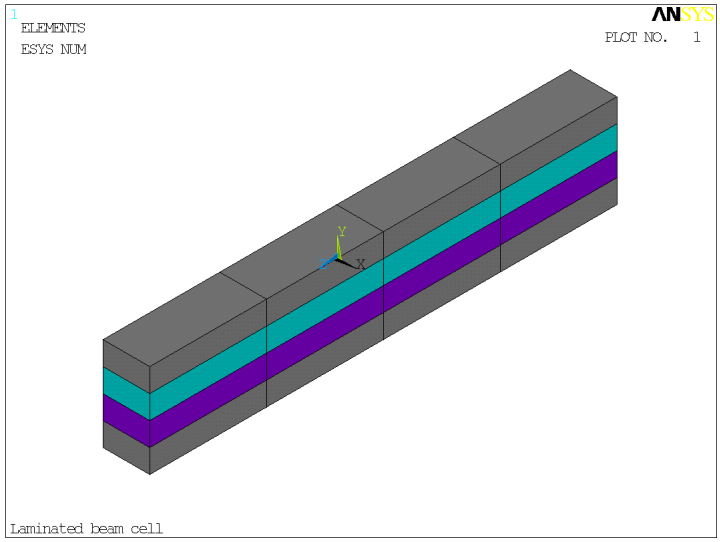

(b) *Cell modelled in ANSYS®*

Figure 3.37: Characteristics of the laminated beam

The mechanical properties of each glass-epoxy layer along their principal axes of orthotropy (x', y', z') are reported in Table 3.3. The dimension of the beam, shown in Figure 3.37a, are $L = 0.2\,m$, $b = 0.02\,m$ and $h = 0.004\,m$. The elementary section, long $\Delta = 0.002\,m$ is modelled using 4×4 SOLID45 elements, as shown in Figure 3.37b: different colors represent different orientation of the layers. The single section, hence, presents 75 DOFs on each side of the segment. The beam is excited in point A (0.5L, $h/2$, $-b/2$), and the response is evaluated in B (L, $h/2$, 0), C (L/2, $h/2$, 0), D (0.25L, $h/2$, 0). The results obtained through WFEM are compared to those of ANSYS® (7575 DOFs) in terms of displacement for a point force. Firstly, $F_x = 1\,N$ is applied in A, and then longitudinal displacements are reported in Figure 3.38. Vertical and transverse displacements are reported in Figures 3.39-3.40, for a unit force direct respectively along y and z axis. The WFEM results are obtained by retaining 16 wavemodes pairs, neglecting the higher-order ones. It can be noted that the FEA and WFEM results are in very good agreement, except for small differences at the anti-resonances of FRFs estimated on point C.

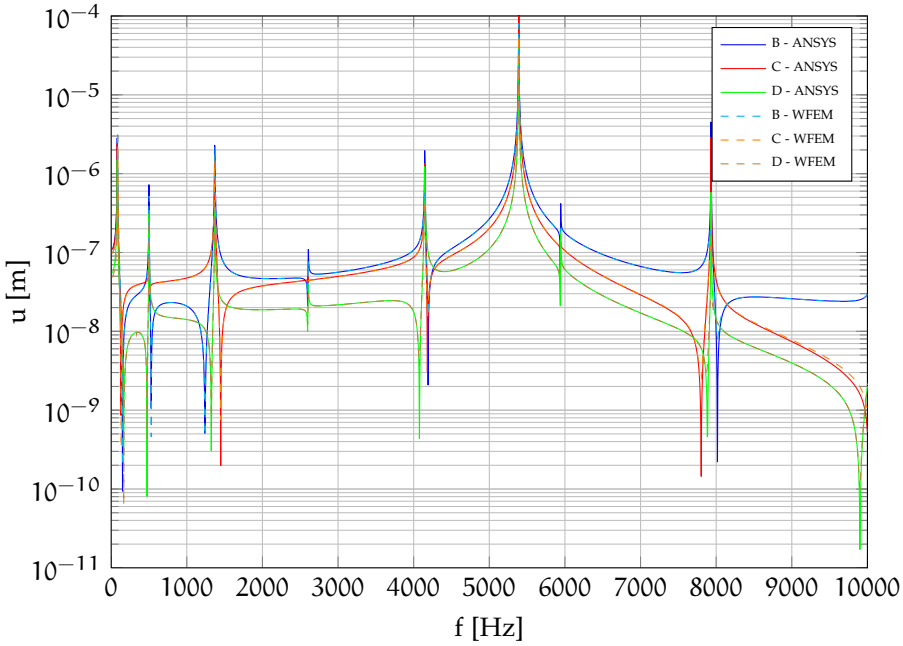

Figure 3.38: Longitudinal displacements of a cantilevered laminated beam [72] subject to a longitudinal point force in point A

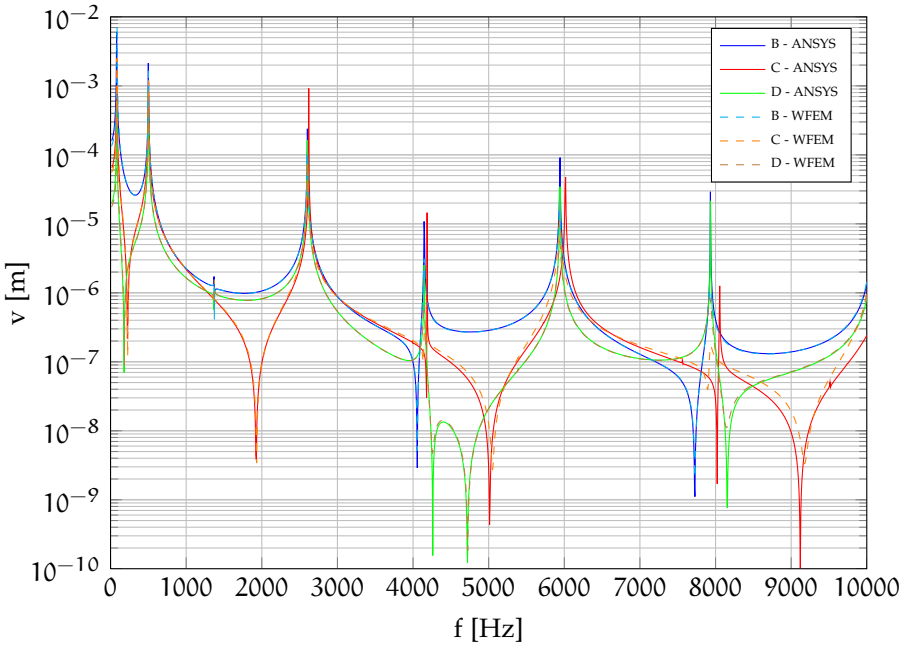

Figure 3.39: Vertical displacements of a cantilevered laminated beam [72] subject to a vertical point force in point A

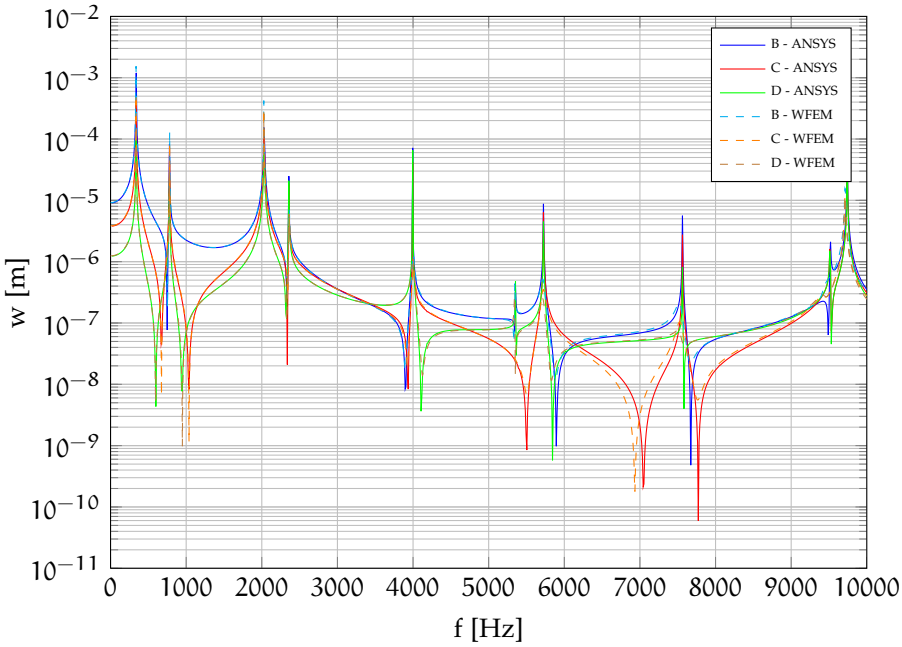

Figure 3.40: Transverse displacements of a cantilevered laminated beam [72] subject to a transverse point force in point A

3.4.3.4 *Dispersion curves of sandwich beams*

A sandwich configuration allows a strong increase of the bending stiffness to mass ratio by including a thick, low density core between two thin and stiff face sheets. At the same time, the general drawback is in the resulting poor acoustic performances, and for this reason many works in literature investigate the vibroacoustics of sandwich structures [107]. In most of them the analysis is performed through the wavenumber estimation [6, 7, 10, 109, 127], therefore a WFE approach may be very helpful for the analyst.

Tavallaey [128] proposes an analytical model for wave propagation analysis in three layered structures, assuming face sheets and core as homogeneous and isotropic. The governing equation are derived and solved using a winding-integral technique. The results are reported for a sandwich beam having a width $b = 116\,\text{mm}$, made by a 50 mm thick PVC core enclosed in glass reinforced plastic face sheets, 2.5 mm thick. Both the core and the face sheet are assumed to be isotropic, and the mechanical properties are reported in Table 3.4.

Table 3.4: Material properties of the investigated sandwich beam [128]

	Face Sheet	Core
E [GPa]	9.8	0.094
ν	0.3	0.3
ρ [kg/m^3]	1580	101

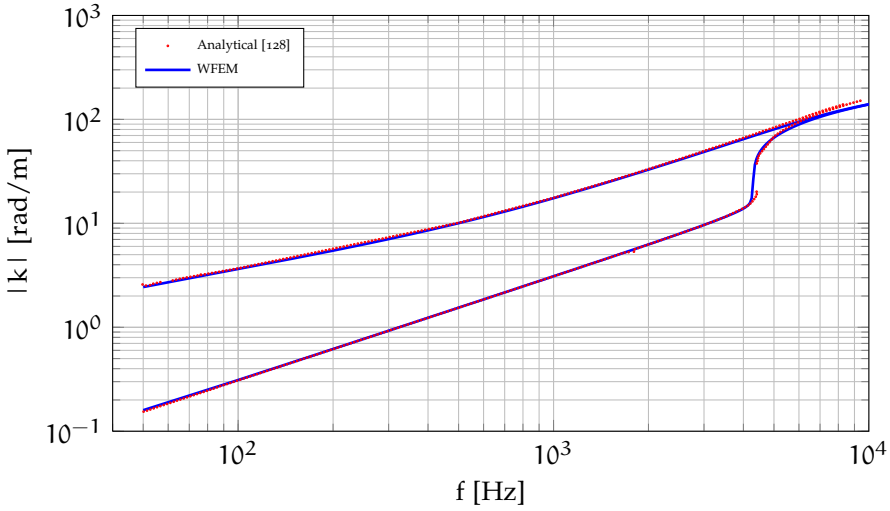

Figure 3.41: First-order propagating wavenumbers of an isotropic sandwich beams [128]

The sandwich is modelled in ANSYS® with 10×16 SOLID45 elements, with $\Delta = 0.002\,\text{m}$. In Figure 3.41, the comparison between the analytical model and the WFE results are shown in the frequency range $40 - 10\,000\,\text{Hz}$ for the first-order

propagating waves of the isotropic sandwich panels. The correlation is quite good in the whole frequency range.

3.4.3.5 *Dispersion curves of natural composite sandwich beams*

Due to environmental awareness and constraints of legislative authorities, there is a growing interest in using natural vegetable fibres as reinforcement of polymeric based composites and/or as cores for sandwich panels. Natural fibres offer several advantages such as biodegradability, low cost, low density and acceptable specific strength properties. In recent studies, the dynamic and damping [129–135] analysis of eco-friendly structures is performed. In particular, Sargianis et al. [133] report an experimental study on the measurement of the bending wavenumber of several sandwich beams, comparing natural fibre and carbon/epoxy face sheets. In Table 3.5, the mechanical properties of the considered material are listed, whereas in Table 3.6 the dimensions of the beam are summarised. Some mechanical properties are assumed as an average from those available in literature, since no information are provided by Sargianis et al. [133].

For each beam, once the elementary cell is chosen, a different FE model is created because of the different cross-section dimensions. In Figure 3.42, the results obtained through WFEM are compared to the experimental ones. The agreement is enough good, considering the uncertainty on the mechanical properties (mostly for the sandwich having balsa and pine wood as cores).

Table 3.5: Face sheet and core properties of natural beams [133] (*: literature value)

Material	Elastic Modulus E_1 [GPa]	Poisson ratio ν_{13}	Density ρ [kg/m^3]
Carbon fiber-epoxy face sheet	100	0.3 (*)	1600
Bamboo-vinyl ester face sheet	2.38	0.3 (*)	1150
Rohacell 51 WF core	0.075	0.499	52
Balsa wood core	2.2 (*)	0.22	332
Pine wood core	9.1 (*)	0.3	475

Table 3.6: Dimensions of natural beam [133]

Name	Materials	Face sheet thickness [mm]	Core thickness [mm]	Beam width [mm]
CE-R	Carbon fiber-Rohacell	0.38	18.4	25.4
B-R	Bamboo fiber-Rohacell	1.9	17.0	41.1
B-B	Bamboo fiber-Balsa	1.9	18.2	40.1
B-P	Bamboo fiber-Pine	1.9	9.5	40.5

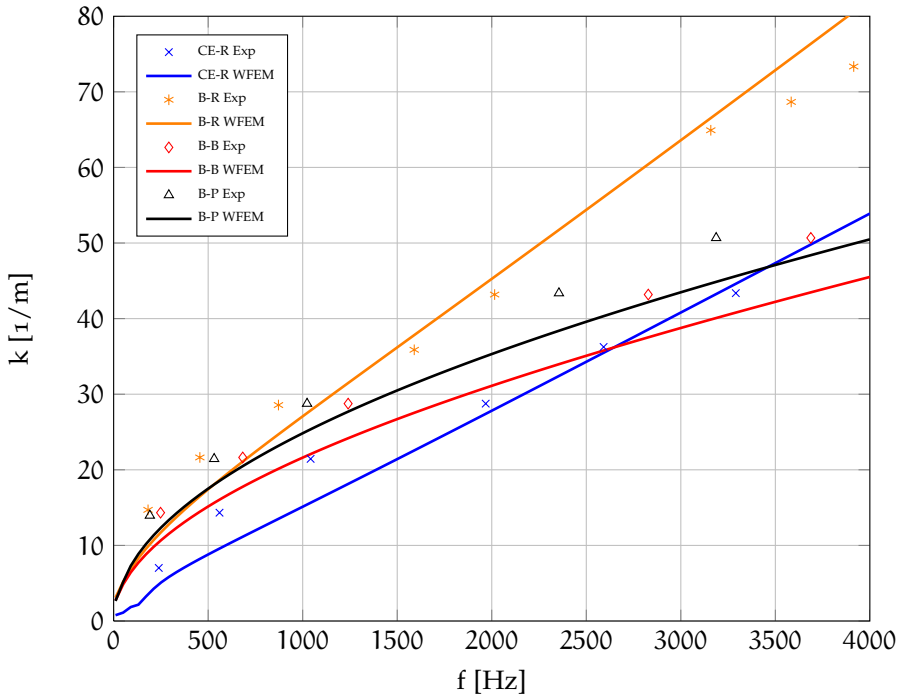

Figure 3.42: Dispersion plot of beams with bamboo-fiber face sheets, compared with carbon fiber face sheets. Continuous curves: WFEM. Only marks: literature results [133]

3.4.4 Forced response of a hybrid sandwich beam: WFEM and experimental results

Experimental results concerning the forced response of a sandwich beam are compared to numerical ones. The beam under investigation is a hybrid structure, obtained by coupling traditional aluminium face sheets to an innovative core such as a polypropylene honeycomb. A vibration test is performed in order to measure the Frequency Response Functions of the beam, which is is compared with numerical results obtained through WFEM and FEM.

3.4.4.1 *Test specimen*

The investigated sandwich beam, shown in Figure 3.43 has in-plane dimensions 395 mm $\times$ 60 mm. It is made by enclosing a polypropylene honeycomb core (with thickness $t_c = 19\,\text{mm}$) between two aluminium face sheets, having thickness $t_s = 0.7\,\text{mm}$. The polypropylene honeycomb core is assumed to be isotropic, since only few mechanical properties are available. The material characteristics of face sheets and core are reported in Table 3.7

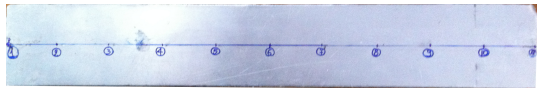

(a) *Top view (with experimental mesh)*

(b) *Lateral view*

Figure 3.43: Aluminium-Honeycomb PP sandwich beam

Table 3.7: Material properties of the Aluminium-PP Honeycomb sandwich beam

	Aluminium Face Sheet	PP Honeycomb Core
E [GPa]	6.9	0.48
ν	0.33	0.4
ρ [kg/m^3]	2750	1000

3.4.4.2 *Experimental setup*

The dynamic response of the sandwich beam was experimentally investigated through a modal test, adopting the so-called roving-hammer technique. The beam was suspended using elastic cords in order to simulate free-free boundary conditions. This particular boundary condition has several advantages, in particular the reduction of added damping due to the constraint. An uni-axial accelerometer (PCB 333B32, Figure 3.44a) was used to measure the response along the direction perpendicular to the plane of the beam. The accelerometer was placed on a free tip of the beam. An impact hammer (ENDEVCO Modal Hammer 2302, Figure 3.44b) was preferred over an electro-dynamic shaker to provide the excitation since the beam is small and light. Excitations were provided over all the points of the experimental mesh, constituted by 11 equally spaced nodes along the longitudinal axis of the beam (only the flexural waves were estimated). Vibration measurements were taken in the frequency range $200 - 1600$ Hz, with a frequency step $\Delta f = 1$ Hz. The frequency response data were recorded using the acquisition system LMS SCADAS III (Figure 3.44c) and then analysed by means of the software LMS Test.Lab 8B.

3.4.4.3 *Experimental result: modal parameters*

The post-processing of the FRFs through LMS Test.Lab 8B allowed the extraction of the modal parameters, in terms of natural frequency, modal damping and modal shapes. In Table 3.8, these are reported for the frequency range of analysis. The extraction of the modal damping is useful in order to consider it in the numerical models.

(a) *accelerometer*

(b) *modal hammer*

(c) *acquisition system*

Figure 3.44: Experimental instrumentation

Table 3.8: Experimental modal parameters of the Aluminium-PP Honeycomb sandwich beam

Mode n.	Frequency [Hz]	Damping (%)
1	525.7	3.2%
2	912.0	4.0%
3	1374.6	4.4%

3.4.4.4 *Numerical models*

The beam is numerically investigated through WFEM and FEM, retaining only the displacement along the vertical direction (as made for the experimental test).

The finite element model of the elementary cell is shown in Figure 3.45a, meshed with 6×6 SOLID45 elements over the cross-section, with $\Delta = 5\,\text{mm}$. The WFE model has 49 DOFs. The cell model is replicated along the x-axis in order to obtain the FE model of the whole beam, reported in Figure 3.45b, to be investigated through the ANSYS® harmonic analysis. This model have a total of 3920 DOFs. In Figure 3.45, different colors stand for different materials used for face sheets and core.

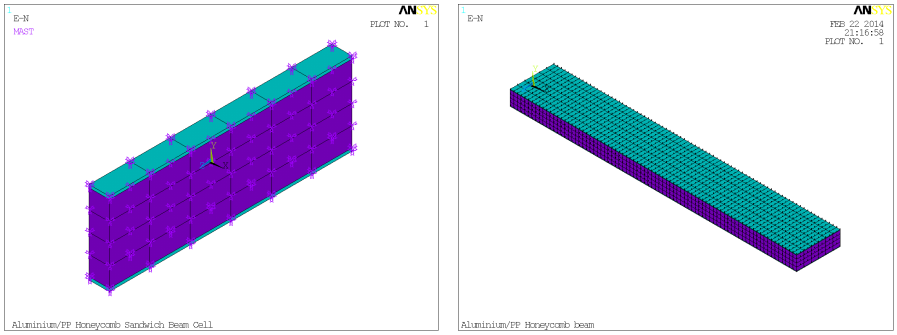

(a) *Elementary cell* **(b)** *Beam*

Figure 3.45: Aluminium-PP Honeycomb sandwich beam. Elementary cell and beam modelled using SOLID45 elements

3.4.4.5 *Numerical-Experimental comparison*

Numerical and experimental FRFs are compared. The response function shown in Figure 3.46 are obtained by applying a force on a free tip of the beam and evaluating the displacement on the other free tip.

As can be observed in Figure 3.46, numerical FRFs are not able to perfectly describe the experimental one, mostly for the first peak. This is due to the assumption made on the isotropy of the honeycomb core, as well as the effect of the boundary conditions. However, the error on the magnitude of the peaks is negligible. It is worth to highlight the good agreement between WFE and FE results.

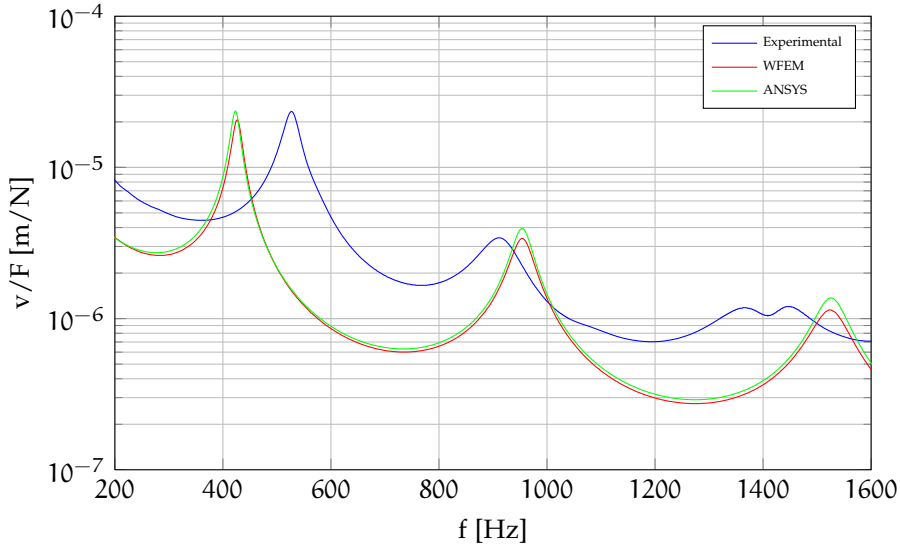

Figure 3.46: Comparison between experimental and numerical FRFs of the Aluminium-PP Honeycomb sandwich beam

4 WAVE AND FINITE ELEMENT METHOD FOR 2-DIMENSIONAL PROBLEMS

This chapter concerns a first approach to the analysis of uniform two-dimensional waveguides through the Wave and Finite Element Method, based on the works made by Manconi and Mace [63, 86]. The procedure is carried out mostly to validate experimental tests on natural fibres composite panel, presented at the end of the chapter. The developed code, validated through benchmarks available in literature, allows the estimation of the wave propagation along one of the principal axis of the plate under investigation (designed with the angle $\theta = 0°$).

4.1 WFEM FOR 2-DIMENSIONAL WAVEGUIDES

The procedure introduce by Manconi and Mace [63, 86] for the analysis of two-dimensional periodic waveguides basically follows the same steps listed for one-dimensional once, except that the eigenvalue problem is formulated directly on the dynamic stiffness matrix, and not on the transfer matrix. The first step is always the identification of an elementary cell of the structure, which has to be modelled through finite elements. The structure, in this case, is homogeneous along the two in-plane directions, but the properties might vary through the thickness.

A schematic example of periodic waveguide is shown in Figure 4.1. The periodic structure is obtained by replicating the reference squared elementary cell n_1, n_2 along the in-plane directions x and y. All other cells can be expressed as a function of the reference one.

The simplest FE model of the elementary cell is shown in Figure 4.2, representing a 4-noded rectangular element.

In this case the nodal DOFs $\mathbf{q}$, and the nodal forces $\mathbf{f}$ vectors can be written as

$$\mathbf{q} = \begin{bmatrix} \mathbf{q}_1^T & \mathbf{q}_2^T & \mathbf{q}_3^T & \mathbf{q}_4^T \end{bmatrix}^T \qquad \mathbf{f} = \begin{bmatrix} \mathbf{f}_1^T & \mathbf{f}_2^T & \mathbf{f}_3^T & \mathbf{f}_4^T \end{bmatrix}^T. \tag{4.1}$$

It is worth noting that $\mathbf{q}_j$ is the vector of the nodal DOFs of all the elements nodes which lie on the j-th corner. Likewise the vector $\mathbf{f}_j$.

In order to analyse the wave investigation in the same way of one-dimensional waveguide, it is needed to express all the nodal DOFs and forces as a function of those of a reference node. The starting point of the method is always the equation of the motion of the cell, which assuming time-harmonic behaviour can be written as:

$$\left(\mathbf{K} + i\omega\mathbf{C} - \omega^2\mathbf{M}\right)\mathbf{q} = \mathbf{f} \tag{4.2}$$

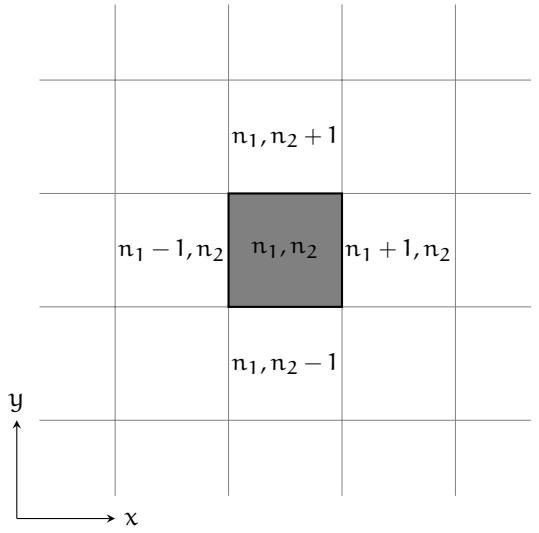

Figure 4.1: Schematic representation of a two-dimensional periodic waveguide

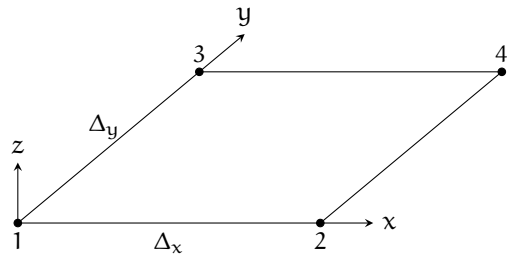

Figure 4.2: Four nodes Finite Element of the elementary cell

Also in this case, the mass, damping and stiffness matrices of the cell can be obtained using commercial FE packages. In the case of uniform and structural damping, a complex stiffness matrix can be considered.

Using the Floquet-Bloch theory, the displacements at each node can be expressed as a function of the displacements at one single node. The main difference with one-dimensional waveguides analysis is the fact that two propagation directions have to be considered. Thus, if the node 1 of the element of Figure 4.2 is taken as reference, the other nodal displacements can be written as

$$\mathbf{q}_2 = \lambda_x \mathbf{q}_1 \qquad \mathbf{q}_3 = \lambda_y \mathbf{q}_1 \qquad \mathbf{q}_4 = \lambda_x \lambda_y \mathbf{q}_1 \tag{4.3}$$

where

$$\lambda_x = e^{i\Delta_x k_x} \qquad \lambda_y = e^{i\Delta_y k_y} \tag{4.4}$$

are the propagation constants along x and y axes, respectively. Thus the nodal displacements of the cell can be written in terms of the only nodal displacements $\mathbf{q}_1$ as

$$\mathbf{q} = \Lambda_R \mathbf{q}_1, \tag{4.5}$$

where the propagation matrix Λ_R is

$$\Lambda_R = \begin{bmatrix} \mathbf{I} \\ \lambda_x \mathbf{I} \\ \lambda_y \mathbf{I} \\ \lambda_x \lambda_y \mathbf{I} \end{bmatrix}. \tag{4.6}$$

Furthermore, assuming the absence of external excitation, equilibrium at node 1 implies that the sum of the nodal forces of all the elements connected to node 1 is zero, consequently

$$\Lambda_L \mathbf{f} = \mathbf{0}, \tag{4.7}$$

where

$$\Lambda_L = \begin{bmatrix} \mathbf{I} & \lambda_x^{-1}\mathbf{I} & \lambda_y^{-1}\mathbf{I} & (\lambda_x\lambda_y)^{-1}\mathbf{I} \end{bmatrix} \tag{4.8}$$

Through the propagation matrices Λ_R and Λ_L, a reduced form of the stiffness, damping and mass matrices can be obtained, and hence a reduced form of the equation of motion. In fact, defining the reduced form of the matrices as

$$\mathbf{K}_r(\lambda_x, \lambda_y) = \Lambda_L \, \mathbf{K} \, \Lambda_R \tag{4.9}$$
$$\mathbf{C}_r(\lambda_x, \lambda_y) = \Lambda_L \, \mathbf{C} \, \Lambda_R \tag{4.10}$$
$$\mathbf{M}_r(\lambda_x, \lambda_y) = \Lambda_L \, \mathbf{M} \, \Lambda_R \tag{4.11}$$

the equation of motion becomes

$$(\mathbf{K}_r + i\omega\mathbf{C}_r - \omega^2\mathbf{M}_r)\mathbf{q}_1 = \mathbf{0}. \tag{4.12}$$

If n is the number of degrees of freedom per node, the dimensions of the mass, damping and stiffness matrices of the cell are $4n \times 4n$, whereas the dimensions of the corresponding reduced forms are $n \times n$.

Similarly to the analysis of one-dimensional waveguides, it is possible to define the reduced Dynamic Stiffness Matrix as

$$\mathbf{D}_r(\lambda_x, \lambda_y, \omega) = \mathbf{K}_r + i\omega\mathbf{C}_r - \omega^2\mathbf{M}_r, \tag{4.13}$$

and hence Eq. (4.12) can be written as

$$\mathbf{D}_r(\lambda_x, \lambda_y, \omega)\mathbf{q}_1 = \mathbf{0}.. \tag{4.14}$$

In this case, the eigenproblem is directly formulated on the Dynamic Stiffness Matrix, without the definition of the transfer matrix. If the DSM of the cell is partitioned as

$$\mathbf{D} = \begin{bmatrix} \mathbf{D}_{11} & \mathbf{D}_{12} & \mathbf{D}_{13} & \mathbf{D}_{14} \\ \mathbf{D}_{21} & \mathbf{D}_{22} & \mathbf{D}_{23} & \mathbf{D}_{24} \\ \mathbf{D}_{31} & \mathbf{D}_{32} & \mathbf{D}_{33} & \mathbf{D}_{34} \\ \mathbf{D}_{41} & \mathbf{D}_{42} & \mathbf{D}_{43} & \mathbf{D}_{44} \end{bmatrix}, \tag{4.15}$$

the reduced eigenvalue problem of Eq. (4.14) can be expressed as

$$\begin{aligned}&[(\mathbf{D}_{11}+\mathbf{D}_{22}+\mathbf{D}_{33}+\mathbf{D}_{44})\,\lambda_x\lambda_y+(\mathbf{D}_{12}+\mathbf{D}_{34})\,\lambda_x^2\lambda_y+\\&+(\mathbf{D}_{13}+\mathbf{D}_{24})\,\lambda_x\lambda_y^2+\mathbf{D}_{32}\lambda_x^2+\mathbf{D}_{23}\lambda_y^2+(\mathbf{D}_{21}+\mathbf{D}_{43})\,\lambda_y+\\&+(\mathbf{D}_{31}+\mathbf{D}_{42})\,\lambda_y+\mathbf{D}_{14}\lambda_x^2\lambda_y^2+\mathbf{D}_{41}]\mathbf{q}_1=\mathbf{o}\end{aligned} \tag{4.16}$$

4.1.1 Other FE implementations

Beside the four-noded rectangular element, other typical finite elements can be employed for modelling two-dimensional waveguides. Depending on the element, different periodic and equilibrium conditions must be imposed. The use of rectangular element with mid-size nodes is here reported [27, 86] since it can be helpful if round-off error occurs (as suggested by Waki et al. [66]), whereas the use of a triangular element is explained by Manconi [86]. Obviously, as in the case of one-dimensional waveguides, if the elementary cell presents internal nodes, the DOFs can be partitioned into boundary and internal, imposing that the nodal force on the internal nodes are zero. Therefore, internal DOFs can be removed by condensation.

4.1.1.1 *Rectangular element with mid-size nodes*

In Figure 4.3, a generic rectangular element with mid-size nodes is represented.

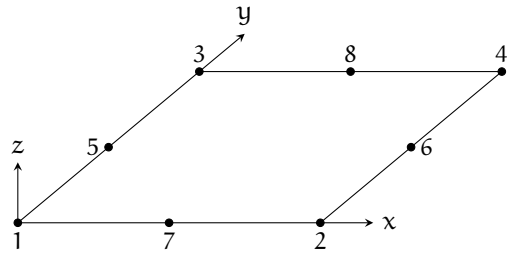

Figure 4.3: Rectangular Finite Element with mid-size nodes

The nodal displacements vector, here, is

$$\mathbf{q}=\begin{bmatrix}\mathbf{q}_1^T & \mathbf{q}_2^T & \mathbf{q}_3^T & \mathbf{q}_4^T & \mathbf{q}_5^T & \mathbf{q}_6^T & \mathbf{q}_7^T & \mathbf{q}_8^T\end{bmatrix}^T. \tag{4.17}$$

By defining the propagation matrix Λ_R as

$$\Lambda_R=\begin{bmatrix}\mathbf{I} & \lambda_x\mathbf{I} & \lambda_y\mathbf{I} & \lambda_x\lambda_y\mathbf{I} & \mathbf{o} & \mathbf{o} & \mathbf{o} & \mathbf{o}\\ \mathbf{o} & \mathbf{o} & \mathbf{o} & \mathbf{o} & \mathbf{I} & \lambda_x\mathbf{I} & \mathbf{o} & \mathbf{o}\\ \mathbf{o} & \mathbf{o} & \mathbf{o} & \mathbf{o} & \mathbf{o} & \mathbf{o} & \mathbf{I} & \lambda_y\mathbf{I}\end{bmatrix} \tag{4.18}$$

it is possible to express the periodicity condition:

$$\mathbf{q}=\Lambda_R\begin{bmatrix}\mathbf{q}_1\\ \mathbf{q}_5\\ \mathbf{q}_7\end{bmatrix} \tag{4.19}$$

Equilibrium of forces at the mid-size nodes on the left and bottom side leads, respectively, to

$$\mathbf{f}_5 + \lambda_x^{-1}\mathbf{f}_6 = 0 \tag{4.20}$$

$$\mathbf{f}_7 + \lambda_y^{-1}\mathbf{f}_8 = 0 \tag{4.21}$$

and hence

$$\Lambda_L = \begin{bmatrix} \mathbf{I} & \lambda_x^{-1}\mathbf{I} & \lambda_y^{-1}\mathbf{I} & \lambda_x^{-1}\lambda_y^{-1}\mathbf{I} & \mathbf{o} & \mathbf{o} & \mathbf{o} & \mathbf{o} \\ \mathbf{o} & \mathbf{o} & \mathbf{o} & \mathbf{o} & \mathbf{I} & \lambda_x^{-1}\mathbf{I} & \mathbf{o} & \mathbf{o} \\ \mathbf{o} & \mathbf{o} & \mathbf{o} & \mathbf{o} & \mathbf{o} & \mathbf{o} & \mathbf{I} & \lambda_y^{-1}\mathbf{I} \end{bmatrix} \tag{4.22}$$

Manconi [86] suggests an approximation for reducing the size of the resulting eigenvalue problem, by enforcing further periodicity conditions between nodes 1, 5 and 7. In fact, it is possible to project the displacement vectors $\mathbf{q}_7$ and $\mathbf{q}_5$ on the node 1, by writing

$$\mathbf{q}_7 = \lambda_x^{1/2}\mathbf{q}_1, \tag{4.23}$$

$$\mathbf{q}_5 = \lambda_y^{1/2}\mathbf{q}_1. \tag{4.24}$$

In this case, the matrices Λ_R and Λ_L become

$$\Lambda_R = \begin{bmatrix} \mathbf{I} & \lambda_x\mathbf{I} & \lambda_y\mathbf{I} & \lambda_x\lambda_y\mathbf{I} & \lambda_y^{1/2}\mathbf{I} & \lambda_x\lambda_y^{1/2}\mathbf{I} & \lambda_x^{1/2}\mathbf{I} & \lambda_x^{1/2}\lambda_y\mathbf{I} \end{bmatrix}^T \tag{4.25}$$

$$\Lambda_L = \begin{bmatrix} \mathbf{I} & \lambda_x^{-1}\mathbf{I} & \lambda_y^{-1}\mathbf{I} & (\lambda_x\lambda_y)^{-1}\mathbf{I} & \lambda_y^{-1/2}\mathbf{I} & \lambda_x^{-1}\lambda_y^{-1/2}\mathbf{I} & \lambda_x^{-1/2}\mathbf{I} & \lambda_x^{-1/2}\lambda_y^{-1}\mathbf{I} \end{bmatrix}^T \tag{4.26}$$

4.2 THE EIGENPROBLEM

The eigenproblem expressed by Eq. (4.14) takes various forms, depending on the physical nature of the problem and the type of result which have to be achieved. The eigenproblem, whose solutions provide FE estimation of dispersion relations and wavemodes for continuous structures, clearly involves three parameters: λ_x, λ_y and ω.

Among the increased complexity of the formulation, some analogies can be found with the one-dimensional problem. In particular, since mass, stiffness and damping matrices are real and symmetric, then the Dynamic Stiffness Matrix is the same too. Furthermore, if Eq. (4.16) is divided by $\lambda_x\lambda_y$ and then transposed, it can be demonstrated that, if (λ_x, λ_y) is a solution for a given circular frequency ω, then also $(\lambda_x, 1/\lambda_y)$, $(1/\lambda_x, \lambda_y)$, $(1/\lambda_x, 1/\lambda_y)$ are solutions of the eigenproblem: these represent the same disturbance travelling along the positive and negative in-plane directions.

Since the eigenvalue problem is three-parametric, three different algebraic eigenvalue problems can be defined [63, 86]. If both propagation constants are known

and real, a linear eigenvalue problem results in ω for propagating waves. Instead, if the circular frequency and the direction of wave propagation are known, a polynomial eigenvalue problem or a transcendental eigenvalue problem results in the wavenumber k, depending on the ratio of propagation constants. Finally, if one propagation constant and the circular frequency are known, a quadratic polynomial problem must be solved for the other propagation constant.

4.2.1 Linear eigenvalue problem

If k_x and k_y are chosen and real, the problem (4.16) results a linear eigenvalue problem in ω^2. This approach can be used to calculate the dispersion relations for free waves propagating through an undamped structure with wavenumber $k = \sqrt{k_x^2 + k_y^2}$ in a direction $\theta = \arctan k_y/k_x$. Indeed, it can be proved that in undamped structures the reduced matrices in Eq. (4.8) are positive definite Hermitian matrices, i.e. real values of propagation constants will lead to n real solutions for ω. The corresponding eigenvectors of the problems define the wave-modes at these frequencies, although some of them are artifacts of the Finite Element discretization and periodicity (as in the case of one-dimensional problem).

4.2.2 Polynomial eigenvalue problem (PEP)

Another type of eigenproblem must be solved if the circular frequency ω and the direction of wave propagation θ are fixed. The direction of propagation can be expressed as a function of propagation constants. In fact, being $\lambda_x = e^{i\Delta_x k_x}$ and $\lambda_y = e^{i\Delta_y k_y}$, the ratio of wavenumbers' amplitude is related to the wave propagation angle:

$$\tan\,\theta = \frac{k_y}{k_x}. \tag{4.27}$$

The form of the eigenproblem is strictly connected to the this ratio. In fact, if $k_y/k_x = m_2/m_1$ is rational, i.e. integers with no common divisor, a polynomial eigenvalue problem (PEP) results in λ_x and λ_y. Instead, the eigenvalue problem becomes transcendental if the ratio is irrational [86].

In the case of polynomial eigenvalue problem, the propagation constants can be expressed as a function of (integer) m_1, m_2:

$$k_x\Delta_x = m_1\sigma, \qquad k_y\Delta_y = m_2\sigma \tag{4.28}$$

Then, introducing $\gamma{=}e^{i\sigma}$ the eigenvalue problem is written as

$$\begin{aligned}&[\mathbf{A}_8\gamma^{2m_1+2m_2} + \mathbf{A}_7\gamma^{2m_1+m_2} + \mathbf{A}_6\gamma^{m_1+2m_2} + \mathbf{A}_5\gamma^{m_1+m_2} + \mathbf{A}_4\gamma^{2m_1} + \\ &+\mathbf{A}_3\gamma^{2m_2} + \mathbf{A}_2\gamma^{m_2} + \mathbf{A}_1\gamma^{m_1} + \mathbf{A}_0]\mathbf{q_1} = \mathbf{0}\end{aligned} \tag{4.29}$$

where, given the DSM expressed in Eq. (4.15), the matrices $\mathbf{A}$ are:

$$\begin{aligned}
\mathbf{A}_8 &= \mathbf{D}_{14} \\
\mathbf{A}_7 &= (\mathbf{D}_{12} + \mathbf{D}_{34}) \\
\mathbf{A}_6 &= (\mathbf{D}_{13} + \mathbf{D}_{24}) \\
\mathbf{A}_5 &= (\mathbf{D}_{11} + \mathbf{D}_{22} + \mathbf{D}_{33} + \mathbf{D}_{44}) \\
\mathbf{A}_4 &= \mathbf{D}_{32} \\
\mathbf{A}_3 &= \mathbf{D}_{23} \\
\mathbf{A}_2 &= (\mathbf{D}_{21} + \mathbf{D}_{43}) \\
\mathbf{A}_1 &= (\mathbf{D}_{31} + \mathbf{D}_{42}) \\
\mathbf{A}_0 &= \mathbf{D}_{41}
\end{aligned} \tag{4.30}$$

Since the matrices $\mathbf{A}$ are of order $n \times n$, the polynomial problem of Eq. (4.29) is of order $2(m_1 + m_2)$, with $2n(m_1 + m_2)$ solution for γ.

Furthermore, if the given direction of propagation is parallel to the x-axis or to the y-axis, i.e. $\theta = 0$ or $\theta = \pi/2$, the eigenvalue problem becomes a quadratic eigenvalue problem (QEP), which is the investigated eigenproblem.

4.2.3 Quadratic eigenvalue problem (QEP)

If the frequency ω and one component of the wavenumber k are known, a quadratic eigenvalue problem(QEP) results. For example this might represents the wave propagation in a closed cylindrical shell where the wavenumber around the circumference can only take certain discrete values. Considering known the component k_y, the eigenproblem of Equation (4.16) becomes quadratic in λ_x:

$$[\mathbf{A}_2\lambda_x^2 + \mathbf{A}_1\lambda_x + \mathbf{A}_0]\mathbf{q}_1 = \mathbf{0} \tag{4.31}$$

where

$$\begin{aligned}
\mathbf{A}_2 &= (\mathbf{D}_{14} + \mathbf{D}_{12} + \mathbf{D}_{34} + \mathbf{D}_{32}) \\
\mathbf{A}_1 &= (\mathbf{D}_{31} + \mathbf{D}_{42} + \mathbf{D}_{11} + \mathbf{D}_{22} + \mathbf{D}_{33} + \mathbf{D}_{44} + \mathbf{D}_{13} + \mathbf{D}_{24}) \\
\mathbf{A}_0 &= (\mathbf{D}_{41} + \mathbf{D}_{23} + \mathbf{D}_{21} + \mathbf{D}_{43})
\end{aligned} \tag{4.32}$$

QEPs are an important class of nonlinear eigenvalue problems that are less familiar and less routinely solved than the standard eigenvalue problem (SEP) and the generalized eigenvalue problem (GEP), therefore they need special attention [136, 137].

4.2.4 Solving PEPs through linearisation

Besides the numerical methods which treat polynomial eigenvalue problems in their original form, there are some which linearise a PEP in a generalised eigenvalue problem (GEP), and then apply GEP techniques [138]. Through linearisation, it is possible to transform an eigenvalue problem of order n in n generalised eigenvalue problems (similarly to the transformation of an ordinary differential

equation). For a general PEP, there are several linearisations: it is important to choose one respecting the symmetry and other structural properties of the problem.

Given a generic QEP in the form $\mathbf{Q}(\lambda)$, one linarisation of the problem could be as following

$$\mathbf{L} = \mathbf{A} - \lambda\mathbf{B} \tag{4.33}$$

if there are two unimodular matrix polynomials $\mathbf{E}(\lambda)$ and $\mathbf{F}(\lambda)$, i.e. $\det(\mathbf{E}(\lambda))$ and $\det(\mathbf{E}(\lambda))$ are non-zero constants, such that

$$\mathbf{E}(\mathbf{A} - \lambda\mathbf{B})\mathbf{F} = \begin{bmatrix} \mathbf{Q}(\lambda) & \mathbf{o} \\ \mathbf{o} & \mathbf{I}_n \end{bmatrix}. \tag{4.34}$$

Given the properties of matrices $\mathbf{E}$ and $\mathbf{E}$, $\det(\mathbf{A} - \lambda\mathbf{B})$ agrees with $\det(\mathbf{Q}(\lambda))$ up to a non-zero constant multiplier, hence $\mathbf{L}$ and $\mathbf{Q}$ have the same eigenvalues [136]. The companion linearisation is the most frequently used [137] in its several existing forms. Companion linearisations have a number of desirable properties:

- they are always linearisations even if $\mathbf{Q}(\lambda)$ is non-regular. Moreover they are strong linearisations, i.e. they preserve the partial multiplicities of infinite eigenvalues [139];
- the left and right eigenvectors of $\mathbf{Q}(\lambda)$ are easily recovered from those of the companion form [140];
- they have good conditioning and backward stability properties in the majority of the cases.

For instance, consider the quadratic eigenvalue problem defined in Eq. (4.31). The easiest way to construct a linearisation is to use the following substitution

$$\mathbf{u} = \lambda_x \mathbf{q}_1 \tag{4.35}$$

and rewrite Eq. (4.31) as

$$\mathbf{A}_2\lambda_x^2\mathbf{u} + \mathbf{A}_1\mathbf{u} + \mathbf{A}_0\mathbf{q}_1 = \mathbf{o}. \tag{4.36}$$

This leads to the following generalised eigenvalue problem

$$\begin{bmatrix} \mathbf{o} & \mathbf{I} \\ -\mathbf{A}_0 & -\mathbf{A}_1 \end{bmatrix} \begin{bmatrix} \mathbf{q} \\ \mathbf{u} \end{bmatrix} - \lambda \begin{bmatrix} \mathbf{I} & \mathbf{o} \\ \mathbf{o} & \mathbf{A}_2 \end{bmatrix} \begin{bmatrix} \mathbf{q} \\ \mathbf{u} \end{bmatrix} = \mathbf{o} \tag{4.37}$$

which corresponds to the first companion form. The best known companion linearisation are the first and second companion, given respectively by

$$\mathbf{C}_1 = \begin{bmatrix} \mathbf{o} & \mathbf{I} \\ -\mathbf{A}_0 & -\mathbf{A}_1 \end{bmatrix} - \lambda \begin{bmatrix} \mathbf{I} & \mathbf{o} \\ \mathbf{o} & \mathbf{A}_2 \end{bmatrix} \tag{4.38}$$

$$\mathbf{C}_2 = \begin{bmatrix} -\mathbf{A}_0 & \mathbf{o} \\ \mathbf{o} & \mathbf{I} \end{bmatrix} - \lambda \begin{bmatrix} \mathbf{A}_1 & \mathbf{A}_2 \\ \mathbf{I} & \mathbf{o} \end{bmatrix} \tag{4.39}$$

Other two companion linearisations can be obtained directly from the first two:

$$\mathbf{C}_3 = \begin{bmatrix} \mathbf{A}_1 & \mathbf{0} \\ \mathbf{A}_0 & \mathbf{A}_1 \end{bmatrix} - \lambda \begin{bmatrix} \mathbf{0} & \mathbf{A}_1 \\ -\mathbf{A}_2 & \mathbf{0} \end{bmatrix} \tag{4.40}$$

$$\mathbf{C}_4 = \begin{bmatrix} \mathbf{0} & -\mathbf{A}_1 \\ \mathbf{A}_2 & \mathbf{0} \end{bmatrix} - \lambda \begin{bmatrix} \mathbf{A}_2 & \mathbf{A}_0 \\ \mathbf{0} & \mathbf{A}_2 \end{bmatrix} \tag{4.41}$$

The choice between the various forms may depend on the nonsingularity of $\mathbf{A}_2$ and $\mathbf{A}_0$: if $\mathbf{A}_2$ is singular, $\mathbf{C}_3$ is the linearisation to be used, but if $\mathbf{A}_0$ is singular $\mathbf{C}_4$ is preferred.

4.3 THE CODE FOR 2D-WFEM

Another code has been written in MATLAB® for the numerical analysis of wave propagation in two-dimensional waveguides by means of the Wave and Finite Element Method. The code is named *WFEM2D.m* and it is here briefly described, according to the flow chart shown in Figure 4.4. As mentioned above, only quadratic eigenvalue problem with $\theta = 0°$ are solved, describing the wave propagation along the x axis.

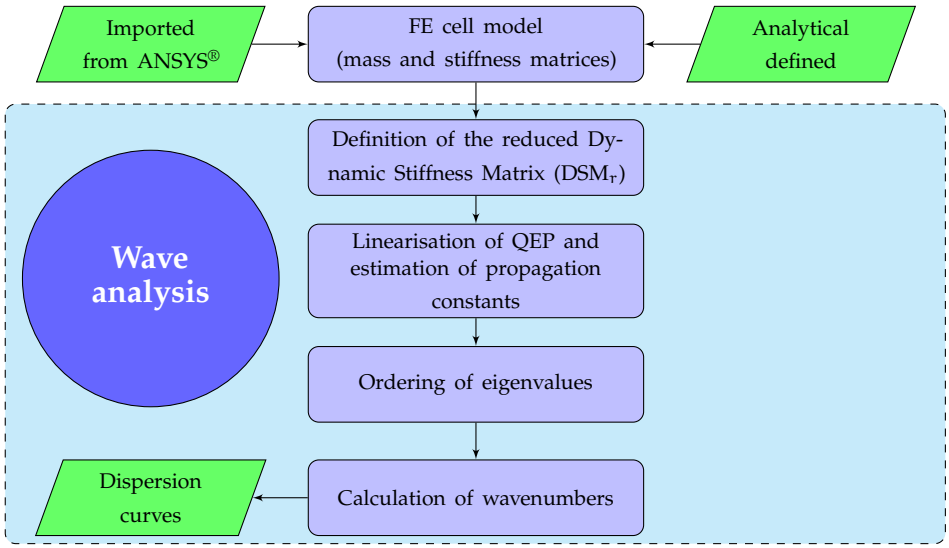

Figure 4.4: Flow chart of the code *WFEM2D.m*

The flow chart is shorter than that of *WFEM1D.m*, since the analysis of two-dimensional structures has involved only the wave propagation and not the forced response. First of all, mass and stiffness finite element matrices of the elementary cell are imported in MATLAB® workspace from ANSYS® during the pre-processing phase, and then the reduced Dynamic Stiffness Matrix is defined.

Once the quadratic eigenvalue problem is formulated, it is linearised by means of the first companion linearisation, and hence the eigenproblem is solved. Given the estimated eigenvalues, they are sorted in descending order of their real part (the sorting through the Modal Assurance Criterion does not work well because the eigenvectors are parallel to each other). For the two-dimensional case, in fact, only dispersion relations are carried out, without information on the wave-modes. Thus, wavenumbers are calculated, and dispersion curves plotted. Since the eigenvalues are not tracked (as made for one-dimensional case), the results are presented through scatter plots.

4.4 RESULTS

In this section, the dispersion curves of different kind of infinite plates are calculated through the Wave and Finite Element Method. These results constitutes only a first approach to two-dimensional waveguides, since all the analysis concerns the resolution of a quadratic eigenvalue problem with $\theta = 0°$.

Comparisons with analytical results allow to validate the approach for simple waveguides, as in the case of isotropic infinite plates. Furthermore, for complex waveguides such as orthotropic or layered plates, the numerical results are compared to the ones available from the literature. At the end, the dispersion curves of natural fibres composite are evaluated, comparing the results with those of experimental test.

The waveguides analysed in this section are flat. As done for the one dimensional waveguides, the application of different ANSYS® elements is exploited. The analysis of dispersion curves is performed by modelling the cell of the waveguide using two different elements: SHELL181 and SOLID45.

4.4.1 Isotropic plates

The simplest two-dimensional waveguide is constituted by a thin isotropic plates, whose analytical dispersion relations are described in Chapter 2. The reference plate is assumed to be made of aluminium ($E = 70\,\text{GPa}$, $\nu = 0.33$, $\rho = 2700\,\text{kg/m}^3$), 0.005 m thick.

The cell is firstly modelled by employing the simplest considered plate element: SHELL181. This element is suitable for analysing thin to moderately-thick shell structures, since it is based on the Mindlin-Reissner shell theory (which takes into account the effect of shear deformation and rotary inertia). SHELL181, shown in Figure 4.5, is a 4-node element with six degrees of freedom at each node: translations in x, y, and z directions, and rotations about the x, y and z-axes.

The dispersion curves for freely propagating waves of an infinite aluminium plate (no damping is considered) are shown in Figure 4.6, together with the analytic solutions. The results are shown in the frequency range $0 - 20\,\text{kHz}$ since this is the range in which the acoustical analysis of structures is usually performed. The waveguide cell is modelled by using a square SHELL181 element, having $\Delta_x = \Delta_y = 0.006\,\text{m}$. The length of the cell is chosen through a compromise to

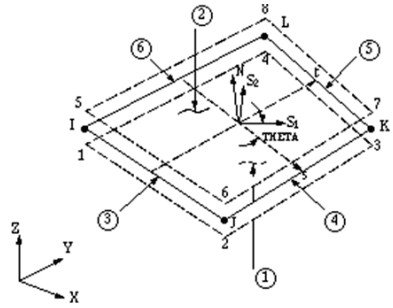

Figure 4.5: SHELL181 element [126]

avoid round-off errors at low frequencies and finite element discretisation approximation at high frequencies. A very good agreement between the numerical curves and the analytical ones can be appreciated for the three branches (from the top: flexural, shear and longitudinal waves) in the whole frequency range.

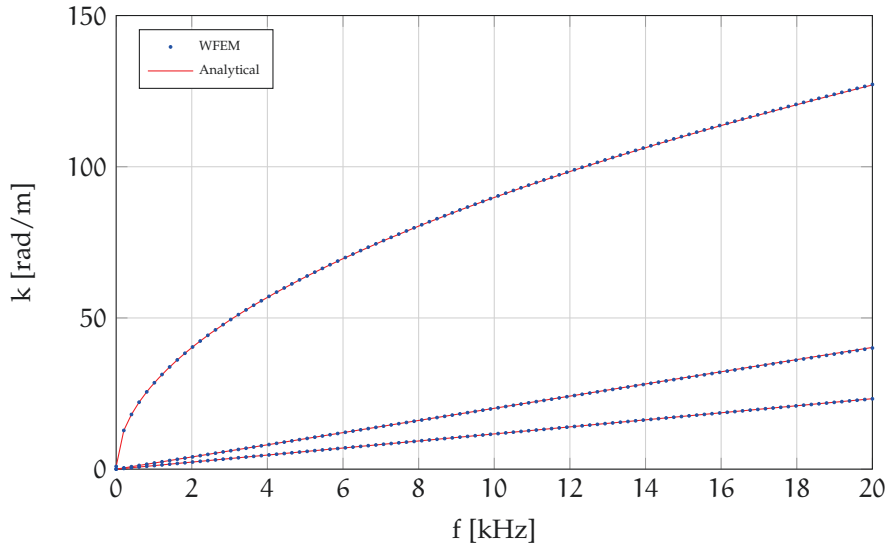

Figure 4.6: Dispersion curves of a thin ($h = 0.005\,m$) aluminium plate. Numerical results obtained by modelling the cell with a SHELL181 element ($\Delta_x = \Delta_y = 0.006\,m$)

Obviously, by changing the size of the cell, numerical errors may occur, similarly to what happens for one-dimensional waveguides. The branch more influenced by numerical errors is the flexural ones. In particular, in Figure 4.7 the bending dispersion curves are plotted for three different size of the element. The choice of a small segment ($\Delta_x = \Delta_y = 0.01\,m$) leads again to errors at high frequencies due to the finite element discretisation effect: starting from 4000 Hz, the curve deviates from the ones obtained by using $\Delta_x = \Delta_y = 0.006\,m$. On the other side, by decreasing the size of the cell up to $\Delta_x = \Delta_y = 0.001\,m$, round-off errors occur at low frequencies due to the arithmetic precision of the computer. The considerations made for the one-dimensional cell are valid again, but in this

case the round-off errors influence the bending wavenumber at high frequencies as well (the bending wavenumber is overestimated), therefore the size of the cell must be chosen accurately as a function of the thickness, of the material and of the frequency range of interest.

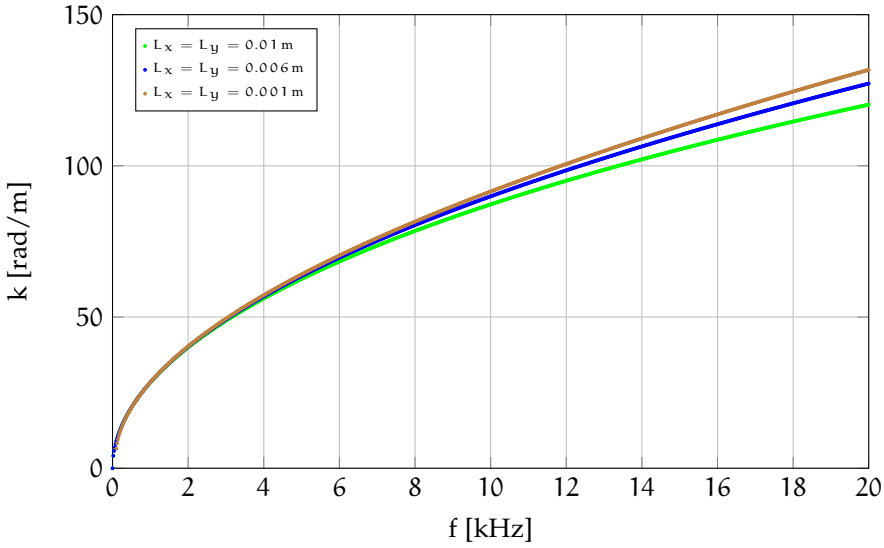

Figure 4.7: Effect of the size of the cell on the dispersion curves of a thin ($h = 0.005\,m$) aluminium plate (cell modelled with SHELL181 element)

If the minimum wavelength becomes comparable to the thickness of the plate, this last can be no longer considered thin. Therefore, at high frequencies (depending on the thickness of the plate under investigation) the plate should be analysed as thick. In this case, first-order theories for flat plate may lead to inaccurate results, and it is necessary refining the model. For this reason, the same waveguide is now modelled by using brick elements, e.g. SOLID45 in ANSYS®. In Figure 4.8, the ANSYS® model of the elementary cell is shown, meshed by using five elements through the thickness. The length of the side is $\Delta_x = \Delta_y = 0.001\,m$.

First of all, a mesh convergence study is performed on the number of elements to be used through the thickness. In Figure 4.9, the propagating waves, i.e. corresponding to purely real wavenumbers, are shown up to 500 kHz, calculated by using an increasing number of elements through the thickness: 20 SOLID45 are sufficient to obtain a good accuracy. Furthermore, among the primarily flexural, shear and extensional branches propagating since the lowest frequencies, other waves cut-on at very high frequencies. This is even more evident if the range of the analysis is increased. The complete dispersion plot (obtained using the model with 20 SOLID45) is shown up to 700 kHz in Figure 4.10, wherein both real (Figure 4.10a) and imaginary (Figure 4.10b) parts of the wavenumbers are plotted. From the plots, it is possible to understand that for frequencies less than 312 kHz there are only three propagating waves (i.e. having imaginary part equal to zero), corresponding to bending, shear and longitudinal waves. At 312 kHz, two pure imaginary wavenumbers, corresponding to evanescent waves, become

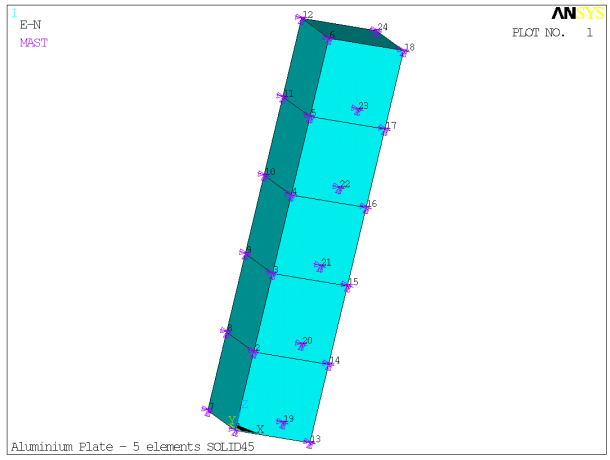

Figure 4.8: Elementary cell of an aluminium plate modelled with five elements SOLID45

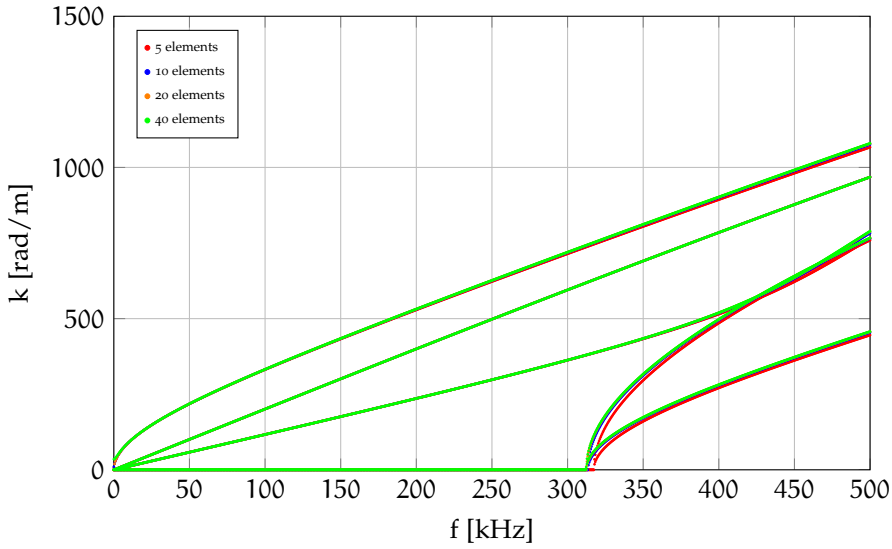

Figure 4.9: Mesh convergence study for a thick plate modelled with SOLID45 elements

pure real, meaning that two high-order waves start to propagate. This frequency is called *cut-on frequency of the waves*. Furthermore, at 569 kHz, a pair of complex conjugate wavenumbers bifurcates into a pair of propagating waves. One of them has a particular behaviour, later explained. Other two higher-order waves cut-on at 634 kHz.

In Figure 4.11, the dispersion curves are shown in logarithmic y-axis and in a reduced frequency range in order to highlight the behaviour of the wave which cuts on at 569 kHz. As said above, the pair of complex wave *a* bifurcates into a pair of propagating waves *b*-*c*. In particular, the curve *b* has a negative gradient, i.e. the wavenumber decreases as the frequency increase. According to the definition of group velocity (Eq. (2.10)), this wave has a negative group velocity:

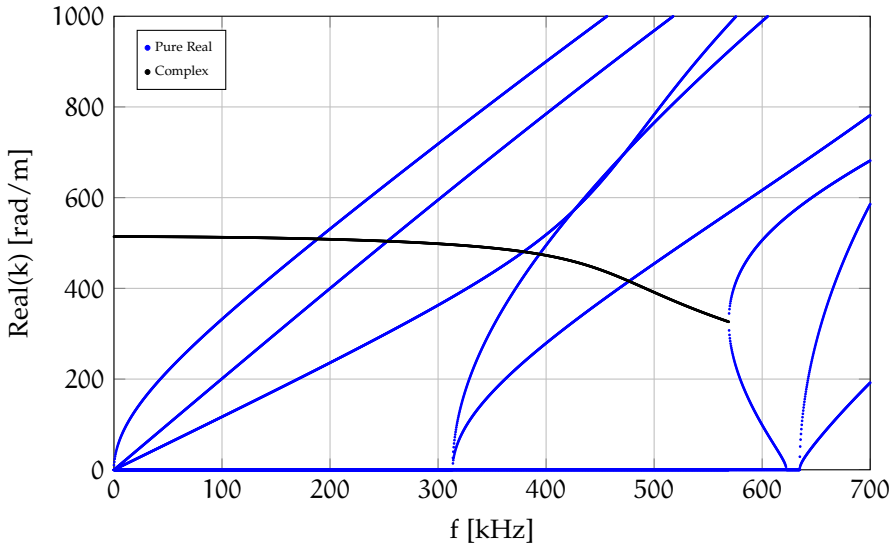

(a) *Real part of dispersion curves*

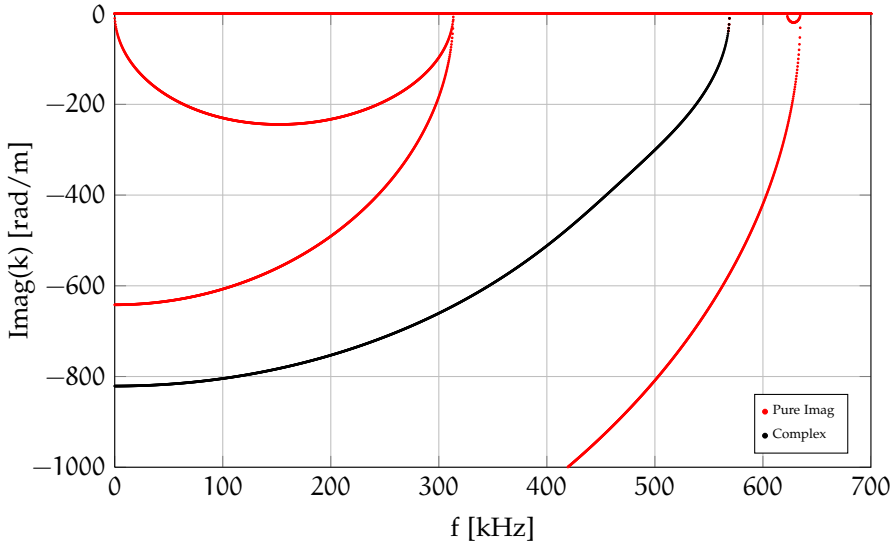

(b) *Imaginary part of dispersion curves*

Figure 4.10: Dispersion curves of an aluminium plate

the wave carries energy in the negative direction, but with a positive wavenumber. Quoting Mace et al. [58], *the motion thus resembles a Michael Jackson Moonwalk [141]*. Waves with negative group velocity are object of discussion in literature [142–147], since Tolstoy and Usdin [148] tried to explain the significance of negative group velocity. Recent works [145–147] agree in associating this behaviour to higher order symmetric Lamb waves (starting from S_1 wavemode).

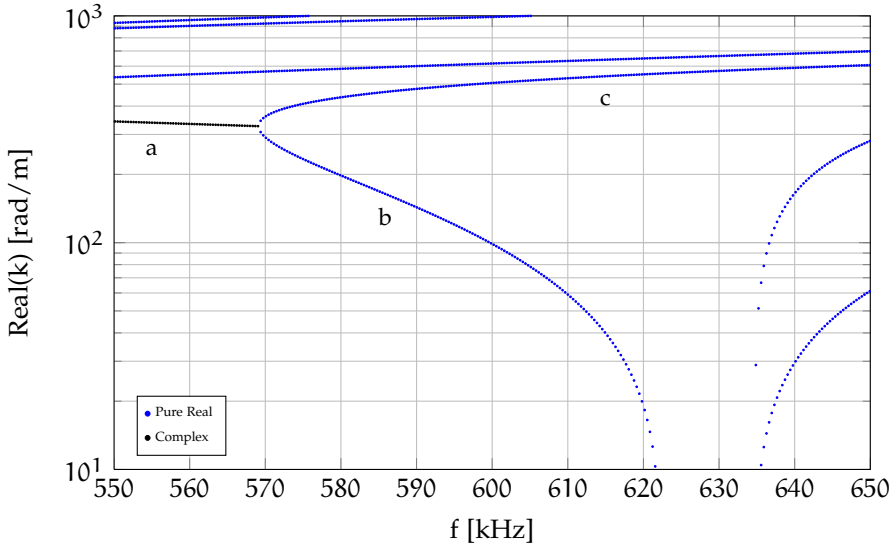

Figure 4.11: Dispersion curves of an aluminium plate - Zooming at high frequencies (Y-axis log)

4.4.2 Composite and laminated plates

Beside the isotropic plates, the WFEM is suitable to investigate also orthotropic, composite or sandwich panels. In this section, dispersion curves are calculated for orthotropic and laminated infinite panels, comparing the results obtained through Wave/Finite Element Method to those obtained with the Spectral Finite Element Approach developed by Barbieri et al. [149].

4.4.2.1 *Orthotropic plate*

Consider the carbon/epoxy composite plate 0.005m thick, having a mass density $\rho = 1590\,\mathrm{kg/m^3}$, whose mechanical properties along its principal axes of orthotropy (x', y', z') are described in Table 4.1.

Table 4.1: Mechanical properties of an orthotropic carbon/epoxy plate

Young's moduli [GPa]			Shear moduli [GPa]			Poisson's ratios		
$E_{x'}$	$E_{y'}$	$E_{z'}$	$G_{x'y'}$	$G_{x'z'}$	$G_{y'z'}$	$\nu_{x'y'}$	$\nu_{x'z'}$	$\nu_{y'z'}$
171.42	9.08	9.08	5.29	5.29	3.97	0.32	0.32	0.499

The FE model of the elementary cell consist of one SHELL181 element, with dimensions $\Delta_x = \Delta_y = 0.001$ m. The dispersion curves of the carbon/epoxy plate are plotted in Figure 4.12, in which both the WFEM and SFEM results are shown. As can be observed, the accordance between the two methods is quite good, but SFEM requires the definition of a spectral element case-by-case, whereas the WFEM exploits the ANSYS® elements library.

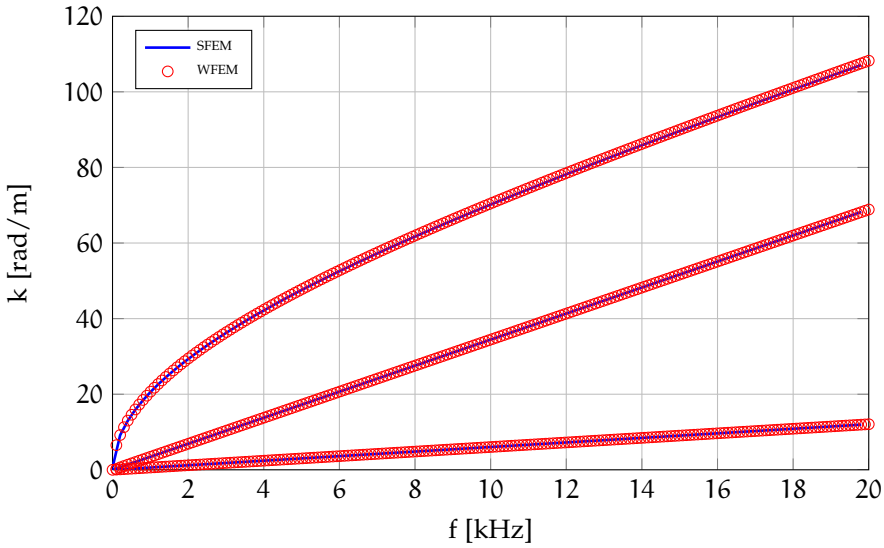

Figure 4.12: Dispersion curves of an orthotropic infinite plate

4.4.2.2 *Laminated composite plates*

Barbieri et al. [149] investigate the wave propagation in laminated composite plates, composed by two different materials. The properties of the plate are summarised in Table 4.2. (Barbieri et al. [149] report only few of them, fixing the others in order to satisfy the assumptions of plane stress. Herein the missing properties are assumed and reported). The Finite Element model of the elementary cell is obtained with 12 elements SOLID45, one for each layer, i.e. the reduced WFE model has 72 DOFs. The dispersion curves obtained by means of the two approaches are shown in Figure 4.13.

4.4.3 Sandwich panels

As last example, the dispersion curves a of sandwich panel are calculated through WFEM and then compared to literature results.

Consider an isotropic sandwich panel. Shorter [150] employs a SFEM method to describe the dispersion relations of a sandwich panel having a foam core ($E = 0.03\,\text{GPa}$, $\nu = 0.2$, $\rho = 48\,\text{kg/m}^3$, $h = 15\,\text{mm}$) and aluminium skins ($E = 71\,\text{GPa}$, $\nu = 0.33$, $\rho = 2700\,\text{kg/m}^3$, $h = 0.6\,\text{mm}$).

The FE model of the elementary cell is build in ANSYS® with 27 SOLID45 elements having height 0.6 mm. The in-plane dimensions of the cell are $\Delta_x = \Delta_y = 2\,\text{mm}$. In Figure 4.14, the dispersion curves of the isotropic sandwich are shown. The agreement of the WFEM results with the literature ones is quite good, mostly at high frequencies. Slight differences are instead appreciated at low frequencies, due to round-off errors. It is worth to highlight again the presence of a wave with negative group velocity, predicted by both methods.

Table 4.2: Mechanical properties of a laminated composite plates [149]

		Material A	Material B
Young's moduli [GPa]	$E_{x'}$	65	145
	$E_{y'}$	65	7.79
	$E_{z'}$	6.5	1.45
Shear moduli [GPa]	$G_{x'y'}$	3.86	4
	$G_{x'z'}$	7.15	1.59
	$G_{y'z'}$	5.85	1.30
Poisson's ratio	$\nu_{x'y'}$	0.05	0.34
	$\nu_{x'z'}$	0.01667	0.113
	$\nu_{y'z'}$	0.01667	0.113
Density [kg/m^3]	ρ	1467	1550
Thickness [mm]	h	2.37	2.37
Lay-up sequence		$[0A, 45B, 90B, 45B, 0B, 90B]_s$	

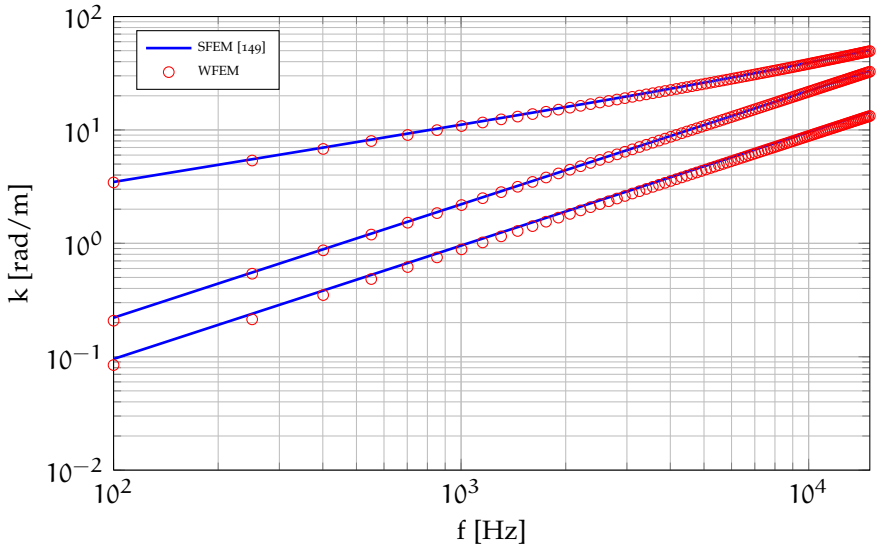

Figure 4.13: Dispersion curves of a laminated composite plate [149]

4.4.4 Natural Fibre Composite Laminate: comparison with experimental results

The use of Natural Fibre Composites (NFC) in transportation engineering applications is increasing, especially in automotive industry. For instance, Mercedes S-class uses SI43kg of natural fibre reinforced thermoplastics in door cards, seat based and other internal applications [151], whereas 2005 Ford Mondeo presents

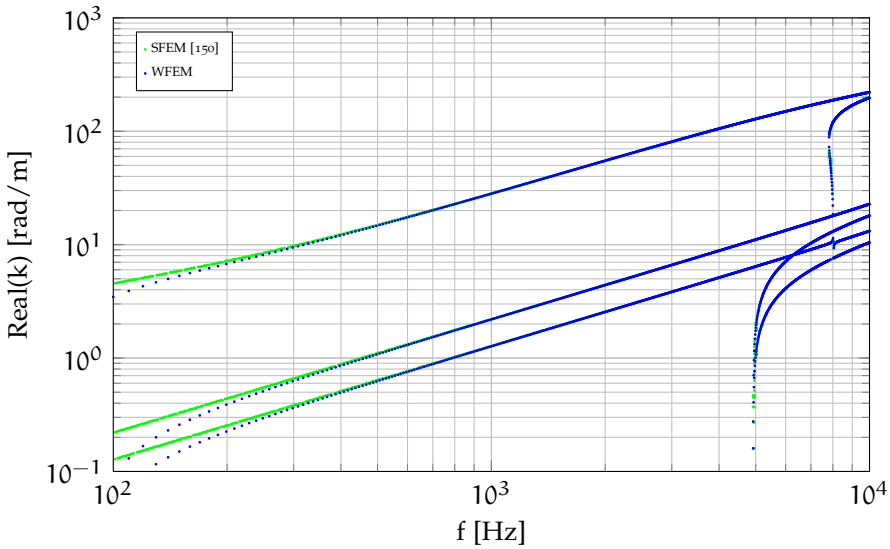

Figure 4.14: Real valued dispersion curves for an isotropic sandwich panel [150]

door linings made of polypropylene reinforced with kenaf [152]. Several works about bio-based panels have been carried out by the author's research group [131, 132, 134]. Within this wide experimental campaign, the dispersion relations (in terms of group velocity) of flat NFC panels were experimentally carried out, and reported by Petrone [153], and one of the goal of this work is to validate experimental results with numerical ones.

4.4.4.1 *Test specimen*

The panel under investigation is an unidirectional laminated NFC, constituted by 8 plies of Flax/PE with a lay-up sequence $[0]_8$. The panel have dimensions $0.706\,\mathrm{m} \times 0.496\,\mathrm{m} \times 0.0036\mathrm{m}$ and density $\rho = 1025\,\mathrm{kg/m^3}$. Its mechanical properties are reported in Table 4.3.

Table 4.3: Mechanical properties of the unidirectional Flax/PE panel

Young's moduli [GPa]			Shear moduli [GPa]			Poisson's ratios		
E_x	E_y	E_z	G_{xy}	G_{xz}	G_{yz}	ν_{xy}	ν_{xz}	ν_{yz}
9.5	1.3	1.3	0.55	0.55	0.4	0.4	0.4	0.6

4.4.4.2 *Experimental setup*

The experimental test is basically based on the identification of a given type of wave propagating in the plate, properly excited. These kind of waves are known as *guided waves*, since they may travel at large distance in structures with a very

small attenuation. They are usually used for structural health monitoring applications (SHM) [91]. Besides structural health monitoring, guided waves can be used also in the fields of non-destructive testing and material characterization [154–156].

Among the various available waves [157], *Lamb waves* are ultrasonic waves, guided between two parallel free surfaces (i.e. upper and lower surfaces of a plate). The setup of the experimental test was arranged in order to excite the specimen with a known Lamb wave, and then to evaluate how much time this wave spends to cover a finite distance in different directions. Four piezoelectric PICERAMIC PIC 255 (Figure 4.16c), having diameter $d = 10\,mm$ and thickness $t = 0.25\,mm$, were bonded on the plate surface. The first one is positioned onto the centre of the panel, and used as actuator. The other ones, instead, are used as sensors: they are placed 150 mm far away from the actuator, along three different directions (0°, 45° and 90°, according to the longitudinal axis of the panel).

The specimen was excited by a known excitation. In this case, a 4.5 sine cycles curve with Hanning window was used, in order to obtain a narrow-band bell curve in the frequency domain, as shown in Figure 4.15. Narrow-band excitations are needed in order to limit the problem of the dispersiveness of Lamb waves, strongly dependent on the frequency. The excitation, provided by the actuator, was generated by a signal generator HP Agilent 33120A (Figure 4.16a). The complete acquisition process was performed by using an oscilloscope Agilent InfiniiVision DSO7014A (Figure 4.16b). In Figure 4.17, a schematic representation of the experimental setup is shown on the panel surface.

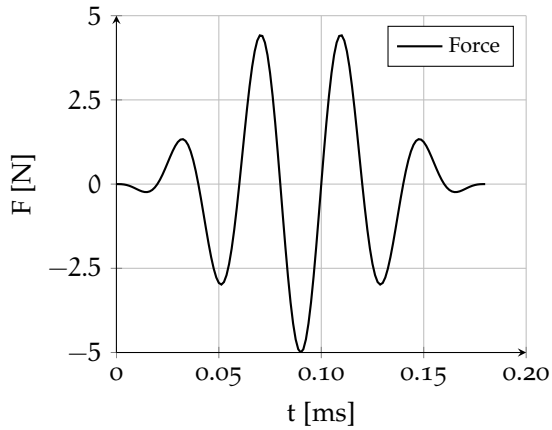

Figure 4.15: Excitation curve (4.5 sine cycles with Hanning window) at 25 kHz

Once the excitation is provided by the actuator, the wavefront starts to propagate in an omni-directional way, with different group velocities depending on the mechanical properties along a specific direction. The experimental setup allows to evaluate the group velocity of the waves travelling along three direction. For each sensor, the time spent by the wavefront to travel across 150 mm must be measured. This is performed through the Short-Time Fourier Transform (STFT) of the signals acquired at the actuator and at the receivers positions, which allow

(a) *signal generator* **(b)** *oscilloscope* **(c)** *piezoelectric*

Figure 4.16: Experimental instrumentation setup

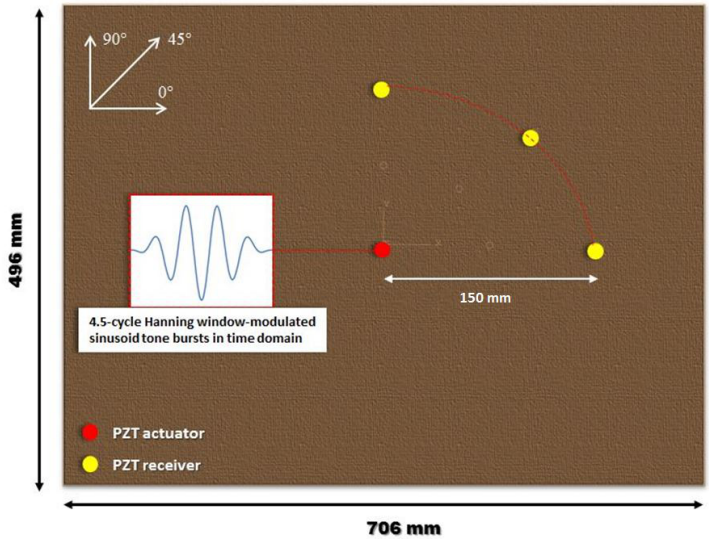

Figure 4.17: Schematic representation of the experimental setup onto the panel surface

to estimate the time of flight (TOF), i.e. the time interval between the maximum energy of the actuator and of the receiver wavefronts.

For example, the Figure 4.18 shows the signals of the actuator and of the receiver in the 0° direction for an excitation frequency 25 kHz. The TOF is highlighted as the time interval between the points of maximum energy of the signals. Once the TOF is measured, the group velocity is simply calculated as the ratio of the distance (150 mm) over the time of flight. It is worth to notice the presence of a second wavefront in Figure 4.18: it represents the acquisition of wave package reflected at the boundaries of the plate. (For this reason, the sensor should be placed as far away from the edges as possible).

The tests were performed in the frequency range $10 - 40$ kHz, with a a step of 5 kHz. The upper frequency limit is defined by the reflection of symmetric Lamb wave from the plate edges, overlapping the antisymmetric wave package under investigation at the sensor position.

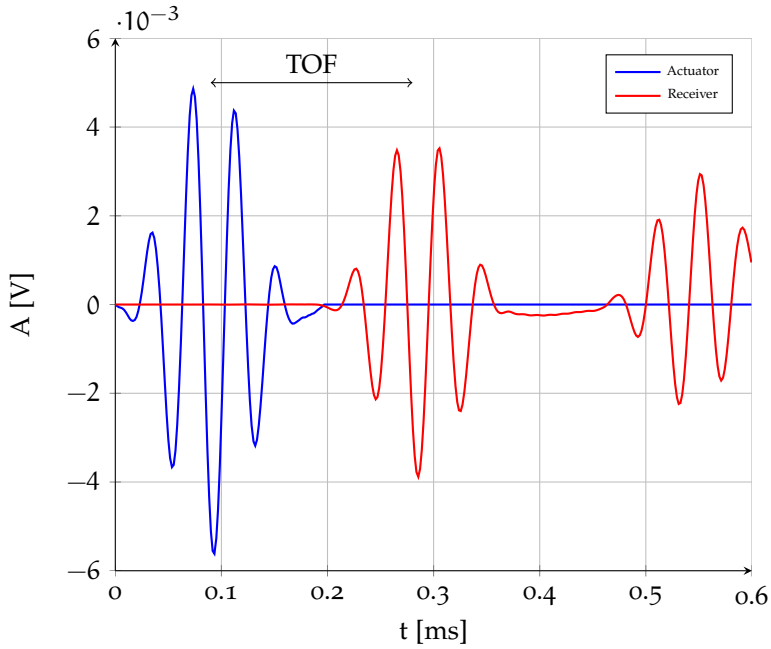

Figure 4.18: TOF of unidirectional Flax-PE panel at 25 kHz along 0° direction

4.4.4.3 *WFE model*

The WFE model of the waveguide is realised, as usual, through ANSYS®. The elementary cell has in-plane dimensions 0.1 mm × 0.1 mm: the cell is small to guarantee that the side are at least 10 times shorter than the minimum wavelength in the whole frequency range of analysis. The FE model of the cell is modelled with an element SHELL181 (in this range, the plate can be assumed as thin). The material properties are those reported in Table 4.3.

Since the code is able to estimate the wavenumbers associated to waves propagating only along x axis ($\theta = 0°$), in order to evaluate the group velocity also along the y axis ($\theta = 90°$), the FE model of the cell is rotated of 90° around z axis.

Once the wavenumbers are known as a function of the frequency, the group velocity is numerically evaluated according its definition.

4.4.4.4 *Numerical-Experimental correlation*

In Figure 4.4, experimental and numerical, results in terms of wave propagation speed along x and y axes, are shown. The same results are summarised in Table 4.4 as well. The WFEM allows a very good prediction of the experimental results in the whole frequency range, since the relative error is always lower than 10%.

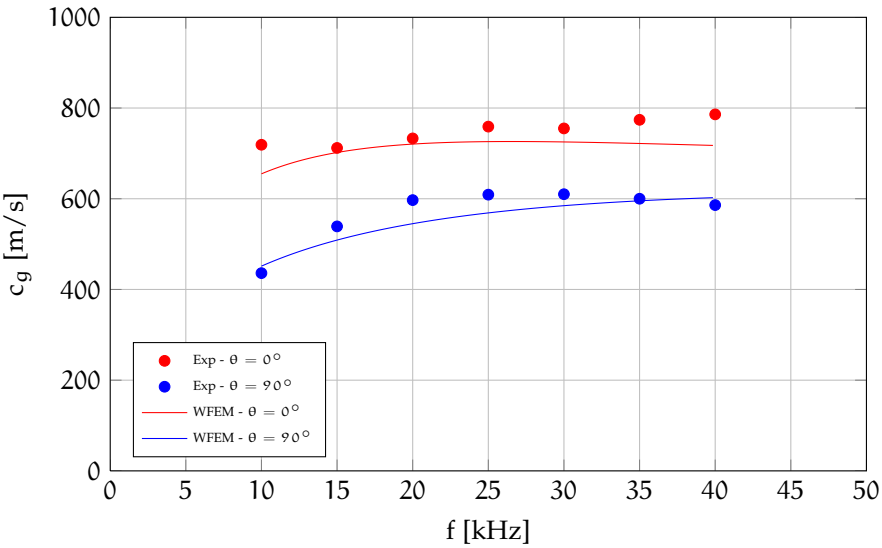

Figure 4.19: Group velocity for the unidirectional Flax/PE panel

Table 4.4: Group velocity for the unidirectional Flax/PE panel

	$\theta = 0°$			$\theta = 90°$		
f [Hz]	c_{g-exp} [m/s]	c_{g-WFE} [m/s]	Δc_g %	c_{g-exp} [m/s]	c_{g-WFE} [m/s]	Δc_g %
10	719	655	8.9	436	451	−3.4
15	712	703	1.2	539	508	5.7
20	733	721	1.6	597	545	8.7
25	759	726	4.3	609	569	6.6
30	755	726	3.8	610	585	4.0
35	774	722	6.7	600	595	0.0
40	786	718	8.6	586	601	−0.3

5 CONCLUSIONS

In this dissertation, some investigations have been performed on the use of the Wave and Finite Element Method. The analysis have concerned: (i) the wave analysis of one- and two-dimensional periodic waveguides; (ii) the forced response of one-dimensional structures.

From the analysis of the literature, it emerged that the Wave and Finite Element Method has received an increasing attention in the last 10 years for the analysis of periodic structures. In fact, differently from other numerical methods, this technique allows to model a single, elementary cell by using conventional Finite Element packages, avoiding the definition of special elements. Mass and stiffness finite element matrices of the element are post-processed by applying the Bloch's theory, together with continuity of displacements and equilibrium of forces at the interface, in order to define a dynamic stiffness matrix. This leads to the formulation of an eigenvalue problem whose solutions are the waves' propagation constants. Once the propagation constants are known, it is possible to obtain the dispersion curves of the waveguide under investigation. From the dispersion relations, furthermore, it is possible to estimate the forced response of a finite structure by applying the wave propagation approach.

The Wave and Finite Element Method for one-dimensional waveguides has been explained. Once mass and stiffness finite element matrices was defined, the eigenproblem has been formulated on the transfer matrix, expressed as a function of the dynamic stiffness matrix. Starting from the eigenvalues of the problem, the wavenumbers have been calculated in order to plot the dispersion relations, whereas the eigenvectors have been used to evaluate the forced response of finite structures. In the case of complex shapes, it has been highlighted the necessity of a reduced wave basis, neglecting high order evanescent waves. The forced response of finite structures have been estimated through a wave propagation approach, based on the calculation of the amplitudes of the propagating waves and of the reflection coefficients at the boundaries. The analysis of one-dimensional structures, both in terms of wave propagation and forced response, has been performed through a MATLAB® code, named *WFEM1D.m*, able to import the finite element matrices of the elementary cell carried out with ANSYS®. The code has been validated with available analytic solutions for rod and beam elements, both in terms of dispersion curves and forced response. A sensitivity analysis has been performed in order to evaluate the influence of the cell length on the dispersion curves. Errors at high frequencies may occur if the flexural wavelength becomes comparable with the cell length. Furthermore, the use of brick elements to mesh the cross-section of the elementary cell may lead to low-frequencies errors too, due to the finite precision arithmetic of the computers. It has been shown that

this errors strongly depends on the material properties and on the cell length. For this reason, the cell length should be chosen through a compromise in order to reduce finite element discretisation errors (at high frequencies) and round-off errors (at low frequencies). WFEM has been used to investigate one-dimensional structures with different cross-section, in order to exploit its potentiality. In particular, the dispersion curves of a thin-walled tubular section, a simply supported strip plate and a sandwich beam, as well as the Frequency Response Function of a layered beam, have been carried out, showing a good agreement with results available in literature. Furthermore, the forced response of a hybrid sandwich beam, constituted by aluminium face sheets and polypropylene honeycomb, has been estimated and compared to experimental results, obtained through a modal test. The comparison of the numerical and experimental FRF has shown an acceptable correlation, considering that the honeycomb core has been assumed as isotropic.

A first approach to two-dimensional waveguides has been introduced, with the primary scope to validate some experimental tests on the wave propagation through natural fibres composite panels. In the case of infinite panels, the eigenproblem has been formulated on a reduced dynamic stiffness matrix. Eigenproblems of different forms have arisen because of the three-parametric dependence. In particular, for our purposes a quadratic eigenvalue problem has been considered, in order to investigate the wave propagation along the direction $\theta = 0°$. The eigenproblem has been linearised through first companion linearisation, and solved in order to evaluate the eigenvalues, i.e. the propagation constants. In this case, the forced response has not been analysed, since some issues arose in the eigenvectors tracking. In order to plot the dispersion relations of infinite panels, the WFEM for two-dimensional waveguides has been implemented into another MATLAB® code, named *WFEM2D.m*, in which the finite element matrices are imported from ANSYS®. A sensitivity analysis has been performed on shell and solid elements, showing the same numerical issues as in the one-dimensional code. The analysis of a thick aluminium plate at high frequencies has highlighted the capability of this method to predict dispersion relations also for waves having negative group velocity. Dispersion curves for laminated and sandwich panels have been carried out and compared to SFEM results available from the literature, showing a very good agreement. Finally, the group velocities along $0°$ and $90°$ directions have been estimated for a natural fibres composite panels and compared to experimental results. The experimental test regarded the propagation of ultrasonic guided waves, i.e. Lamb waves, whose group velocities were estimated at different frequencies by measuring the time spent by the excited waves to travel over the distance between the actuator and the receivers.

In conclusion, the Wave and Finite Element Method has allowed the analysis of different types of waveguides through the Finite Element discretisation of an elementary cell, together with the application of periodicity conditions.

The main advantages of this technique can be summarised as follows.

- The elementary cell can be discretised through conventional Finite Elements, and then FE libraries of commercial packages can be used without the definition of specific elements.

- The computational cost is independent of the length of the elementary cell, as well as the size of the structure. This property makes the WFEM particularly appealing for the analysis of structures in the mid-frequency range, where full FE models are computational expensive and SEA results are approximated.

On the other hand, some drawbacks can be highlighted, on which future works will focus:

- the finite arithmetic precision of computer determines round-off errors in the dynamic stiffness matrix, which arise at low-frequencies mostly if the cross-section is discretised with brick elements. However, this issue does not affect the results in the mid- and high-frequency range.
- The tracking of eigenwaves, performed through a Modal Assurance Criterion, is a time-consuming task, and it does not work correctly for two-dimensional waveguides.
- There is not a well-posed criterion for the definition of the reduced wave basis, needed for the calculation of the forced response.

Appendix

A EXAMPLE OF COMMAND LIST FOR ANSYS®

Command list to import in ANSYS® in order to obtain mass and stiffness matrices of a cell made of steel, 0.001 m long, having square cross-section with area $A = 10^{-6}$ m.

```
/BATCH,list
/CLEAR

/PREP7,Solid Steel Beam     !Preprocessor session
/TITLE,Solid Steel Beam     !Title of the job
/REPLOT

!DEFINITION OF MATERIAL PROPERTIES
Em=2.0E+011                 !Young modulus
rho=7.8E+003                !Density
nu=3.3E-001                 !Poisson ratio

!DEFINITION OF THE MATERIAL
MP,EX,1,Em
MP,PRXY,1,nu
MP,DENS,1,rho

!DEFINITION OF THE NODES
n,1,0,-5.e-4,-5.e-4
n,2,0,5.e-4,-5.e-4
n,3,0,5.e-4,5.e-4
n,4,0,-5.e-4,5.e-4
n,5,0.001,-5.e-4,-5.e-4
n,6,0.001,5.e-4,-5.e-4
n,7,0.001,5.e-4,5.e-4
n,8,0.001,-5.e-4,5.e-4

!DEFINITION OF THE FINITE ELEMENT
ET,1,SOLID45                !Finite element SOLID45
KEYOPT,1,4,0                !Options of the element
E,1,2,3,4,5,6,7,8           !Connecting the nodes.

!SOLUTION
/SOLU                       !Solution session
ANTYPE,SUBSTR               !Type of analysis: substructuring
SEOPT,steel_square,3,1      !Substructure analysis options
M,ALL,ALL                   !Definition of master degrees of freedom
```

```
/OUTPUT,steel_square.txt    !Definition output file
SOLVE                       !Analysis
/OUTPUT                     !Writing the text output to the file
FINISH                      !End of the job
```

BIBLIOGRAPHY

[1] K. F. Graff. *Wave Motion in Elastic Solids*. Dover Publications, 1975.

[2] L. Cremer, M. Heckl, and B. A. T. Petersson. *Structure-Borne Sound: Structural Vibrations and Sound Radiation at Audio Frequencies*. Springer-Verlag, 3rd edition, 2005.

[3] R. A. DiTaranto. Theory of vibratory bending for elastic and viscoelastic layered finite-length beams. *Journal of Applied Mechanics*, 32(4), 1965.

[4] D. J. Mead and S. Markus. The forced vibration of a three-layer, damped sandwich beam with arbitrary boundary conditions. *Journal of Sound and Vibration*, 10(2):163–175, 1969.

[5] V. S. Sokolinsky and S. R. Nutt. Consistent higher-order dynamic equations for soft-core sandwich beams. *AIAA Journal*, 42(2):374–382, 2004.

[6] G. Kurtze and B. G. Watters. New wall design for high transmission loss or high damping. *The Journal of the Acoustical Society of America*, 31(6):739–748, 1959.

[7] J. A. Moore. *Sound transmission loss characteristics of three layer composite wall constructions*. PhD Thesis, Department of Mechanical Engineering, Massachusetts Institute of Technology, Cambridge, Massachusetts (USA), May 1975.

[8] C. L. Dym and M. A. Lang. Transmission of sound through sandwich panels. *The Journal of the Acoustical Society of America*, 56(5), 1974.

[9] C. L. Dym and D. C. Lang. Transmission loss of damped asymmetric sandwich panels with orthotropic cores. *Journal of Sound and Vibration*, 88(3):299–319, 1983.

[10] A. C. Nilsson. Wave propagation in and sound transmission through sandwich plates. *Journal of Sound and Vibration*, 138(1):73–94, 1990.

[11] J. N. Reddy. *Mechanics of Laminated Composite Plates and Shells: Theory and Analysis*. CRC Mechanical Engineering Series. Taylor & Francis, 2nd edition, 2003.

[12] S. Ghinet, N. Atalla, and H. Osman. The transmission loss of curved laminates and sandwich composite panels. *The Journal of the Acoustical Society of America*, 118(2), 2005.

[13] R. Kumar and R. W. B. Stephens. Dispersion of flexural waves in circular cylindrical shells. *Proceedings of the Royal Society of London. A. Mathematical and Physical Sciences*, 329(1578):283–297, 1972.

[14] C. R. Fuller. The effects of wall discontinuities on the propagation of flexural waves in cylindrical shells. *Journal of Sound and Vibration*, 75(2):207–228, 1981.

[15] D. G. Karczub. Expressions for direct evaluation of wave number in cylindrical shell vibration studies using the Flügge equations of motion. *The Journal of the Acoustical Society of America*, 119(6), 2006.

[16] J. R. Banerjee. Development of an exact dynamic stiffness matrix for free vibration analysis of a twisted Timoshenko beam. *Journal of Sound and Vibration*, 270(1–2):379–401, 2004.

[17] L. Brillouin. *Wave Propagation in Periodic Structures: Electric Filters and Crystal Lattices*. Dover Publications, 2nd edition, 1953.

[18] J. F. Doyle. *Wave propagation in structures: spectral analysis using fast Discrete Fourier Transform*. Springer, 1997.

[19] S. Gopalakrishnan, A. Chakraborty, and D. R. Mahapatra. *Spectral Finite Element Method: Wave Propagation, Diagnostics and Control in Anisotropic and Inhomogeneous Structures*. Computational Fluid and Solid Mechanics. Springer, 2007.

[20] U. Lee. *Spectral Element Method in Structural Dynamics*. Wiley & Sons, 2009.

[21] O. C. Zienkiewicz and R. L. Taylor. *The Finite Element Method. Volume 2: Solid Mechanics*. Butterworth-Heinemann, 5th edition, 2000.

[22] M. Petyt. *Introduction to Finite Element Vibration Analysis*. Cambridge University Press, 2nd edition, 2010.

[23] V. Koloušek and R. F. McLean. *Dynamics in engineering structures*. Butterworths, 1973.

[24] W. T. Thomson. Transmission of elastic waves through a stratified solid medium. *Journal of Applied Physics*, 21(2), 1950.

[25] D. J. Mead. Wave propagation in continuous periodic structures: research contributions from southamption, 1964–1995. *Journal of Sound and Vibration*, 190(3):495–524, 1996.

[26] R. M. Orris and M. Petyt. A finite element study of harmonic wave propagation in periodic structures. *Journal of Sound and Vibration*, 33(2):223–236, 1974.

[27] A. Y. A. Abdel-Rahman. *Matrix analysis of wave propagation in periodic systems*. PhD Thesis, Institute of Sound and Vibration Research, University of Southampton, Southampton, UK, July 1979.

[28] D. J. Mead. A general theory of harmonic wave propagation in linear periodic systems with multiple coupling. *Journal of Sound and Vibration*, 27(2):235–260, 1973.

[29] D. J. Thompson. Wheel-rail noise generation, part iii: Rail vibration. *Journal of Sound and Vibration*, 161(3):421–446, 1993.

[30] L. Gry. Dynamic modelling of railway track based on wave propagation. *Journal of Sound and Vibration*, 195(3):477–505, 1996.

[31] L. Houillon, M. N. Ichchou, and L. Jezequel. Wave motion in thin-walled structures. *Journal of Sound and Vibration*, 281(3–5):483–507, 2005.

[32] J.-M. Mencik and M. N. Ichchou. Multi–mode propagation and diffusion in structures through finite elements. *European Journal of Mechanics - A / Solids*, 24(5):877–898, 2005.

[33] S. Akrout, M. N. Ichchou, J.-M. Mencik, and L. Jezequel. Structural guided waves energy velocities by finite element method. In *Proceedings of the 12th International Congress on Sound and Vibration (ICSV 12)*, 2005. 11 - 14 July, Lisbon, Portugal.

[34] M. N. Ichchou, S. Akrout, and J.-M. Mencik. Guided waves group and energy velocities via finite elements. *Journal of Sound and Vibration*, 305(4–5):931–944, 2007.

[35] S. R. F. Arruda, K. M. Ahmida, M. N. Ichchou, and J.-M. Mencik. Structural guided waves energy velocities by finite element method. In *Proceedings of the 12th International Congress on Sound and Vibration (ICSV 12)*, 2005. 11 - 14 July, Lisbon, Portugal.

[36] J.-M. Mencik and M. N. Ichchou. Wave finite elements in guided elasto-dynamics with internal fluid. *International Journal of Solids and Structures*, 44(7..8):2148–2167, 2007.

[37] M. N. Ichchou, J. Berthaut, and M. Collet. Multi-mode wave propagation in ribbed plates. part i: wavenumber-space characteristics. *International Journal of Solids and Structures*, 45(5):1179–1195, 2008.

[38] M. N. Ichchou, J. Berthaut, and M. Collet. Multi-mode wave propagation in ribbed plates. part ii: Predictions and comparisons. *International Journal of Solids and Structures*, 45(5):1196–1216, 2008.

[39] J.-M. Mencik and M. N. Ichchou. A substructuring technique for finite element wave propagation in multi-layered systems. *Computer Methods in Applied Mechanics and Engineering*, 197(6–8):505–523, 2008.

[40] M. N. Ichchou, J.-M. Mencik, and W. Zhou. Wave finite elements for low and mid-frequency description of coupled structures with damage. *Computer Methods in Applied Mechanics and Engineering*, 198(15–16):1311–1326, 2009.

[41] W. J. Zhou, M. N. Ichchou, and J.-M. Mencik. Analysis of wave propagation in cylindrical pipes with local inhomogeneities. *Journal of Sound and Vibration*, 319(1–2):335–354, 2009.

[42] J.-M. Mencik. On the low- and mid-frequency forced response of elastic structures using wave finite elements with one-dimensional propagation. *Computers & Structures*, 88(11–12):674–689, 2010.

[43] W. J. Zhou and M. N. Ichchou. Wave propagation in mechanical waveguide with curved members using wave finite element solution. *Computer Methods in Applied Mechanics and Engineering*, 199(33–36):2099–2109, 2010.

[44] W. J. Zhou, M. N. Ichchou, and O. Bareille. Finite element techniques for calculations of wave modes in one–dimensional structural waveguides. *Structural Control and Health Monitoring*, 18(7):737–751, 2011.

[45] J.-M. Mencik. Model reduction and perturbation analysis of wave finite element formulations for computing the forced response of coupled elastic systems involving junctions with uncertain eigenfrequencies. *Computer Methods in Applied Mechanics and Engineering*, 200(45–46):3051–3065, 2011.

[46] M. N. Ichchou, F. Bouchoucha, M. A. Ben Souf, O. Dessombz, and M. Haddar. Stochastic wave finite element for random periodic media through first–order perturbation. *Computer Methods in Applied Mechanics and Engineering*, 200(41–44):2805–2813, 2011.

[47] T. Huang, M. N. Ichchou, O. A. Bareille, and M. Collet. Wave propagation in smart structures through numerical approach. In *Proceedings of the 5th International Conference on Adaptative Modeling and Simulation (ADMOS 2011)*, 2011. 6 - 8 June, Paris, France.

[48] D. Chronopoulos, B. Troclet, M. N. Ichchou, and J. P. Lainé. A unified approach for the broadband vibroacoustic response of composite shells. *Composites Part B: Engineering*, 43(4):1837–1846, 2012.

[49] J.-M. Mencik. A model reduction strategy for computing the forced response of elastic waveguides using the wave finite element method. *Computer Methods in Applied Mechanics and Engineering*, 229–232:68–86, 2012.

[50] J.-M. Mencik and M.-L. Gobert. Wave finite element based strategies for computing the acoustic radiation of stiffened or non-stiffened rectangular plates subject to arbitrary boundary conditions. In *Proceedings of the 11th International Conference on Computational Structures Technology (CIVIL-COMP)*, 2012. 4 - 7 September, Dubrovnik, Croatia.

[51] T. L. Huang, M. N. Ichchou, and O. A. Bareille. Multi-mode wave propagation in damaged stiffened panels. *Structural Control and Health Monitoring*, 19(5):609–629, 2012.

[52] J.-M. Mencik. A wave finite element-based formulation for computing the forced response of structures involving rectangular flat shells. *International Journal for Numerical Methods in Engineering*, 95(2):91–120, 2013.

[53] D. Chronopoulos, B. Troclet, O. A. Bareille, and M. N. Ichchou. Modeling the response of composite panels by a dynamic stiffness approach. *Composite Structures*, 96(0):111–120, 2013.

[54] M. A. Ben Souf, M. N. Ichchou, O. A. Bareille, and M. Haddar. On the dynamics of uncertain coupled structures through a wave based method in mid- and high-frequency ranges. *Computational Mechanics*, 52(4):849–860, 2013.

[55] M. A. B. Souf, O. A. Bareille, M. N. Ichchou, B. Troclet, and M. Haddar. Variability of coupling loss factors through a wave finite element technique. *Journal of Sound and Vibration*, 332(9):2179–2190, 2013.

[56] M. A. B. Souf, O. A. Bareille, M. N. Ichchou, F. Bouchoucha, and M. Haddar. Waves and energy in random elastic guided media through the stochastic wave finite element method. *Physics Letters A*, 377(37):2255–2264, 2013.

[57] D. Chronopoulos, M. N. Ichchou, B. Troclet, and O. A. Bareille. Computing the broadband vibroacoustic response of arbitrarily thick layered panels by a wave finite element approach. *Applied Acoustics*, 77:89–98, 2014.

[58] B. R. Mace, D. Duhamel, M. J. Brennan, and L. Hinke. Finite element prediction of wave motion in structural waveguides. *Journal of Acoustical Society of America*, 117(5):2835–2843, May 2005.

[59] D. Duhamel, B. R. Mace, and M. J. Brennan. Finite element analysis of the vibrations of waveguides and periodic structures. *Journal of Sound and Vibration*, 294(1–2):205–220, 2006.

[60] Y. Waki, B. R. Mace, and M. J. Brennan. Flexural wave propagation in a plate strip with free boundaries using the wave finite element method. In *Proceedings of the 36th International Congress and Exposition on Noise Control Engineering (INTER-NOISE 2007)*, 2007. 28 - 31 August, Instanbul, Turkey.

[61] Y. Waki, B. R. Mace, and M. J. Brennan. Vibration analysis of a tyre model using the wave and finite element method. In *Proceedings of the 19th International Congress on Acoustics (ICA 2007)*, 2007. 2 - 7 September, Madrid, Spain.

[62] E. Manconi and B. R. Mace. Modelling wave propagation in cylinders using a wave/finite element technique. In *Proceedings of the 19th International Congress on Acoustics (ICA 2007)*, 2007. 2 - 7 September, Madrid, Spain.

[63] B. R. Mace and E. Manconi. Modelling wave propagation in two-dimensional structures using finite element analysis. *Journal of Sound and Vibration*, 318(4–5):884–902, 2008.

[64] B. R. Mace. Waves and finite elements. In *Proceedings of the 7th European Conference on Structural Dynamics (EURODYN 2008)*, 2008. 7 - 9 July, Southampton, UK.

[65] E. Manconi and B. R. Mace. Wave propagation in viscoelastic laminated composite plates using a wave/finite element method. In *Proceedings of the 7th European Conference on Structural Dynamics (EURODYN 2008)*, 2008. 7 - 9 July, Southampton, UK.

[66] Y. Waki, B. R. Mace, and M. J. Brennan. Numerical issues concerning the wave and finite element method for free and forced vibrations of waveguides. *Journal of Sound and Vibration*, 327(1–2):92–108, 2009.

[67] E. Manconi and B. R. Mace. Wave propagation in helically wire-reinforced pipes from finite element analysis. In *Proceedings of the 2nd International Conference on Computational Methods in Structural Dynamics and Earthquake Engineering (COMPDYN 2009)*, 2007. 22 - 24 June, Rhodes, Greece.

[68] E. Manconi and B. R. Mace. Wave propagation in axisymmetric structures from finite element analysis. In *Proceedings of the 2nd International Conference on Computational Methods in Structural Dynamics and Earthquake Engineering (COMPDYN 2009)*, 2007. 22 - 24 June, Rhodes, Greece.

[69] E. Manconi and B. R. Mace. Wave characterization of cylindrical and curved panels using a finite element method. *The Journal of the Acoustical Society of America*, 125(1), 2009.

[70] E. Manconi and B. R. Mace. Dynamic and acoustic properties of viscoelastic laminated structures. In *Proceedings of the 17th International Congress on Sound and Vibration (ICSV 17)*, 2010. 18 - 22 July, Cairo, Egypt.

[71] E. Manconi and B. R. Mace. Estimation of the loss factor of viscoelastic laminated panels from finite element analysis. *Journal of Sound and Vibration*, 329(19):3928–3939, 2010.

[72] J. M. Renno and B. R. Mace. On the forced response of waveguides using the wave and finite element method. *Journal of Sound and Vibration*, 329(26):5474–5488, 2010.

[73] J. M. Renno and B. R. Mace. Calculating the forced response of two-dimensional homogeneous media using the wave and finite element method. *Journal of Sound and Vibration*, 330(24):5913–5927, 2011.

[74] J. M. Renno and B. R. Mace. A hybrid approach for the calculation of the scattering properties of joints. In *Proceedings of the 5th International Conference on Adaptative Modeling and Simulation (ADMOS 2011)*, 2011. 6 - 8 June, Paris, France.

[75] J. M. Renno and B. R. Mace. Vibration modelling of helical springs with non-uniform ends. *Journal of Sound and Vibration*, 331(12):2809–2823, 2012.

[76] J. M. Renno, E. Manconi, and B. R. Mace. Calculation of coupling loss factors using a hybrid finite element/wave and finite element method. In *Proceedings of the 4th International Conference on Noise and Vibration: Emerging Methods (NOVEM 2012)*, 2012. 1 - 4 April, Sorrento, Italy.

[77] J. M. Renno and B. R. Mace. Calculation of reflection and transmission coefficients of joints using a hybrid finite element/wave and finite element approach. *Journal of Sound and Vibration*, 332(9):2149–2164, 2013.

[78] J. M. Renno and B. R. Mace. Calculating the forced response of cylinders using the wave and finite element method. In *Proceedings of the 11th International Conference on Recent Advances in Structural Dynamics (RASD 2013)*, 2012. 1 - 3 July, Pisa, Italy.

[79] E. Manconi, B. R. Mace, and R. Garziera. The loss-factor of pre-stressed laminated curved panels and cylinders using a wave and finite element method. *Journal of Sound and Vibration*, 332(7):1704–1711, 2013.

[80] R. H. Lyon and R. G. DeJong. *Theory and application of Statistical Energy Analysis*. Butterworth-Heinemann, 1995.

[81] B. R. Mace. Wave reflection and transmission in beams. *Journal of Sound and Vibration*, 97(2):237–246, 1984.

[82] D. W. Miller and A. von Flotow. A travelling wave approach to power flow in structural networks. *Journal of Sound and Vibration*, 128(1):145–162, 1989.

[83] L. S. Beale and M. L. Accorsi. Power flow in two- and three-dimensional frame structures. *Journal of Sound and Vibration*, 185(4):685–702, 1995.

[84] S.-K. Lee, B. R. Mace, and M. J. Brennan. Wave propagation, reflection and transmission in non-uniform one-dimensional waveguides. *Journal of Sound and Vibration*, 304(1–2):31–49, 2007.

[85] Y. Waki. *On the application of Finite Element Analysis to wave motion in one-dimensional waveguides*. PhD Thesis, Institute of Sound and Vibration Research, University of Southampton, Southampton, UK, December 2007.

[86] E. Manconi. *Modelling wave propagation in two-dimensional structures using a wave/finite element technique*. PhD Thesis, Department of Industrial Engineering, University of Parma, Parma, Italy, March 2008.

[87] F. Fahy and P. Gardonio. *Sound and Structural Vibration (Second Edition)*. Academic Press, Oxford, 2nd edition, 2007.

[88] J. D. Achenbach. *Wave propagation in elastic solids*. North–Holland series in applied mathematics and mechanics. North–Holland Pub. Co., 1973.

[89] S. A. Hambric. Structural acoustics tutorial–part 1: Vibrations in structures. *Acoustics Today*, 2(4), 2006.

[90] E. Carrera, G. Giunta, and M. Petrolo. *Beam Structures: Classical and Advanced Theories*. John Wiley & Sons, Ltd, 2011.

[91] V. Giurgiutiu. *Structural Health Monitoring: with Piezoelectric Wafer Active Sensors*. Structures and Fracture ebook Collection Series. Elsevier Science, 2007.

[92] A. W. Leissa. The free vibration of rectangular plates. *Journal of Sound and Vibration*, 31(3):257–293, 1973.

[93] D. Russell. Acoustics and Vibration Animations, 2014. Available from http://www.acs.psu.edu/drussell/demos.html. Accessed on March 6th, 2014.

[94] M. R. D. Influence of rotatory inertia and shear on flexural vibrations of isotropic, elastic plates. *Journal of Applied Mechanics*, 18:31–38, 1951.

[95] K. M. Liew, Y. Xiang, S. Kitipornchai, and C. M. Wang. *Vibration of Mindlin Plates: Programming the p-Version Ritz Method*. Elsevier Science, 1998.

[96] X. Q. Wang and R. M. C. So. Various standing waves in a Timoshenko beam. *Journal of Sound and Vibration*, 280(1–2):311–328, 2005.

[97] D. J. Mead. Waves and modes in finite beams: Application of the phase-closure principle. *Journal of Sound and Vibration*, 171(5):695–702, 1994.

[98] C. W. de Silva. *Vibration: Fundamentals and Practice*. Taylor & Francis, 2006.

[99] W. M. Ewingg, W. S. Jardetzky, and F. Press. *Elastic Waves in Layered Media*. McGraw-Hill, 1957.

[100] L. Brekhovskikh. *Waves in Layered Media*. Applied mathematics and mechanics. Elsevier Science, 2nd edition, 2012.

[101] Y. Stavsky. Bending and stretching of laminated aeolotropic plates. *Transactions of the American Society of Civil Engineers*, 127(1):1194–1219, 1962.

[102] J. M. Whitney and N. J. Pagano. Shear deformation in heterogeneous anisotropic plates. *Journal of Applied Mechanics*, 37(4):1031–1036, 1970.

[103] E. Carrera. An assessment of mixed and classical theories on global and local response of multilayered orthotropic plates. *Composite Structures*, 50(2):183–198, 2000.

[104] J. N. Reddy. An evaluation of equivalent-single-layer and layerwise theories of composite laminates. *Composite Structures*, 25(1-4):21–35, 1993.

[105] E. Carrera and S. Brischetto. A survey with numerical assessment of classical and refined theories for the analysis of sandwich plates. *Applied Mechanics Reviews*, 62(1):17 pages, 2009.

[106] Y. Frostig and O. T. Thomsen. High-order free vibration of sandwich panels with a flexible core. *International Journal of Solids and Structures*, 41(5–6):1697–1724, 2004.

[107] V. D'Alessandro, G. Petrone, F. Franco, and S. De Rosa. A review of the vibroacoustics of sandwich panels: Models and experiments. *Journal of Sandwich Structures and Materials*, 15(5):541–582, 2013.

[108] R. D. Ford, P. Lord, and A. W. Walker. Sound transmission through sandwich constructions. *Journal of Sound and Vibration*, 5(1):9–21, 1967.

[109] C. P. Smolenski and E. M. Krokosky. Dilational-mode sound transmission in sandwich panels. *The Journal of the Acoustical Society of America*, 54(6):1449–1457, 1973.

[110] C. L. Dym, C. S. Ventres, and M. A. Lang. Transmission of sound through sandwich panels: A reconsideration. *The Journal of the Acoustical Society of America*, 59(2), 1976.

[111] J. A. Moore and R. H. Lyon. Sound transmission loss characteristics of sandwich panel constructions. *The Journal of the Acoustical Society of America*, 89(2), 1991.

[112] J. A. Moore and R. H. Lyon. Mode canceling composite panel for greater than mass-law transmission loss in the principal speech bands, July 1976. Patent US 4106588.

[113] T. Wang, V. S. Sokolinsky, S. Rajaram, and S. R. Nutt. Assessment of sandwich models for the prediction of sound transmission loss in unidirectional sandwich panels. *Applied Acoustics*, 66(3):245–262, 2005.

[114] L. Hinke, B. R. Mace, and M. J. Brennan. Finite element analysis of waveguides, 2004. ISVR Technical Memorandum N. 932, Southampton.

[115] C. Claeys. *Design and Analysis of Resonant Metamaterials for Acoustic Insulation*. PhD Thesis, Faculty of Engineering Sciences, Department of Mechanical Engineering, Division PMA, KU Leuven, Heverlee, Belgium, March 2014.

[116] D. J. Mead. Wave propagation and natural modes in periodic systems: I. Mono-coupled systems. *Journal of Sound and Vibration*, 40(1):1–18, 1975.

[117] D. J. Mead. Wave propagation and natural modes in periodic systems: II. Multi-coupled systems, with and without damping. *Journal of Sound and Vibration*, 40(1):19–39, 1975.

[118] W. X. Zhong and F. W. Williams. Wave problems for repetitive structures and symplectic mathematics. *Journal of Mechanical and Engineering Science*, 206:371–379, 1992.

[119] W. X. Zhong and F. W. Williams. On the direct solution of wave propagation for repetitive structures. *Journal of Sound and Vibration*, 181(3):485–501, 1995.

[120] D. Duhamel, B. R. Mace, and M. J. Brennan. Finite element analysis of the vibrations of waveguides and periodic structures, 2003. ISVR Technical Memorandum N. 922, Southampton.

[121] C. Mei and B. R. Mace. Wave reflection and transmission in Timoshenko beams and wave analysis of Timoshenko beam structures. *Journal of Vibration and Acoustics*, 127(4):382–394, 2005.

[122] Y. Yong and Y. K. Lin. Propagation of decaying waves in periodic and piecewise periodic structures of finite length. *Journal of Sound and Vibration*, 129(1):99–118, 1989.

[123] L. Meirovitch. *Element of Vibration Analysis*. McGraw-Hill, 1986.

[124] R. J. Guyan. Reduction of stiffness and mass matrices. *AIAA Journal*, 3(2):380, 1965.

[125] R. R. Craig and M. C. C. Bampton. Coupling of substructures for dynamic analysis. *AIAA Journal*, 6(7):1313–1319, 1968.

[126] ANSYS, Inc. *ANSYS® Mechanical APDL - Theory Reference*.

[127] E. Nilsson and A. C. Nilsson. Prediction and measurement of some dynamic properties of sandwich structures with honeycomb and foam cores. *Journal of Sound and Vibration*, 251(3):409–430, 2002.

[128] S. S. Tavallaey. *Wave Propagation in Sandwich Structures*. PhD Thesis, MWL The Marcus Wallenberg Laboratory for Sound and Vibration Research. Kungl Tekniska Hogskolan KTC, Stockholm, Sweden, February 2001.

[129] M. A. Dweib and B. Hu and A. O'Donnell and H. W. Shenton and R. P. Wool. All natural composite sandwich beams for structural applications. *Composite Structures*, 63(2):147–157, 2004.

[130] S. V. Joshi and L. T. Drzal and A. K. Mohanty and S. Arora. Are natural fiber composites environmentally superior to glass fiber reinforced composites? *Composites Part A: Applied Science and Manufacturing*, 35(3):371–376, 2004.

[131] G. Petrone, S. Rao, S. D. Rosa, B. R. Mace, F. Franco, and D. Bhattacharyya. Initial experimental investigations on natural fibre reinforced honeycomb core panels. *Composites Part B: Engineering*, 55:400–406, 2013.

[132] G. Petrone, V. D'Alessandro, F. Franco, B. R. Mace, and S. De Rosa. Modal characterization on recyclable foam sandwich panels. In *Proceedings of the 9th International Conference on Composite Science and Technology (ICCST/9)*, 2013. 24 - 26 April, Sorrento, Italy.

[133] J. J. Sargianis, H.-I. Kim, E. Andres, and J. Suhr. Sound and vibration damping characteristics in natural material based sandwich composites. *Composite Structures*, 96:538–544, 2013.

[134] G. Petrone, V. D'Alessandro, F. Franco, and S. De Rosa. Damping evaluation on eco-friendly sandwich panels through reverberation time (RT60) measurements. *Journal of Vibration and Control*, 2014. First published online on February 14th, 2014. 11 pages.

[135] A. Stocchi, L. Colabella, A. Cisilino, and V. Alvarez. Manufacturing and testing of a sandwich panel honeycomb core reinforced with natural-fiber fabrics. *Materials & Design*, 55:394–403, 2014.

[136] F. Tisseur and K. Meerbergen. The quadratic eigenvalue problem. *Society for Industrial and Applied Mathematics*, 43(2):235–286, 2001.

[137] S. Hammarling, C. J. Munro, and F. Tisseur. An algorithm for the complete solution of quadratic eigenvalue problems. *ACM Transactions on Mathematical Software*, 39(3):18:1–18:19, 2013.

[138] M. Berhanu. *The Polynomial Eigenvalue Problem*. PhD Thesis, Manchester Institute for Mathematical Sciences, School of Mathematics, The University of Manchester, Manchester, UK, August 2005.

[139] P. Lancaster. Linearization of regular matrix polynomials. *Electronic Journal of Linear Algebra*, 17:21–27, 2008.

[140] N. J. Higham, D. S. Mackey, F. Tisseur, and S. D. Garvey. Scaling, sensitivity and stability in the numerical solution of quadratic eigenvalue problems. *International Journal for Numerical Methods in Engineering*, 73(3):344–360, 2008.

[141] M. Jackson. Billie-jean, 1982. Album Thriller.

[142] J. Wolf, T. D. K. Ngoc, R. Kille, and W. G. Mayer. Investigation of lamb waves having a negative group velocity. *The Journal of the Acoustical Society of America*, 83(1), 1988.

[143] M. F. Werby and H. Uberall. The analysis and interpretation of some special properties of higher order symmetric Lamb waves: The case for plates. *The Journal of the Acoustical Society of America*, 111(6), 2002.

[144] P. L. Marston. Negative group velocity lamb waves on plates and applications to the scattering of sound by shells. *The Journal of the Acoustical Society of America*, 113(5), 2003.

[145] A. L. Shuvalov and O. Poncelet. On the backward lamb waves near thickness resonances in anisotropic plates. *International Journal of Solids and Structures*, 45(11–12):3430–3448, 2008.

[146] T. Hussain and F. Ahmad. Lamb modes with multiple zero-group velocity points in an orthotropic plate. *The Journal of the Acoustical Society of America*, 132(2), 2012.

[147] T. Peets, D. Kartofelev, K. Tamm, and J. Engelbrecht. Waves in microstructured solids and negative group velocity. *EPL (Europhysics Letters)*, 103(1):16001p1–16001p6, 2013.

[148] I. Tolstoy and E. Usdin. Wave propagation in elastic plates: Low and high mode dispersion. *The Journal of the Acoustical Society of America*, 29(1):37–42, 1957.

[149] E. Barbieri, A. Cammarano, S. De Rosa, and F. Franco. Waveguides of a composite plate by using the spectral finite element approach. *Journal of Vibration and Control*, 15(3):347–367, 2009.

[150] P. J. Shorter. Wave propagation and damping in linear viscoelastic laminates. *The Journal of the Acoustical Society of America*, 115(5):1917–1925, 2004.

[151] Mercedes Benz. The New Mercedes-Benz S-Class: Design for the Environment, 2005. Available from http://www.schwab-kolb.com/daimler/en/dc000227.htm. Accessed on February 18th, 2014.

[152] Ford Motor Company. From Bangladesh to a Mondeo, Kenaf Adds to Ford's Use of Ecological-friendly Materials, 2005. Available from http://media.ford.com. Accessed on February 18th, 2014.

[153] G. Petrone. *Characterisation of bio-based structures: models and experiments*. PhD Thesis, Department of Industrial Engineering, University of Napoli Federico II, Napoli, Italy, March 2014.

[154] L. Yam, Z. Wei, L. Cheng, and W. Wong. Numerical analysis of multi-layer composite plates with internal delamination. *Computers & Structures*, 82(7-8):627–637, 2004.

[155] Z. Su, L. Ye, and Y. Lu. Guided Lamb waves for identification of damage in composite structures: a review. *Journal of Sound and Vibration*, 295(3-5):753–780, 2006.

[156] M. Sale, P. Rizzo, and A. Marzani. Semi-analytical formulation for the guided waves-based reconstruction of elastic moduli. *Mechanical system signal processing*, 25(6):2241–2256, 2011.

[157] J. L. Rose. *Ultrasonic Waves in Solid Media*. Cambridge University Press, 2004.

LIST OF PUBLICATIONS

PEER–REVIEWED JOURNALS

- Vincenzo D'Alessandro, Giuseppe Petrone, Francesco Franco, Sergio De Rosa. A review of the vibroacoustics of sandwich panels: Models and experiments. *Journal of Sandwich Structures and Materials*, September 2013, Volume 15, Pages 541-582, 2013.
  DOI: 10.1177/1099636213490588

- Farbod Alijani, Marco Amabili, Giovanni Ferrari, Vincenzo D'Alessandro. Nonlinear vibrations of laminated and sandwich rectangular plates with free edges. Part 2: Experiments & comparisons, *Composite Structures*, November 2013, Volume 105, Pages 437-445, 2013.
  DOI: 10.1016/j.compstruct.2013.05.020

- Giuseppe Petrone, Vincenzo D'Alessandro, Francesco Franco, Sergio De Rosa. Damping evaluation on eco-friendly sandwich panels through reverberation time (RT 60) measurements. *Journal of Vibration and Control*, first published online on February 14, 2014.
  DOI: 10.1177/1077546314522507

- Giuseppe Petrone, Vincenzo D'Alessandro, Francesco Franco, Brian R. Mace, Sergio De Rosa. Modal characterization of recyclable foam sandwich panels. *Composite Structures*. In Press, accepted for publication on March 11, 2014. Available online on March 28, 2014.
  DOI: 10.1016/j.compstruct.2014.03.026

- Vincenzo D'Alessandro, Giuseppe Petrone, Sergio De Rosa, Francesco Franco. Modelling of aluminium foam sandwich panels. *Smart Structures and Systems*. Accepted for publication, scheduled for Volume 13(4), April 2014. Special Issue: DeMEASS V.

- Vincenzo D'Alessandro, Giuseppe Petrone, Francesco Franco, Sergio De Rosa. Numerical and experimental investigations on the acoustic power radiated by aluminium foam sandwich panels. Submitted to *Applied Acoustics*. Under review.

CONFERENCE PROCEEDINGS

- Vincenzo D'Alessandro, Marco Amabili, Sergio De Rosa, Francesco Franco. Preliminary identification of sandwich panels. In *Proceedings of the 4th International Conference on Noise and Vibration: Emerging Methods (NOVEM 2012)*.

ISBN 13: 9781605951133. Ed: Dip. Ingegneria Aerospaziale, Universitá degli Studi di Napoli. April 1-4, 2012, Sorrento (Italy). Paper n.20, 10 pag.

- Giuseppe Petrone, Vincenzo D'Alessandro, Francesco Franco, Brian R. Mace, Sergio De Rosa. Modal characterization on recyclable foam sandwich panels. In *Proceedings of the 9th International Conference on Composite Science and Technology (ICCST/9)*. ISBN 13: 9781605951133. Ed: Michele Meo. April 24-26, 2013, Sorrento (Italy). Pages 665-676.
- Vincenzo D'Alessandro, Giuseppe Petrone, Francesco Franco, Sergio De Rosa.The acoustic power radiated from aluminium foam sandwich panels. In *Proceedings of the International Conference on Acoustics AIA-DAGA 2013*. ISBN 13: 9783939296058, Publisher: German Acoustical Society (DEGA). March 18-21, Merano (Italy). Pages 354-357.